NIOSH R01 final report for R01-OH10828

Title Page

Title **SYSTEMIC HEALTH IMPLICATIONS OF OCCUPATIONAL NANOMATERIAL EXPOSURE**

MPIs: Matthew J. Campen and Andrew Ottens
Affiliation: University of New Mexico
Address: 2502 Marble Ave, NE, Albuquerque, NM
Telephone: 505 925-7778
Email: mcampen@salud.unm.edu

Awarded Institute: Same as affiliation and contact information above
Sponsors: National Institute for Occupational Safety and Health
Grant number: R01-OH10828
Project Start and End dates: 09/30/2015 – 09/29/2020
Date of report completion: 20 December, 2020

TABLE OF CONTENTS

List of Terms and Abbreviations

4′,6-diamidino-2-phenylindole (DAPI)
A Disintegrin and Metalloproteinase (ADAM)
A Disintegrin and Metalloproteinase with Thrombospondin (ADAMTS)
Akaike information criterion (AIC)
Analysis of Variance (ANOVA)
Area under the curve (AUC)
Blood Brain Barrier (BBB)
Body Mass Index (BMI)
Bronchoalveolar Lavage Fluid (BALF)
C-C motif chemokine ligand 2 (Ccl2)
C-C motif chemokine ligand 5 (Ccl5)
Carbon nanotubes and fibers (CNT/F)
Cardiovascular Disease (CVD)
Central Nervous System (CNS)
Cerebrospinal Fluid (CSF)
Chemokine C-X-C motif ligand 1 (CXCL1 aka KC-GRO)
Cluster of Differentiation (CD)
Command line interface (CLI)
Dispersion Media (DM)
Elemental Carbon (EC)
Engineered nanomaterials (ENM)
Gamma-Aminobutyric Acid (GABA)
Glial fibrillary acidic protein (GFAP)
Glutamic acid decarboxylase 65-kilodalton isoform (GAD65)
Graphical user interface (GUI)
Human Coronary Artery Endothelial Cells (HCAECs)
Human Umbilical Vein Endothelial Cells (HUVECs)
Inhalable elemental carbon (IEC)
Interferon-γ (IFN-γ)
Interleukin (IL)
Intracellular adhesion molecule 1 (Icam1)
Ionized calcium binding adaptor molecule 1 (Iba1)
Knockout (KO)
Marimastat (Mar)
Matrix Metalloproteinase (MMP)
Mouse Primary Cerebrovascular Endothelial Cells (mCECs)
Multiwalled Carbon Nanotubes (MWCNT)
National Institute for Occupational Safety and Health (NIOSH)
Partial Least Squares Discriminant Analysis (PLS-DA)
Phosphate-buffered Saline (PBS)
Physiological Saline Solution (PSS)
Principle Component Analysis (PCA)
Quantitative Polymerase Chain Reaction (qPCR)
Recommended exposure limit (REL)
Respirable elemental carbon exposure (RC_EC)
Ribonucleic Acid (RNA)
Room Temperature (RT)
Serum Cumulative Inflammatory Potential Assay (SCIP)
Thrombospondin (TSP)
Tissue inhibitors of metalloproteinases (TIMPs)
Transforming growth factor beta (Tgfb)
Transmission Electron Microscopy (TEM)
Tris(2-carboxyethyl)phosphine (TCEP)
Tumor necrosis factor alpha (Tnfa)
Variable importance scores (VIP)

Vascular cell adhesion molecule 1 (Vcam1)
Vesicular glutamate transporter 1 (VGLUT1)
Zonula occludens-1 (ZO-1)

FINAL REPORT ABSTRACT:

Introduction: Nanomaterials have become a major engineering and industrial endeavor for a wide variety of applications, however concerns regarding risk to human health have arisen due to the multitude of physicochemical variables associated with compositional variations and the difficulty of rapid screening for possible toxicity. We've previously demonstrated a link between nanomaterial exposure, specifically multi-walled carbon nanotube (MWCNT), and serum compositional changes that promote inflammatory pathways and vascular dysfunction. This project sought to determine the origin and assess the functional inflammatory potential of MWCNT exposure-derived serum byproducts. To this end, a multipronged research approach was designed using functional *in vitro* assays, advanced peptidomic analysis, controlled rodent exposures and samples from an occupationally-exposed human cohort.

Results: To determine the role of matric metalloproteinases (MMPs) in MWCNT-exposure derived serum-bioactivity, a broad-spectrum MMP inhibitor was selectively delivered to the lung of C57BL/6 mice prior to oropharyngeal MWCNT exposure. We observed a significant pulmonary inflammatory response to MWCNT exposure that was independent of MMP blockade. However, cultured mouse cerebrovascular endothelial cells treated with serum from MWCNT-exposed mice pretreated with MMP blockade exhibited ~50% recovery in barrier integrity compared to 75% in vehicle only pretreated MWCNT-exposed animals. Analysis of biofluids from these animals revealed that upwards of 85% of the MWCNT-induced peptidomic signal released into the circulation was returned to control levels with MMP blockade. Moreover, a distinct MWCNT-induced peptidomic shift was observed within the CSF. Identified MWCNT-responsive peptides depicted a mechanism involving aberrant fibrinolysis in connection with blood-brain barrier permeation, astrocyte and microglial reactivity with dose-dependent differences and a pro-degradative anti-plastic hyperexcited state.

Cultured endothelial cells treated with serum from occupationally-exposed individuals participating in a NIOSH exposure assessment study showed only modest changes in inflammatory response patterns likely due to tight occupational controls with most personal breathing zone measures below 10 $\mu g/m^3$. Using our in-lab developed software, EndogeSeq, we identified 27 of the 104 most-discriminant peptides in the serum of 24 subjects divided evenly between high and low-exposure groups. Peptide compilation was functionally related to pulmonary injury, vascular dysfunction, altered translation, and autophagy/endocytosis processes consistent with pathogenesis observed in model CNT/F exposures.

Conclusion: Animal studies revealed that while lung MMP activity does not play a significant role in mediating MWCNT-induced pulmonary inflammation, pulmonary MMP activity largely drives MWCNT-induced serum bioactivity which disrupts the endothelial barrier. These data substantiate the role of MMP proteolytic fragment generation in the lung, its release into the circulation and the reactive bioactivity of that peptidomic response. Moreover, MWCNT-exposure in mice induces a distinct peptidomic response in the CSF reflecting a compromised blood-brain barrier, neuroinflammation, and hyperexcited neuronal state consistent with early-pathobiology of neurodegenerative disease. Analysis of serum from a subset of occupationally-exposed workers revealed a robust and highly discriminatory shift within the circulating peptidome that is linearly correlated with the log of personal breathing zone metrics of exposure. Taken together, our data support further development of peptide biomarkers for monitoring *in vivo* responses to CNT/F exposure and the use of such diagnostics in longitudinal observational studies.

Section 1 of the Final Progress Report

Nanoparticles are incorporated into an ever-growing array of consumer products and the manufacturing of carbon nanotubes and carbon fibers (CNT/F) is currently the fastest-growing engineered nanomaterials industry.[3,4] However, growing concerns regarding both human health outcomes and environmental impacts have raised questions with respect to the safety of CNT/F production and application.[5,6] Initial literature on CNT toxicity has revealed common findings of inhalation exposure including disruption of lung tissue architecture, recruitment of inflammatory cells and activation of inflammatory responses.[7-14]

Building on our previous work we hypothesized that peptide fragments released into the circulation following lung multiwalled CNT (MWCNT) reactivity would result in neurovascular dysfunction and blood-cerebrospinal fluid-barrier permeability. To test this hypothesis, we designed a multipronged research approach using functional *in vitro* assays, advanced peptidomic analysis, controlled rodent exposures, and samples from an occupationally-exposed human cohort. Our overarching goal was to determine the origin and assess the functional inflammatory potential of MWCNT exposure-derived byproducts.

Significant or Key Findings:

Aim 1: Ascertain the origin of modified circulatory components related to airway metalloproteinase (MMP) activity and inflammation. In Aim 1, we explored the role of MMPs in MWCNT-exposure derived serum-bioactivity by selectively delivering a broad-spectrum MMP inhibitor (Marimastat) to the lung. Results from these studies revealed significant pulmonary neutrophil infiltration, an increase in total BALF protein, and elevated cytokine expression in lung tissue in a dose-dependent manner in C57BL/6 mice that was independent of Marimastat pretreatment. However, in assessing cultured mouse cerebrovascular endothelial cells treated with serum from MWCNT-exposed mice, we observed ~50% recovery in barrier integrity with MMP blockade pre-treatment, which was down as much as 75% in MWCNT-exposed animals that received only vehicle pre-treatment. Peptidomic analysis revealed that upwards of 85% of the MWCNT-exposure induced peptidomic signal released into circulation was returned to control levels with MMP blockade pre-treatment in the lung. This substantiated the role of MMP proteolytic fragment generation in the lung, its release into the circulation and the reactive bioactivity of that peptidomic response.

Taken together, findings from Aim 1 revealed that lung MMP activity does not play a significant role in mediating MWCNT-induced pulmonary inflammation but MWCNT-induced circulating peptides and inflammatory bioactivity are generated, in large part, by pulmonary MMP activity. The biological pathways underlying nanomaterial-mediated respiratory pathology seem, at least on the surface, to mirror those of air pollution exposures including activation of inflammatory signaling, oxidative stress, enzyme activation and ECM remodeling.[15-17] These data therefore suggest that many downstream, extrapulmonary effects of inhaled particulates, such as MWCNT, may be related to pulmonary MMP activation and spillover of fragmented peptides and matrikines into the circulation, which in turn drive endothelial inflammatory responses and impair barrier function.

Aim 2: Assess pulmonary MWCNT-induced neurovascular impacts and "serome" access into the central nervous system (CNS). While exposure to air pollutants has repeatedly shown an association with neurological outcomes, the mechanisms underlying the involvement of the lung-brain axis remain unclear.[18-20] We have shown that circulating "serome" factors induced by pulmonary reactivity from MWCNT exposure impact cardiovascular function and induce blood-brain barrier impairment.[8] The objective of Aim 2 was to test our hypothesis that MWCNT-lung reactivity releases byproducts into the circulation that then result in neurovascular dysfunction and blood-CSF-barrier permeability as a novel CNS-access mechanism. Enriched peptide fractions from cerebral spinal fluid (CSF) and serum from the MWCNT-exposed C57BL/6 mice from Aim 1 were analyzed using ion mobility-enabled data-independent mass spectrometry for label-free peptidomic analysis. Results from these studies revealed that MWCNT exposure generated a prominent peptidomic response in the blood and CSF; however, there was very limited correlation between the factors responsive to MWCNT-exposure. Instead, we determined that there was a distinct MWCNT-induced peptidomic shift within the CSF with 292 significant responses. Identified MWCNT-responsive peptides depicted a mechanism involving aberrant fibrinolysis (fibrinopeptide A) in connection with blood-brain barrier permeation (HOXA4), neuroinflammatory (TMEM131L) reactivity by astrocytes and microglia with dose-dependent differences, and a pro-degradative (STAM, PGK) anti-plastic (AFF1, VPS18) state with a quantified imbalance between excitation (VGLUT1) and inhibition (GAD65) to result in a hyperexcited (MAP1B) phenotype.

Overall, data from Aim 2 demonstrated that in response to MWCNT exposure, a distinct peptidomic response is generated in CSF reflecting a compromised blood-brain barrier, neuroinflammation, and hyperexcited neuronal state consistent with early-pathobiology of neurodegenerative disease. In addition, Aim 2 focused on

engineering new software to overcome challenges in identifying molecular byproducts endogenous to biofluids ("EndogeSeq"), such as induced with MWCNT-pulmonary exposure. The latest version of the EndogeSeq platform has been released and allows handling of both quantitative and identification functions for peptidomic analysis. During the engineering of EndogeSeq we aimed to optimize a scoring algorithm that was sensitive to detecting real endogenous peptides while minimizing false-positives that would limit overall performance. Molecular identification enabled by EndogeSeq is critical to decoding circulating factor origins and delineating the downstream transduced bioactivation mechanisms enabling a deeper understanding of how pulmonary exposures initiate systemic health impacts.

Aim 3: Characterize MWCNT-induced inflammatory potential and seromic response in samples derived from an occupationally-exposed human cohort. We allied with a NIOSH cross-sectional epidemiologic and carbon nanotube/nanofiber (CNT/CNF) exposure assessment cohort study. For this we assessed collected serum specimens for endothelial activation linked to CNT/CNF personal breathing zone measurements of elemental carbon. In the first subaim, human coronary artery endothelial cells (HCAECs) and human umbilical vein endothelial cells (HUVECs) were treated with serum from exposed workers and the induction of seromic factors was evaluated to build a blood diagnostic of occupational ENM exposure. Findings from the serum cumulative inflammatory potential assays in both HCAECs and HUVECs were modest. While recent studies with colleagues in China found that this *in vitro* serum inflammatory potential assay behaved predictably in a cohort of workers exposed to much higher levels of carbon nanoparticles (657 $\mu g/m^3$), we conclude that the modest effects seen in the present study are largely due to tight occupational controls in the US-based cohort. With most personal breathing zone measures below 10 $\mu g/m^3$ we conclude that this cohort was largely well-protected. However, a few subjects did have substantial exposures.

We next studied a peptidomic response to occupational CNT/F exposure and its diagnostic potential for monitoring workers across the industry. Using a case-control design with serum from 24 subjects divided evenly between two exposure cohorts we were able achieve higher power in addressing an induced serum peptidomic response. Workers in a high exposure cohort were acutely exposed to > 0.5 $\mu g/cm^3$ inhalable elemental carbon (IEC) in a two-day shift; i.e., exceeding 50% of the NIOSH recommended exposure limit of 1 $\mu g/cm^3$. Workers in a low exposure cohort received < 0.1 $\mu g/cm^3$ IEC and served as an industry control population. Some 11,546 serum peptides were reproducibly quantified across at least 50% of workers, demonstrating a complex circulating peptidome in humans. Moreover, 934 of these peptides measured in at least 75% of subjects were significantly altered in concentration between High and Low exposure cohorts. From these, we were able to devise a five-peptide biomarker model that was 100% predictive in discriminating those with high CNT/F exposure from those with low exposure in a separate validation cohort. Moreover, these peptides provided between a 3 and 4 order dynamic range with a strong ($R^2 > 0.7$) linear correlation to the logarithmic combination of the personal breathing zone measures of CNT/F exposure. Using EndogeSeq we were able to identify 27 of the 104 most-discriminant peptides. The compilation of peptides were functionally related to vascular dysfunction, pulmonary injury, altered translation and autophagy/endocytosis processes consistent with pathogenesis observed in model CNT/F exposures.

Translation of Findings: Findings from Aim 3 reveal that while health effects among CNT/F workers have yet to be clearly demonstrated in the US, there is a robust and highly discriminatory shift within the circulating peptidome that is linearly correlated with the log of personal breathing zone metrics of exposure. Moreover, the identified peptides reflect pathobiology that is consistent with negative pulmonary and vascular outcomes observed in modeled CNT/F exposure. These data support further development of peptide biomarkers for monitoring *in vivo* responses to CNT/F exposure among workers and the use of such diagnostics in longitudinal observational studies. The overall confirmation that pulmonary responses to MWCNT lead to generation of a bioactive circulatory peptidomic shift is important for better understanding acute and long-term systemic health effects of nanomaterial inhalation.

Research Outcomes/Impact: Through a translational approach from in vitro, preclinical, and occupational cohort studies, we have better defined the potential for lung-generated peptide species to negatively impact vascular endothelial cell homeostasis, especially with regards to BBB function. Potential downstream outcomes on neurological function were defined for extreme scenarios. In general, we found that occupational exposure levels in a cohort studies are low enough to avoid such outcomes, but peptidomic markers from low-level exposed workers suggests that some pulmonary response and systemic peptidomic spillover is occurring. While we are unclear how such peptidomic changes impact health long-term, they do present a potential metric for exposure assessment.

Section 2 of the Final Progress Report

BACKGROUND

Engineered nanomaterials (ENM) have become a major engineering and industrial endeavor for a wide variety of applications.[21] Risks to human health are a concern due to the multitude of physicochemical variables associated with the essentially unlimited compositional variations for these materials, and the difficulty of rapidly screening *all* new ENMs for toxic potency.[9,11] The primary concerns are for occupational or accidental high-dose inhalation exposures, although chronic, low-level exposures may also have substantial health ramifications. Novel methods for screening the toxic potential of ENMs are needed that are high-throughput and have coherence with human disease outcomes.

From a toxicological standpoint, several routes of ENM exposure are plausible, although for the present proposal we have focused on inhalation. Oral, dermal, and ocular routes can occur, but the lower rate of uptake, surface area, and vulnerability of those organs provides rationale for prioritizing the inhalation route. Intravenous and subcutaneous routes are also foreseeable, as ENMs become used for drug delivery, medical devices, or other therapeutic roles. While the impact of alternate exposure routes cannot be dismissed, recent studies comparing routes in a head-to-head manner find that inhalation exposure is more potent a driver of systemic toxicity of particles than direct intravenous or gastrointestinal exposure.[22,23] In fact, it has been posited that endogenous blood proteins may confer protection against direct effects of nanotubes on endothelial cells via incorporation into the nanotube corona.[24]

While numerous groups have attempted to ascertain risk by directly treating endothelial cells with ENMs in culture, such a bolus effect and high direct exposure is unrealistic and ignores the biochemical interactions with ENMs in the lung and blood. Most importantly, *in vitro* studies of direct ENM exposure to endothelial cells typically only observe toxic or inflammatory effects at concentrations of 10-50 µg/ml, when even workplace concentrations are unlikely to exceed 50 $\mu g/m^3$ – a concentration factor of 1,000,000 that is not physiologically conceivable.[25,26] The present proposal overcomes such limitations by employing methods that incorporate more anatomically realistic pulmonary (inhalation/instillation) exposures, followed by inflammatory assessment of the "serome", which is a nearly complete snapshot of the factors to which coronary and cerebrovascular endothelial cells are exposed.

Systemic Inflammatory Effects of ENMs: Vascular Outcomes. Numerous population health studies identify a correlation between exposure to airborne particulate matter (PM) and cardiovascular disease (CVD; coronary artery disease, ischemic heart disease, stroke).[27-29] Recent studies have shown that exposure to ENMs may drive progression of CVD. Systemic inflammation, increased atherosclerotic lesion area, enhanced prothrombotic potential, and vascular dysfunction have been associated with pulmonary exposures to ENMs.[30-35] In addition, these studies have shown that cardiovascular effects may be more sensitive than gross pulmonary toxicity evaluations (e.g., bronchoalveolar lavage cytotoxicity or lung inflammation).

Inhaled ENMs have been investigated for the potential to induce systemic inflammation and promote progression of aortic atherosclerotic lesions. Nurkiewicz et al[33,36] have shown that pulmonary exposures to titanium dioxide particulates led to the observation of adherent inflammatory cells and deposition of myeloperoxidase in the systemic vasculature. Li et al[31] showed increase plaque size in ApoE $^{-/-}$ hypercholesterolemic mice instilled with carbon nanotubes every other week for 8 weeks. These changes were not associated with increases in circulating inflammatory markers (such as IL-6), suggesting that an unknown driver(s) was causing the vascular inflammation. A similar study by Niwa et al[32] found that carbon nanoparticles could also promote atherosclerosis progression and that acute intratracheal insufflations of the nanoparticle did lead to increased systemic inflammation.

Systemic Inflammatory Effects of ENMs: Neurological Outcomes. Several recent studies show neurotoxic effects of inhaled particles. Welding fumes, which typically contain particulates in the 200-300 nm diameter range, are able to induce striatal inflammation, indicated by expression of TNFα, Ifnγ and iNOS mRNA in healthy Sprague-Dawley rats.[37] Coincident, the welding fume PM instillation also led to loss of dopaminergic mitochondrial function. Intranasal exposure to titanium dioxide led to upregulation of hippocampal TNFα, NFkB and toll-like receptors 2 and 4, which aligned with a loss of spatial learning and memory in CD-1 mice. [38] These outcomes are consistent with neuroinflammation induced by diesel emissions, which contain nano-sized particulates in addition to gases such as oxides of nitrogen and carbon monoxide. [39]

The brain is arguably the most protected systemic organ, due to the blood-brain barrier (BBB). Even at unjustifiably high systemically-administered doses of nanoparticles, it is difficult to observe accumulation in the brain, and invariably the concentration in the brain is <1% of other organs.[40] MWCNTs are no different, with minimal systemic distribution and brain levels are estimated at <0.001% of the original inhalation dose (5 mg/m^3 x 5h/d x 12 d).[23] Furthermore, the detected MWCNT material in the brain was often in capillaries or capillary walls, suggesting that even less material crossed the BBB.[41] The authors note that the blood flow to the brain, which is roughly 20% of total cardiac output,[42] would predict a greater percentage of deposition relative to liver or kidneys, but the BBB is resistant to MWCNT deposition. Thus, there is a gap of knowledge to explain how neuroinflammation and neural toxicity occur when ENMs fail to directly access the CNS.

Our proposed paradigm, that circulatory modifications are the principal outcome of lung-ENM interactions, is consistent with the idea that all systemic organs may be vulnerable. We propose that much of the observed extrapulmonary translocation is academic and purely related to exceedingly high doses used in toxicological proof-of-concept research. More realistic doses, we propose, induce chemical modifications of the serum that imparts inflammatory bioactivity. We have observed the induction of serum in controlled human studies with exposures to diesel emissions (100 µg/m^3) and nitrogen dioxide (0.5 ppm) for short 2h exposures.[2] Furthermore, inflammatory serum bioactivity is induced in MWCNT-exposed mice and mass spectrometry findings confirm a broad profile of peptidomic changes that likely drive this effect, as detailed in this report.

Human Cardiovascular Risk Determination with a Translationally-Coherent Ex Vivo Approach: We have developed an *in vitro,* translational method to assess the inflammatory potential of circulating factors. [2,43] We found that human plasma samples obtained after controlled exposure to diesel emissions or NO_2 could induce expression of cellular adhesion molecules (ICAM, VCAM, and P-selectin) in primary hCAECs, as compared to plasma obtained before exposures or after sham (filtered air) exposures.[2] Despite the relatively low concentrations of air pollution exposure, which fail to elicit measurable changes in lung function or pulmonary inflammation, these studies highlight that circulating pro-inflammatory mediators are inducible by pollutants that never pass the epithelial lining fluid of the lung, such as NO_2. [44,45]

This assay holds great promise to help further understand the pathways that lead from the exposed lung to the systemic health impacts, as well as assess factors that determine individual susceptibility and relative potency of inhaled toxicants. We applied this same assay paradigm to a study of grape seed extract (resveratrol) efficacy in humans and found that after a month of treatment, plasma from resveratrol-treated subjects caused less hCAEC activation compared to each individual's baseline plasma, while placebo had no effect, consistent with our hypothesis for this natural supplement. [43] Moreover, numerous traditional markers, including IL-6 and TNFα failed to reveal any significant effects, positive or otherwise.

Omic Biofluid Signatures of Circulating Molecular Byproducts - A New Translational Approach to Detection of ENM Induced Pathobiology: We have also identified a new and diverse complement of inducible biomolecules within biofluids with significant diagnostic potential. Enabled by the recent advent of data-independent mass spectrometric analysis for label-free quantitative study of exposure-induced unknowns in biofluids, our collaborative studies with NIOSH uncovered a compliment of >1,000 blood-borne biomolecular responses to lung-xenobiotoic interactions, which we have termed the "serome". Indeed, we are afforded ample classification power by the diversity of molecular responses such as to differentiate exposed animals at different doses of MWCNT treatment and vehicle control animals (**Fig. 1**). Importantly, we deduced the novel introduction of peptide byproducts as a prominent component of the serome, with evidence to suggest proteolytic production upon pulmonary exposure with release into circulation to signal systemic effects.

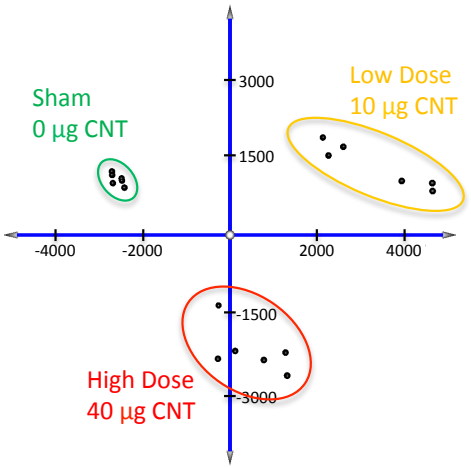

Figure 1. Classifying MWCNT exposure by "serome" signature. Study subjects were effectively discriminated by unsupervised principal component analysis. A signature of moderate-sized by-product molecules was induced within the blood serum of MWCNT treated animals (the "serome"), accurately classifying by treatment and dose. In total, 2,507 factors were found responsive to either MWCNT dose (*Kruskal-Wallis; 5% FDR).*

We also demonstrated that pathobiologically induced peptide byproducts can pass through a compromised BBB, as we exemplified in response to traumatic brain injury, and are reproducibly quantified within human peripheral fluids.[46] Further our human studies demonstrate multivariate biomolecular correlation with assess neurological dysfunction. These findings, importantly, demonstrate the translational

potential of this newly identified biomolecular cohort in biofluids to resolve common pathobiology among heterogenous human cohorts.

SIGNIFICANCE

CVD affects roughly 50% of the US population and is not surprisingly a major concern for worker health. CVD risk is elevated in firefighters, [47] miners, [48] and welders, [49] all of whom have a high risk of inhalational exposures to particulates. In addition to mental and physical stress on the job, numerous environmental exposures have been associated with increased risk of CVD and adverse cardiac/cerebrovascular outcomes (stroke, infarction), including welding/soldering fumes and traffic pollution. [47,50,51] Contemporary clinically- or experimentally-derived determinations of risk, while valuable, are imprecise, especially for toxicological assessments. In a recent editorial, the gap in experimental methods was noted for the study of chronic vascular disease. Landsiedel and colleagues wrote, "Inhalation studies on the potential to develop chronic diseases, or studies to check the potential analogy to CVD associated with adverse health effects from ambient air pollution, are largely missing."[6] Based on our preliminary work with this endothelial cell activation assay, we strongly believe this method can meet the needs of 1) comparative toxicity between ENMs, 2) linkages to chronic vascular disease, and 3) translational human significance.

This project therefore sought to address the impact of carbon nanotube exposure in the lung on the generation of circulating peptide fragments and functional inflammatory potential. The research strategy entailed a multipronged approach, using functional in vitro assays, advanced peptidomic sequencing, controlled rodent exposures, and samples from an occupationally-exposed human cohort. We addressed the research question through 3 specific aims:

Aim 1: Ascertain the origin of modified circulatory components related to airway metalloproteinase activity and inflammation.

AIM 2: Assess pulmonary ENM-induced neurovascular impacts and "serome" access into the central nervous system (CNS).

Aim 3: Characterize MWCNT-induced inflammatory potential and seromic response in samples derived from an occupationally-exposed human cohort.

RESEARCH APPROACH AND OUTCOMES

Aim 1: Ascertain origin of modified circulatory components related to airway metalloproteinase activity and inflammation.

Evidence suggests that circulating factors may be related to a) direct reactions of ENMs and pulmonary cellular/molecular components or b) degradation byproducts of increased metalloproteinase activity and that the circulating components act through endothelial cell surface pattern recognition receptors. Evidence for substantial upregulation of lung MMP12 following MWCNT inhalation, combined with the observation of fibrin peptide fragments in the serum that possess cleavage domains specific to MMP12, provides substantial justification to examine this, as well as related metalloproteinases.

We have previously found that exposure to MWCNT by both inhalation and pharnygeal aspiration leads to serum compositional changes that promote inflammatory pathways and vascular dysfunction, an effect recapitulated in recent studies of ozone, diesel, and nitrogen dioxide, [2,17] Microarray analysis of the serum-treated endothelial cells revealed 1) an upregulation of inflammatory pathways and 2) downregulation of cell cycle and cell motility genes. This latter finding was demonstrated as a functional impact in a wound-healing assay, where confluent cells treated with serum from control or MWCNT-exposed mice were "scratched" and regrowth measured over 6h (**Figure 2**). Serum from both the low and high dose MWCNT induced a significant retardation of regrowth, consistent with findings in the microarray. These findings are consistent with both gaseous and complex emissions

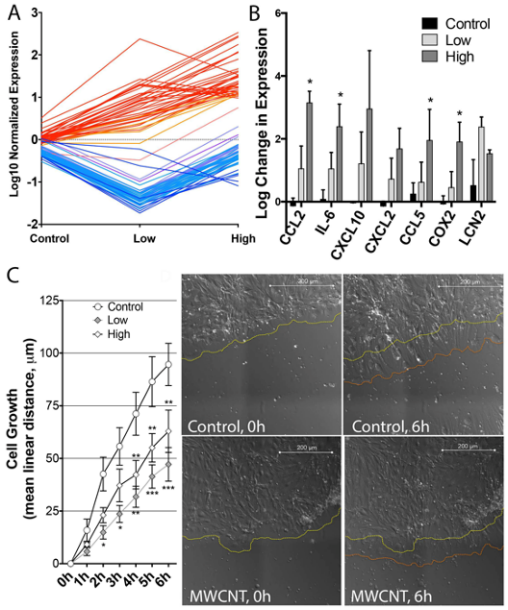

Figure 2. Microarray analysis (A) of mCVECs treated with serum from MWCNT-exposed mice revealed significant dose related induction of inflammatory factors, including chemokines and inflammatory enzymes involved in atherosclerosis (B), along with reduction of genes essential to cell cycle and cytokinesis. To address the functional impact of the down-regulated pathways, we conducted a wound-healing assay (C), which showed that mCVECs incubated with serum from MWCNT-exposed mice had significant reductions in cell growth compared to those treated with control serum. Asterisks*,** indicate p<0.05, 0.01 by 2-way ANOVA, n=6/group.

exposures[2,17,52] and clearly establish inflammatory bioactivity of serum components following MWCNT exposure.

Upregulation of Lung MMP Gene Expression: Gene array findings reported a strong upregulation of MMP12 in the lungs of mice exposed to MWCNTs by inhalation (significant at the 0.5 and 5.0 mg/m^3 levels; **Figure 3**). This finding is consistent with pulmonary transcriptional response to welding fume particles, an exposure that has been demonstrated to promote atherosclerosis in mouse models.[53,54] Activity is not directly related to transcription, however, and numerous MMPs may be endogenously expressed and activated without affecting gene expression.

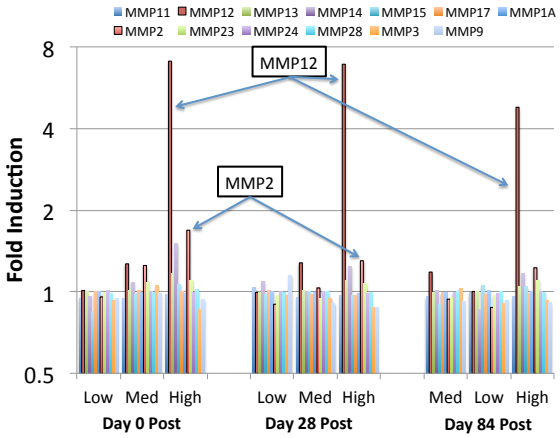

Figure 3. Transcriptional changes in lungs from mice inhaling MWCNT (0.05, 0.5, or 5.0 mg/m^3) for 19 days. A strong, persistent increase in MMP12 expression was noted out to 84 days post exposure. MMP2 was also significantly elevated, but to a lesser extent.

AIM 1.1. Role of pulmonary matrix metalloproteinases in multiwalled carbon nanotube-mediated pulmonary and systemic inflammatory activation.

In this first study, we explored the role of MMPs in driving MWCNT-exposure derived serum bioactivity by utilizing a broad-spectrum MMP inhibitor, Marimastat, delivered selectively to the lung.

MATERIALS AND METHODS

Animal Model and Sample Collection

Specific pathogen-free male 6-8 week old C57BL/6J mice (Jackson Laboratory) were used in this study. Animals were housed in an Association for Assessment and Accreditation of Lab Animal Care International-approved animal facility at the University of New Mexico with procedures approved by Institutional Animal Care and Use Committee of the University of New Mexico. Animal care and use procedures were conducted in accordance with the US Public Health Service's Policy on Humane Care and Use of Laboratory Animals (https:// grants.nih.gov/grants/olaw/references/phspol.htm) and the National Institutes of Health's Guide for the Care and Use of Laboratory Animals (https://grants.nih.gov/grants/olaw/Guide-for-the-Care-and-Use-of-Laboratory-Animals.pdf). Food and water were provided *ad libitum* in ventilated cages in a temperature- and humidity-controlled environment with a 12-h light/dark cycle.

The C57BL/6J mice were treated under light isoflurane anesthesia via oropharyngeal aspiration with broad spectrum MMP inhibitor, Marimastat (Alfa Aesar - J67288) in DMSO at a final concentration of 10 mg/kg of body weight or 1% DMSO in 1X phosphate buffered saline (PBS; **Figure 4**). One hour following Marimastat dosing, mice were administered MWCNT under light isoflurane anesthesia via oropharyngeal aspiration at doses of 0 µg, 10 µg or 40 µg (n = 5). The MWCNTs were prepared in dispersion media (DM) consisting of mouse serum albumin (0.6 mg/mL) and 1,2-dipalmitoyl-sn-glycero-3-phosphocholine (10 µg/mL). The MWCNT material used in this study, MWCNT-7, has been extensively characterized [13,55]. The average diameter was 49

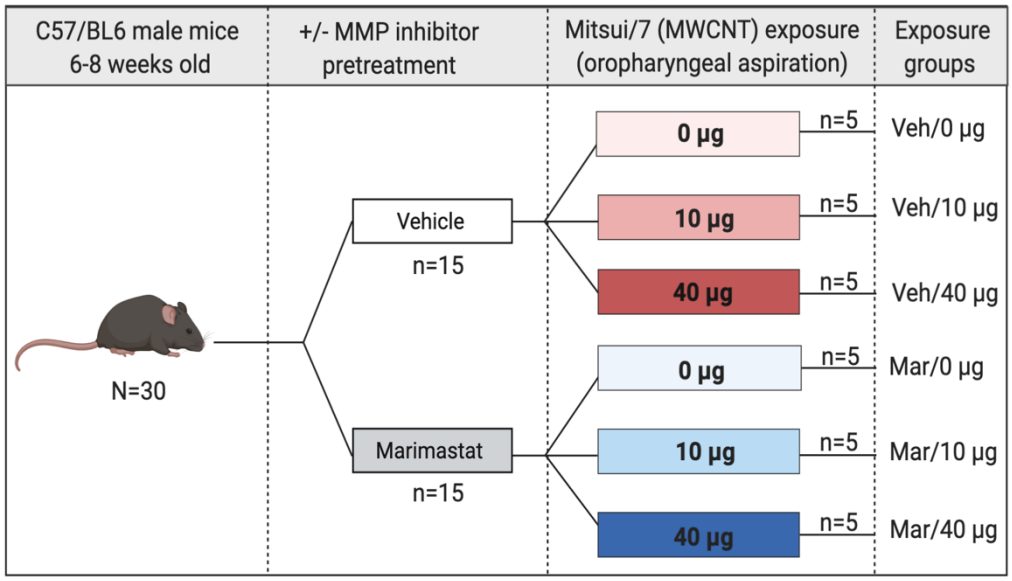

Figure 4: Aim 1.1 Experimental Design. Male C57BL/6 mice aged 6-8 weeks were randomized into 6 groups of 5 mice each. Animals were weighed and dosed with 10mg/kg body weight Marimastat via oropharyngeal aspiration 1 hour prior to dosing with dispersion media (DM), 10µg or 40µg of MWCNT via oropharyngeal aspiration. Animals were euthanized 24-hours post MWCNT exposure and tissues collected to assess pulmonary inflammation, serum peptide profile and serum bioactivity.

nm with a length of 3.86 μm (geometric SD = 1.94). Purity was >99% carbon. Mice were euthanized at 24 h following MWCNT pulmonary dosing using isoflurane and exsanguination. At the time of euthanasia, blood and bronchoalveolar lavage fluid (BALF) were collected; blood was allowed to clot on ice and then centrifuged to collect serum. Following transcardial perfusion with ice-cold 1X PBS, lungs and heart were collected and flash frozen in liquid nitrogen to determine changes in relative mRNA or protein expression.

Pulmonary Inflammation Assessment

Bronchoalveolar Lavage Fluid (BALF) Cell Composition: Lung lavage fluid was collected by instilling 1 mL of sterile PBS and immediately withdrawing fluid twice via cannulated trachea. Total cell count was determined using a standard hemocytometer. Differential BALF cell counts were assessed by centrifuging 200 μL of BALF onto a cytospin slide preparation and quantified using HEMA3 stain (Protocol, Thermo Fisher Scientific).

BALF Cytokine Levels: MWCNT-induced cytokine protein changes in BALF were determined using the electrochemiluminescent Meso Scale Discovery MULTI-SPOT V-PLEX® Cytokine Assay System Proinflammatory Panel 1 (mouse) kit (K15048D - Meso Scale Diagnostics LLC, Rockville, MD) according to manufacturer's instructions. Briefly, BALF was collected by lavaging lungs of euthanized DM control and MWCNT-exposed mice with ice-cold 1X PBS. Cell fractions were removed by centrifugation and 50 μl/well of the supernatant were loaded onto sample plates pre-coated with a capture antibodies for the following cytokines: IFN-γ (interferon gamma), IL-10 (interleukin 10), IL-12p70 (interleukin 12 active heterodimer), IL-1β (interleukin 1 beta), IL-2 (interleukin 2), IL-4 (interleukin 4), IL-5 (interleukin 5), IL-6 (interleukin 6), KC/GRO (CXCL1, chemokine C-X-C motif ligand 1), and TNF-α (tumor necrosis factor alpha). Plates were incubated with gentle shaking for 2 h at RT. Plates were washed 3X with buffer containing 1X PBS and 0.05% Tween 20. Detection antibody was added to each well and allowed to react for 1 h at RT. Plates were washed as above and Read Buffer was added to each well. Plates were analyzed on an MSD QuickPlex SQ 120 instrument (MSD, AI0AA-0); Discovery Workbench (v. 4.0) software calculated cytokine concentrations using a linear regression analysis of the standard curve. All concentrations were normalized to total BALF protein, determined using a standard Bradford protein assay.

Whole Lung Inflammatory Gene Expression: RNA was isolated from flash frozen lung tissue using the RNeasy Mini Kit (QIAGEN, Germantown, MD), and reverse transcribed prior to gene expression analyses via quantitative real-time PCR (qPCR) in a 96-well format. Expression of mouse *Ccl2* (Mm00441242_m1), *Icam1* (Mm00516023_m1), *Il6* (Mm00446190-m1), *Tnfa* (Mm00443258_m1), *Tgfb* (Mm01178820_m1), and *Vcam1* (Mm01320970_m1) (Applied Biosystems, Foster City, CA) were measured using the TaqmanR Gene Expression protocol (ThermoScientific, Waltham, MA) following the manufacturer's instructions. Relative gene expression normalized to the housekeeping gene TATA-Box Binding Protein (*tbp*; Mm00446973_m1) was determined using the $2^{-\Delta\Delta CT}$ method for all samples with threshold cycle values (CT) under 35. Results are expressed as fold change.

Serum Peptidomic Mass Spectrometry

Endogenous peptidomic analysis was performed on mouse serum specimens collected following treatment with 0 μg, 10 μg or 40 μg of MWCNT, with and without Marimastat pretreatment (n=5/grp) using previously described methodology. [56] Briefly, 40 μL of serum was pre-filtered using a 0.22 μm Ultrafree-MC unit (Millipore) using the manufacturer's instructions. Samples were reduced in 18 mM tris(2-carboxyethyl)phosphine (TCEP) and denatured in 20% acetonitrile and thiol-protection with 30 mM iodoacetamide to dissociate peptide content from carrier moieties. Samples were size-fractionated using YM-30 MicroCon units (Millipore) per manufacturer's instructions with an effective mass cutoff of approximately 8 kDa. The retentate was further dissociated by acidification with 0.4% formic acid to disrupt ionic interactions and re-spun through the YM-30 to combine filtrates. The filtrate was de-salted, de-lipidated and concentrated by solid-phase extraction using a Symmetry C18 reversed-phase column (Waters). The enriched peptide samples (4 μL) were then gradient separated (6% to 44% acetonitrile in 0.1% formic acid) using a 150 mm x 75 μm HSS T3 reversed-phase capillary column on a NanoAcquity UPLC online with a Waters Synapt G2-Si tandem mass spectrometer (Waters). The instrument was operated in UDMSe mode[57] for data-independent analysis at 25000 resolving power and the quadrupole optimized to exclude small-molecule ions below 500 m/z. UDMSe data were peak picked 150 and 50 ion count thresholds for low-energy and high-energy scans, respectively, and deisotoped using PLGS software v3.0.3 (waters). Resultant ion tables were aligned across replicates by retention time (±1.5 min), drift time (±5 bins) and accurate mass (±12 ppm) measures with EndogeSeq. Precursor ion tables were then filtered to retain only highly-reproducible measures (n≥4/grp), with matched product ions (±24 ppm)

retained if present in at least two biological replicates. Left censored data were imputed by random-generated value sets centered at the limit of quantification accounting for the datasets median ion variance and missingness across replicates [58]. The compiled peptidomic data were median centered and log_2 transformed before testing for effects of MWCNT exposure, Marimastat pretreatment or their interaction using 2-way ANOVA and Benjamini-Hochberg multiple-measures correction in Multiple Experiment Viewer (mev.tm4.org), set to a 5% false discovery rate.

Serum Cumulative Inflammatory Potential Assay

Mouse cerebrovascular endothelial cells (mCEC) were obtained from a commercial vendor (Cell Biologics, Chicago, IL) and maintained according to manufacturer's recommendations at 37ºC and 5% CO_2 with complete endothelial cell medium supplemented with 5% fetal bovine serum. All experiments were conducted with cells between passages 3 and 8. To determine the serum cumulative inflammatory potential of MWCNT exposure, mCECs were treated with serum isolated from exposed or control C57BL/6 male mice as previously described [59,60]. Briefly, mCECs were serum starved overnight then incubated in FBS-free culture media supplemented at a final concentration of 5% v/v serum from dispersion media control (0 µg; DM), 10 µg, or 40 µg MWCNT exposed mice for 4 h. RNA was isolated from treated mCECs using the RNeasy Mini Kit (QIAGEN, Germantown, MD), and reverse transcribed prior to gene expression analyses via quantitative real-time PCR (qPCR). Furthermore, in an additional permutation, cells were pretreated with either non-immune IgG or a CD36 neutralizing antibody to test the role of CD36 in mediating responses (quantity of CD36 ab, timing?). Expression of mouse *Ccl2* (Mm00441242_m1), *Icam1* (Mm00516023_m1), *Il6* (Mm00446190-m1), *Tnfa* (Mm00443258_m1), *Tgfb* (Mm01178820_m1)*, Vcam1* (Mm01320970_m1) and *Vegfα* (Mm01281449_m1) (Applied Biosystems, Foster City, CA) were measured using the TaqmanR Gene Expression protocol (ThermoScientific, Waltham, MA) following the manufacturer's instructions. Relative gene expression, normalized to the housekeeping gene *tbp* (TATA-Box Binding Protein; Mm00446973_m1), was determined using the $2^{-\Delta\Delta CT}$ method for all samples with threshold cycle values (CT) under 35 (cite). Results are expressed as fold change.

Monolayer Impedence-Based Quantification of Cell Growth and Barrier Integrity

Electric Cell-substrate Impedance Sensing (ECIS; Applied Biophysics) system was used to quantify the barrier integrity of mCECs in a monolayer following exposure to serum from DM- or MWCNT-exposed mice.[60] Briefly, cells were grown in special culture chambers on top of opposing circular gold electrode array. A constant small alternating current was applied between the electrodes and the changes in electrical potential across the monolayer was measured and resistance changes were recorded every minute. Cells were allowed to come to confluence, then serum-starved overnight. The following day, complete culture media lacking FBS was supplemented with MWCNT or DM serum at a concentration of 5% v/v. The cells were then incubated at 37ºC and 5% CO_2 for 4 hours. Baseline serum-response readings were captured over this period and then an electric current was passed through the gold electrode to disrupt the confluent cell layer ("wounding"). The rate of recovery from wounding was evaluated by assessing the length of time for resistance readings to return to the pre-wounding baselines.

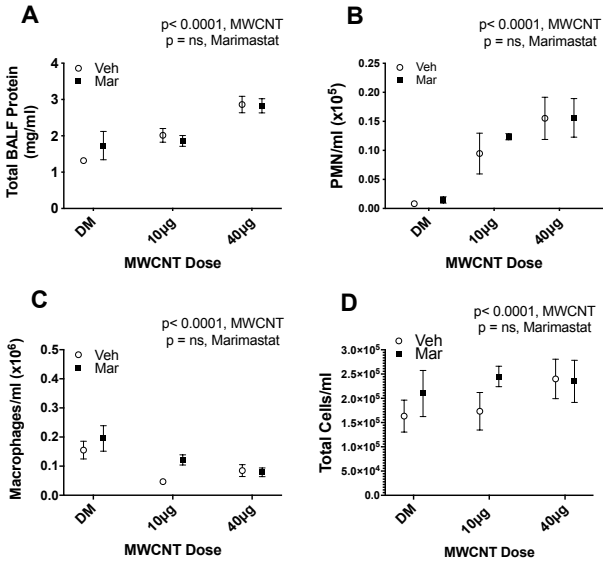

Figure 5. MWCNT-mediated lung inflammation. Bronchoalveolar lavage fluid (BALF) total protein and infiltrating inflammatory cell count. MWCNT exposure-induced pulmonary inflammation was not altered by MMP blockade. **(A)** Total lavage fluid protein concentration assessed via Bradford protein assay. MWCNT-exposure increased BALF total protein in a dose-dependent manner when compared with controls. **(B and C)** BALF white blood cell differentials; Polymorphonuclear neutrophils (PMN) was significantly increased by MWCNT exposure at both low and high doses; Macrophages in BALF was decreased in MWCNT treated cells. **(D)** Total BALF cells were unchanged by MWCNT exposure. P-values based on 2-way ANOVA presented for each figure. N=4-5 per group. Data presented are means ± SEM.

Statistics

All statistics were conducted in GraphPad Prism (v9.0). Data were either assessed as a 2-way ANOVA, considering MWCNT and Marimiastat treatments as the 2 factors. For serum cumulative inflammatory potential assays, a 3-way ANOVA was conducted, including the use of IgG vs CD36 antibody treatment.

RESULTS

Lung Inflammatory Activation

BALF Inflammatory Cell Profile: MWCNT-exposure drives lung inflammation via mechanisms that are predominantly independent of MMP activation. MWCNT-induced pulmonary inflammation was assessed by total protein and differential cell counts of bronchoalveolar lavage fluid (BALF) collected from DM- and Marimastat-pretreated, MWCNT-exposed mice. MWCNT induced a significant dose-dependent increase in total BALF total protein, consistent with previous studies (**Figure 5A**). Accompanying this increase was a significant influx of polymorphonuclear neutrophils (**Figure 5B**). A modest reduction of macrophages was also observed (**Figure 5C**), but overall the total cell counts were stable if not increasing in the MWCNT-exposed mice (**Figure 5D**). These indicators of lung inflammatory activation occurred via mechanisms independent of MMP activity as Marimastat treatment did not alter MWCNT-mediated responses.

BALF Cytokine Expression

To further investigate the elevation of proteins, we assessed cytokines in the BALF using a multiplex electrochemiluminescence assay (MesoScale Discovery). Most conventional inflammatory cytokines (IL-1β, IL-2, IL-4, IL-6, KC-GRO, and TNFα) (**Figure 6**) displayed elevation in a dose-dependent manner following MWCNT treatment and were not affected by MMP inhibition. Some cytokines remained unchanged by MWCNT treatment or MMP inhibition (IFNγ, IL-10, and IL12p70). Interestingly, IL-5 did show inhibition of MWCNT-mediated induction by marimistat and IL-12p70 was just outside of significance (p=0.054) for an MMP inhibition effect (**Figure 6**). These outcomes suggest that certain cytokine induction may be downstream of inflammatory MMP induction, though most are not.

Whole Lung Cytokine Gene Expression

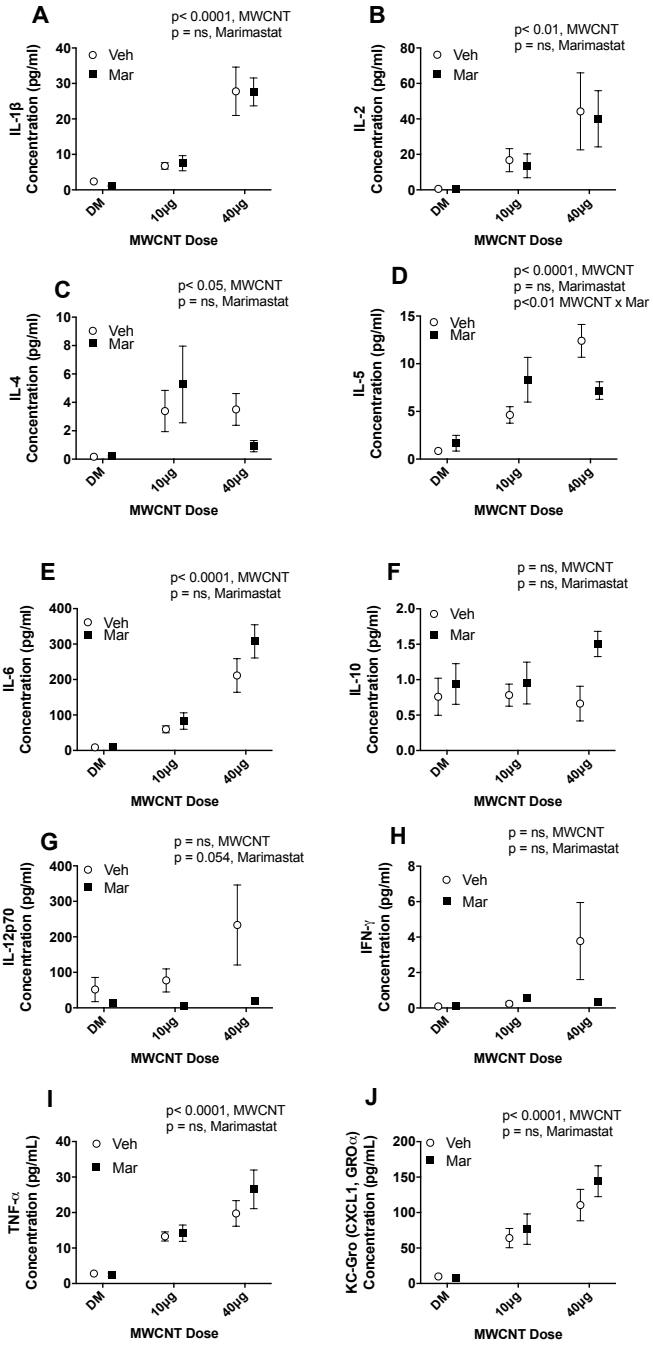

Figure 6. MWCNT-mediated pulmonary cytokine activation. Bronchoalveolar lavage fluid (BALF) inflammatory cytokine profile assessed via Meso Scale Discovery multiplex cytokine assay. MWCNT-exposure increased BALF cytokine protein expression in a dose-dependent manner which was not significantly altered by MMP blockade for most cytokines. Protein expression for **(A)** IL-1β; **(B)** IL-2; **(C)** IL-4; **(D)** IL-5; **(E)** IL-6; **(F)** IL-10; **(G)** IL12p70; **(H)** IFN-γ; **(I)** TNF-α; and **(J)** KC-Gro/CXCL1/GROα. P-values based on 2-way ANOVA presented for each figure. N=4-6 per group. Data presented are means ± SEM.

Finally, we examined pulmonary inflammation in terms of transcriptional changes from lung homogenates. Most cytokine gene expression trends were consistent with protein levels in BALF, with IL-6, IL-1β, and TNFα (**Figure 7**) increasing in a dose-dependent manner with MWCNT treatment, and this increase was unaltered by MMP inhibition. We additionally tested ICAM1 and VCAM1 mRNA (**Figure 7**) expression as markers of vascular injury and both showed non-significant elevation in the lung homogenate following MWCNT exposure. MMP inhibition failed to alter transcriptional changes in the lung.

Serum Peptide Characterization

Consistent with recent studies of serum peptidomic changes after MWCNT exposure[56], both the 10 μg and 40 μg doses of MWCNT led to substantial generation of numerous circulating peptide fragments. The different doses caused significant elevation of a cluster of common peptides (**Figure 8**, lower region of heatmap), and each dose caused the induction of specific peptides unique to that dose (**Figure 8**, upper and middle regions of heatmap). Importantly, pulmonary Marimastat pretreatment almost completely abolished those induced peptides, suggesting that they arise from pulmonary MMP activation following MWCNT exposure.

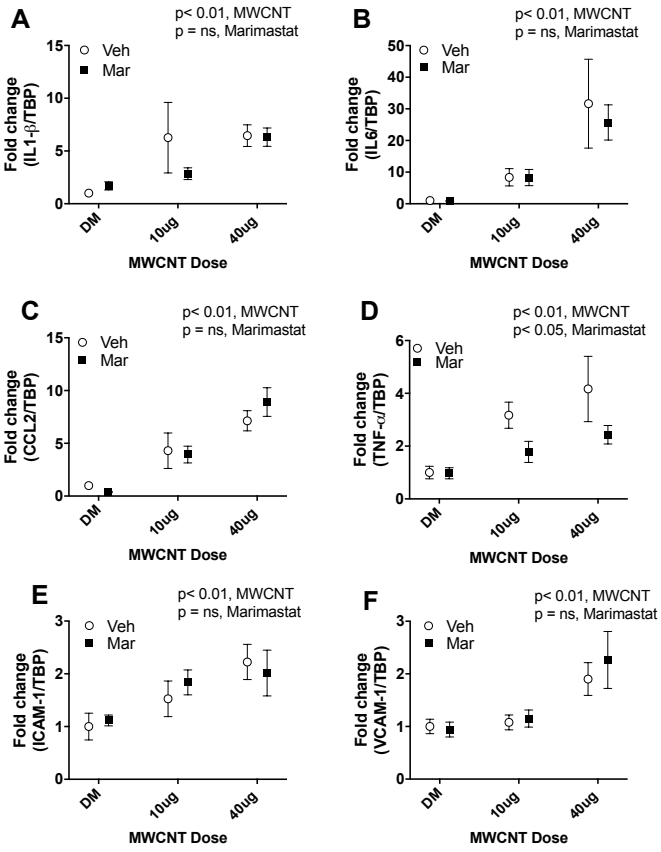

Figure 7. Lung qPCR: Lung cytokine gene expression profile. Gene expression for **(A)** IL1-β; **(B)** IL-6; **(C)** CCL2; **(D)** TNF-α; **(F)** ICAM-1; and **(G)** VCAM-1 are shown. MWCNT generally induced dose-dependent increases in all markers, while MMP inhibition by Marimistat had no effect, except for TNF-a. P-values based on 2-way ANOVA presented for each figure. N=5-6 per group. Data presented are means ± SEM

Serum Cumulative Inflammatory Potential Assessment

To determine the inflammatory bioactivity of the serum following MWCNT dosing and Marimastat pretreatment, serum (5% v/v) from control and exposed mice was added to confluent mCECs for 4h. qPCR assessment of canonical inflammatory response genes from the mCECs revealed significant induction of Ccl2, Vcam1, CD36, and Icam1 (**Figure 9**) by serum from MWCNT-treated mice. Additionally, since previous studies showed a potential role for CD36 in mediating serum-induced vascular reactivity changes[7], we assessed its

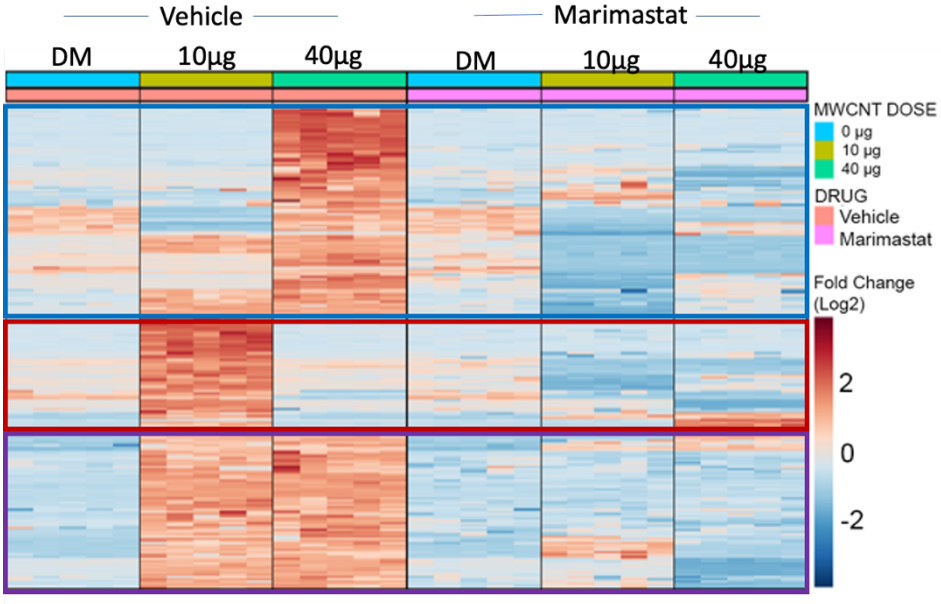

Figure 8. Serum peptidomics heatmap. MWCNT-induced peptide serum profile changes assessed via mass spectrometry. MWCNT exposure increased total serum peptide composition in a differential dose-dependent manner. Each grouping (DM, 10, 40 μg) consists of data from 5 subjects. **Blue box**: Serum peptide composition induced exclusively by high dose (40μg) MWCNT exposure; **Red box:** Serum peptide composition induced by exclusively low dose (10μg) MWCNT exposure; **Purple box:** Serum peptide composition induced by both low and high dose MWCNT exposure. These findings indicate an MMP-mediated mechanism of action for pulmonary MWCNT-induced circulating peptides.

role *in vitro* using an anti-CD36 antibody or a non-immune IgG control pretreatment to test whether serum-induced responses could be attributed to scavenger receptor signaling. A three-way ANOVA analyses was therefore used to test independent or interactive roles of MWCNT, Marimastat, and CD36.

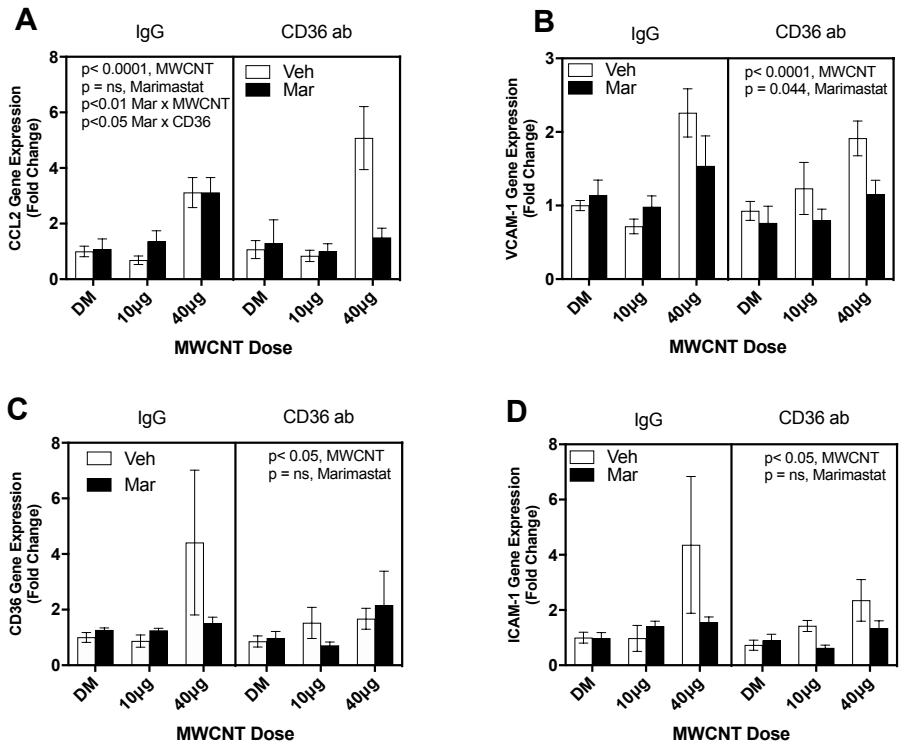

Figure 9. MWCNT *in* vitro serum bioactivity evaluation. Contribution of CD36 to MWCNT-mediated Serum Cumulative Inflammatory Potential (SCIP) in mouse cerebrovascular endothelial cells (mCEC). mCEC in monolayer were treated with a CD36 blocking antibody (ab) or IgG control antibody, followed by 5% v/v serum from C57BL/6 mice exposed to MWCNT in conjunction with MMP blockade. qPCR performed on cell isolates to access cytokine gene expression changes for **(A)** Ccl2; **(B)** Vcam1 **(C)** CD36; and **(D)** Icam1. P-values based on 2-way ANOVA presented for each figure. 3-way ANOVA revealed significant contribution of MWCNT for all genese. Marimastat inhibited Vcam1 expression and, interacting with CD36 antibody, inhibited Ccl2. Similar nonsignificant trends were evident for CD36 and Icam1. N=4-5 per group. Data presented are means ± SEM.

MWCNT serum exposure resulted in significant upregulation of endothelial CCL2 and Vcam1 mRNA ($p < 0.0001$) in both IgG and CD36 antibody treatment groups. Ccl2 expresion was reduced in the CD36 ab + Marimastat group, based on significant interaction terms in the 3-way ANOVA ($p<0.05$). Vcam1 expression, also significantly induced ($p < 0.0001$) by MWCNT-treated serum, was not upregulated in serum from mice treated with MWCNT and Marimastat ($p = 0.044$). CD36 and Icam1 gene expression were both increased by serum from MWCNT-treated mice ($p<0.05$), but neither Marimastat nor CD36 antibodies altered this outcome.

Functional Assessment of MWCNT-mediated Serum Bioactivity

To assess the functional consequences of the MWCNT-generated serum bioactivity, serum from exposed mice was used to assess endothelial barrier integrity changes in an endothelial monolayer using the ECIS assay (**Figure 10**). Following treatment with serum from control (DM, Vehicle) mice, mCEC monolayer resistance increased in a biphasic manner, to 110% of baseline after 1h and then again to 135% of baseline after 15h. Treatment with serum from MWCNT/Vehicle-treated mice reduced barrier integrity acutely and continuously for the 20h assay. MMP blockade with Marimastat abrogated the MWCNT serum-induced barrier disruption, although recovery was not fully back to control levels. Interestingly, Marimastat independently of MWCNT exposure also decreased barrier integrity in the endothelial monolayer; however, this decrease was not as severe as MWCNT serum.

Aim 1.2. Transgenic deficient mouse models and MWCNT. To more specifically probe the role of MMPs in drive circulating bioactivity, we assessed how MMP9 activity influenced: 1) the release of peptide byproducts into the circulation; 2) whether this is an immediate acute response or that potentially bioactive peptides continue to be released following MWCNT exposure given that the material is not readily cleared from the lung; 3) whether repeated exposure enhances the release of bioactive peptides or enhances compensatory responses to decrease the release.

To address those questions, we processed serum for peptidomic mass spectrometric analysis from WT and MMP9^{KO} mice that were treated A) with a high 40 µg MWCNT dose and allowed to recovery for 4 weeks or B) with a moderate 10 µg MWCNT dose once per week of a 4 week period. In this study, we reproducibly measured 4,853 molecules within the peptide-enriched serum fraction. Of these, 87% (4,243) were found to be significantly responsive to MWCNT exposure in WT animals (**Figure 11**). This was a more extensive response than observed previously at only 4-h after treatment, when only 49% of measures were found responsive to

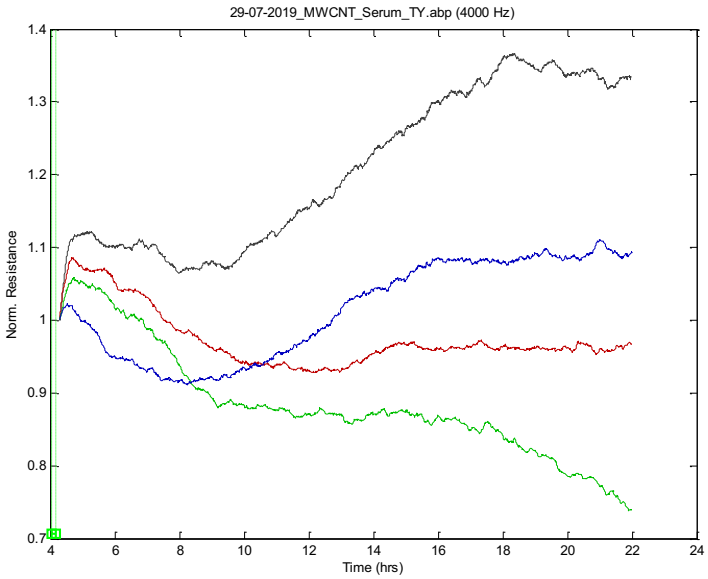

Figure 10. Evaluation of the role of MWCNT-exposure generated serum bioactivity on endothelial barrier integrity. Resistance changes across cellular monolayer over the course of 24 hrs. Mouse cerebrovascular endothelial cells (MCEC) grown in a confluent monolayer were treated with serum from C57BL/6 mice exposed to MWCNT in conjunction with Marimastat. Barrier integrity changes were accessed via Electric Cell-substrate Impedance Sensing (ECIS). Serum from 40µg MWCNT/Veh exposure decreased barrier integrity compared to DM/Veh. MMP blockade partially recovered barrier integrity in MWCNT exposed group (40µg MWCNT/Mar) although not back to DM/Veh control serum levels. MMP blockade alone (40µg MWCNT/Veh) also reduced endothelial barrier integrity although not to levels observed with MWCNT serum exposure. Shown are two replicates of three pooled serum samples per group.

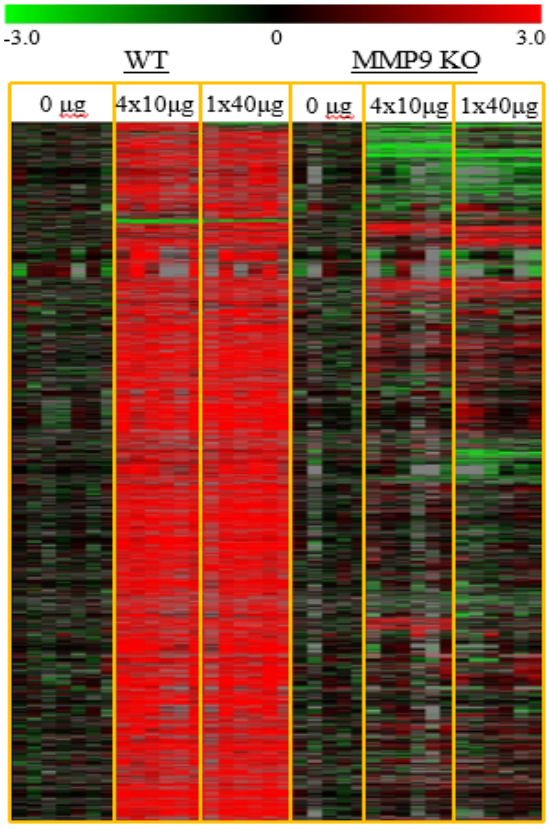

Figure 11. Repeated low-dose or a single high-dose MWCNT pulmonary insult produces a pronounced release of peptide products into circulation, a response that is significantly diminished in MMP-9 knockout (KO) animals. Heatmap of the MWCNT-responsive serum peptidome in wildtype (WT) animals, and the near loss of those responses in MMP9 KO animals. n=5-7/grp; FDR=5%.

treatment, suggesting that peptide byproduct release progresses with time. The peptidomic response to MWCNT was further shifted near exclusively to the introduction of novel peptides into circulation, with hardly any decrease with treatment, which is in contrast to the 4h acute time point where 15% of measures were found to decrease with treatment. Results were largely consistent whether after 4 repeated weekly doses at the lower 10 µg amount (4x10µg) or 4 weeks after a single higher 40 µg dose of MWCNT (1x40µg).

In stark contrast, the release of peptide byproducts into the circulation was mostly absent in MMP-9 KO animals treated with MWCNT. Only 12% (508) of the 4,243 MWCNT-responsive peptide measures remained significantly altered in the absence of MMP-9. Further, the magnitude in response among that 12% was generally lessened in comparison to WT, with the results mostly consistent for the 4x10µg ad 1x40µg 4-week treatment groups. These results substantiate a significant role for MMP-9 in producing the long-term peptide release into the circulation. Other matrix proteases may likely explain the remaining modest response in MMP-9 KO serum. Furthermore, our results cannot rule out a pivotal role for other matrix protease in peptide byproduct release that may be downstream of MMP-9 activation, since MMP-9 is known to regulate the activation of other proteases. Yet these results place proteolytic processing directly in line with the production of molecules isolated within our enriched-peptide fraction that itself has demonstrated bioactivity, as we have published.[8]

AIM 1 Summary: Thus, in this Aim 1 study we demonstrated that 1) lung MMP activity does not play a significant role in mediating MWCNT-induced pulmonary inflammation; 2) MWCNT-induced circulating peptides and inflammatory bioactivity are generated, in large part, by pulmonary MMP activity; and 3) bioactivity of serum from MWCNT-exposed mice disrupts the endothelial barrier (**Figure 12**). The biological pathways underlying nanomaterial-mediated respiratory pathology seem, at least on the surface, to mirror

those of air pollution exposures: activation of inflammatory signaling, oxidative stress, enzyme activation and ECM remodeling [12,14,61]. However the impact of MWCNT inhalation exposure outside the lung, while evident in many studies, remains an incompletely understood phenomenon. The present study therefore suggests that

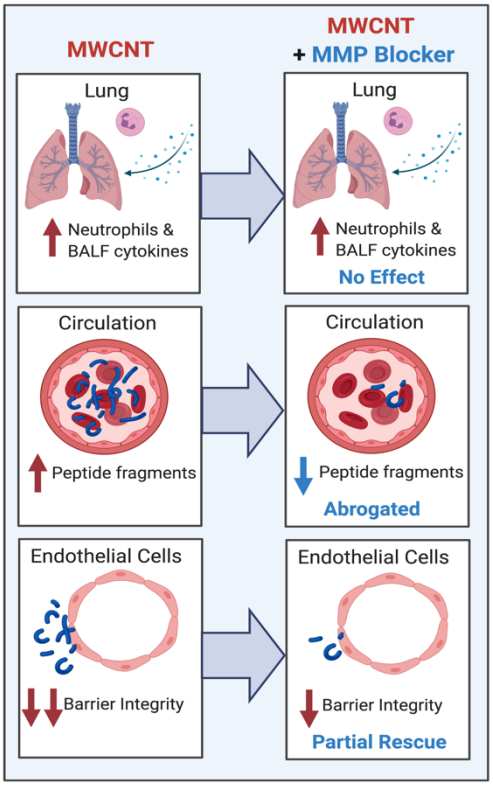

Figure 12. Aim 1 Graphical Summary: Consequences of MWCNT oropharyngeal exposure in C57BL/6 mice. MWCNT induced pulmonary inflammatory activation as evidenced by increased neutrophilia and dose-dependent cytokine BALF profile and whole lung gene expression. MMP blockade did not play a role in the observed pulmonary findings. However, MMP activity was shown in induce serum peptide profile changes in a dose-dependent differential manner. Administration of broad-spectrum MMP inhibitor Marimastat abrogated these serum changes and return peptide profiles to near unexposed levels. The systemic consequences of these serum changes were evaluated *in vitro.* Serum from MWCNT exposed mice decreased endothelial barrier integrity as assessed via ECIS. Marimastat blockade of MMP activity in the lung resulted in serum with considerably less potential for endothelial barrier disruption. These findings provide a mechanism for MWCNT action in the lung and starts to elucidate the systemic consequences of inhalation exposures to MWCNT. Additionally, serum findings provide a base for the exploration of MWCNT exposure and pathological systemic consequences, as well as the identification of biomarkers of both.

many downstream, extrapulmonary effects of inhaled particulates, such as MWCNT, may be related to pulmonary MMP activation and spillover of fragmented peptides or matrikines into the circulation, which in turn drive endothelial inflammatory responses and impair barrier function.

AIM 2: Assess pulmonary ENM-induced neurovascular impacts and "serome" access into the central nervous system (CNS).

As mentioned, inhalation exposure has been found to induce neurological change; yet, the mechanism of systemic transduction to the brain remains unknown. Pulmonary response to inhaled pollutants induces circulating ("serome") factors, which we have shown to impact cardiovascular function. [7,8,15] Here we aim to test our hypothesis that MWCNT-lung reactivity releases byproducts into the circulation that then result in neurovascular dysfunction and blood-CSF-barrier permeability as a novel CNS-access mechanism (**Figure 13A**).

This aim evaluated the transmissivity of lung-derived seromic factors across the blood-CSF choroid barrier. We also engineered new software specially designed to overcome challenges in identifying molecular byproducts endogenous to biofluids ("EndogeSeq"), such as induced with MWCNT-pulmonary exposure. Molecular identity is critical to decoding the origins of and bioactivation mechanisms transduced by induced circulating factors, which we believe propels forward our understanding of how pulmonary exposures initiate systemic health impacts. In addition, we see that identification of specific byproducts transforms our perception of traditional biomarker investigations and potentially facilitate future biomonitoring of worker exposure.

Serome Transduction Mechanism for MWCNT Impacts in the CNS. Liao et al. recently found that worker's exposure to ENM induces cognitive deficits,[62] suggesting analogous neurlogical consequences as seen with air pollution. [19] In explanation, the prevailing position would have the particulate itself translocating from the lung, into the blood, and across the BBB (see [63]). Evidence supports this mechanism for metal oxide particulates, e.g., manganese and titanium oxides. [38,64] However, for non-metalic ENMs, the toxicology reveals that less than 0.001% of fibers actually make it into the brain,[41] suggesting an alternative transduction mechanism. We turned to a new data-independent, unbiased mass spectrometric approach in our laboratory to

investigate ozone exposure-induced changes within the blood given the compelling evidence for cardiovascular and other organ bioactivation.[58] We found that exposure resulted in over a thousand molecular changes, in particular the release of peptide byproducts into the circulation. For example, ozone-inhalation increased the fibrinopeptide in **Figure 13B** 2- to 3-fold (more so at the lower, clinically relevant 0.3 ppm dose). Interestingly, fibrinopeptide is known to accelerate neurovascular damage and increase permiability into the CNS. [65] Also of note, the n- and c-terminals of the fibrinopeptide correspond to known MMP 8/12 and MMP 3/7 cleavage motifs, respectively. Yet, this fibrinopeptide was but one member of an enriched group of peptide byproducts (chi-square; $p=4.37e^{-5}$) from complement cascade proteins (**Figure 13C**) involved in inflammatory processes. Also enriched were peptides from focal adhesion proteins, known to shed bioactive signaling fragments, and found impacted in expression per our earlier qPCR findings. [2] In all, we identified over 1,500 ozone-responsive factors within the serum of exposed animals (ozone "serome"). When we then assessed the seromic response to MWCNT treatment, we found a similar magnitude of responsive biomolecules to that observed with ozone exposure, compelling the present hypothesis that MWCNT-reactivity within the lung releases byproducts into circulation (**Figure 13A**) to impact the neurovasculature and gain access to the CNS.

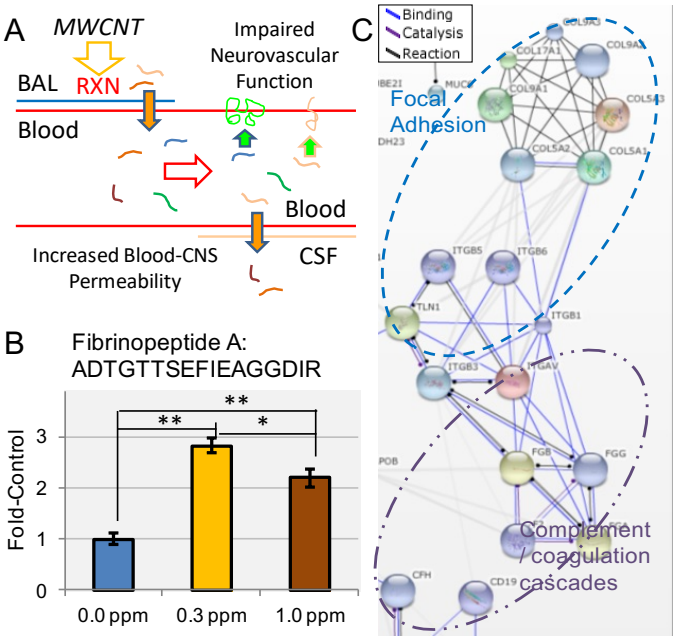

Figure 13. Induced circulating factors with pulmonary xenobiotic exposure. (A) Posited mechanism by which extrapulmonary effects of MWCNT is transduced by moderate-sized byproducts within the blood, such as (B) fibrinopeptides that are known to impair neurovascular function to permit CNS entry. (C) Pulmonary-induced serum peptides are linked with focal adhesion and compliment cascade processes of relevance to systemic vascular and inflammatory impacts.

AIM 2.1. Transmission of MWCNT-induced seromic factors from the lung to blood to CNS.

MATERIALS AND METHODS

Animal model and sample collection

Specific pathogen-free male C57BL/6 J mice (Jackson Laboratory) were housed in an Association for Assessment and Accreditation of Lab Animal Care International approved animal facility at the National Institute for Occupational Safety and Health. Animal care and use procedures were conducted in accordance with the "Public Health Service Policy on Humane Care and Use of Laboratory Animals" and the "Guide for the Care and Use of Laboratory Animals". Food and water were provided ad libitum in ventilated cages in a temperature and humidity controlled environment with a 12-h light/dark cycle. Eight-week-old C57BL/6 J mice, were exposed to MWCNT (Mitsui-7, Hodogaya, Japan, > 99% carbon purity) via oropharyngeal aspiration at 0 µg, 10 µg, or 40 µg (n = 6 per group).[13] The MWCNT material was found negative for LPS using a ToxinSensor Chromagenic LAL Assay Kit (GenScript). MWCNT was prepared in dispersion media (DM) consisting of mouse serum albumin (0.6 mg/mL) and 1,2-dipalmitoyl-sn-glycero-3-phosphocholine (10 µg/mL). The average MWCNT was 49 nm in diameter and 3.86 µm in length (geometric SD = 1.94).[13] Matched serum and bronchoalveolar lavage fluid (BALF) were collected 4 h following aspiration under anesthesia as previously described.[9] The 4 h collection time was selected here to remain consistent with prior published work using this model that demonstrated in vivo and ex vivo vascular outcomes of MWCNT exposure. [7-9]

Endogenous peptide enrichment and mass spectrometry

Matched serum and BALF were processed via the same protocol with proportional adjustment for their different starting volumes of 40 µl for serum and 120 µl for BALF given pilot results showing a 3–4-fold difference in peptide concentration. Biofluids were clarified by centrifugation through a 0.22 µm Ultrafree-MC filtration unit (EMDMillipore, Billerica, MA) using manufacturer instructions. Samples were then denatured for 30 min at room temperature (18 mM TCEP final concentration) in presence of HALT inhibitor cocktail (Thermo Scientific, Rockford, IL) and 20% final concentration acetonitrile. Reduced thiols were acetylated with iodoacetamide at a final concentration 30 mM with a 30 min incubation in the dark at room temperature. Samples were transferred

onto pre-cleaned MicroCon YM-30 centrifugal filter units (EMDMillipore) and centrifuged per manufacturer instructions to isolate endogenous peptides from proteins and vesicles. The retentate was acidified using 0.4% formic acid to further disrupt peptide binding with collection via a second centrifugation of the filter unit. Resultant peptide-enriched filtrates were loaded (4.5 µl) onto a Symmetry C18 reversed-phase column to remove lipids, reagents and salts. The peptidomic fraction for each serum sample was separated using a NanoAcquity UPLC (Waters, Milford, Massachusetts) online with a Waters Synapt G2 tandem mass spectrometer as described previously.[46] Briefly, the peptide fraction was separated on a 150 mm × 75 µm HSS T3 reversed-phase capillary column at 55 °C for 65 min with an elution gradient from 6 to 44% acetonitrile in water (0.1% formic-acid modified). The Synapt G2 was operated with ion mobility enabled data-independent acquisition (UDMSe) at a nominal 25,000 resolving power.[57] The precursor mass range was optimized between 400 and 1800 m/z to account for larger endogenous peptides.

Mass spectral data processing and analysis

Spectra processing was performed employing PLGS v3.0.2 software (Waters) as described previously.[46] Ion tables for matched BALF and serum samples were clustered together in matching retention time (±2 min), drift time (±4 bins), and ion mass (±12 ppm) with EndogeSeq. Results were filtered to include only reproducible ion events observed in two-thirds or more of the biological replicates. For ions categorically falling below the limit of detection across all replicates in a group, a randomly generated set of values was imputed with a mean and coefficient of variance equating the limit of quantification observed across that group's replicates.[58] The clustered ion matrix was then median centered and log2 transformed. Fold changes were calculated relative to the mean for the DM (0 µg MWCNT) vehicle control group. Ions found significantly responsive to MWCNT treatment in serum and BALF biofluids were assessed to identify an overlap with known MMP and ADAM/TS substrates using the MEROPS database[66] and with proteins with predicted secretory domains using the SignalP algorithm.[67] The search workflow included no enzyme specificity for assessing endogenous measures with precursor and product ion match limits of 6 and 12 ppm, respectively. A random-decoy database method was used to control false peptide identification to under a 10% false discovery rate (FDR) using the peptide score, which is highly dependable given the high-resolution tandem mass spectral measures.[68] Matched product ion spectra were visualized using mMass software.[69] Identified peptides were further characterized using the enrichment analysis tools in ToppGene[70] and STRING[71] online software suites, with results adjusted to a 5% FDR.

Matrix protease expression analysis in the lung

Four hours after DM vehicle, 10 µg or 40 µg MWCNT oropharyngeal aspiration, mice were euthanized and their left lung lobe was ligated while bronchoalveolar lavage was performed on the right lung lobe. BALF and whole lung homogenates were assessed for MMP9 protein levels using an enzyme linked immunosorbent assays according to manufacturer's instructions (Boster, Pleasanton, CA).

Broader matrix protease and tissue inhibitors of metalloproteinases were assessed in an existing lung tissue microarray dataset. Animals were exposed for 4 h to Mitsui-7 MWCNT by inhalation to deposit approximately 4 µg or 40 µg as previously described.[72] Lung tissue was assessed for gene expression on an Illumina platform as previously described.[72] In summary, 375 ng of RNA was used to generate cRNA for hybridization to the arrays. MouseRef-8 BeadChips were analyzed on an Illumina BeadStation 500G reader (Illumina, San Diego, CA). Data processing and differential expression analysis was performed using the Limma R package as described elsewhere.[53]

Serum cumulative inflammatory potential assay

Mouse endothelial cells were obtained from a commercial vendor (Cell Biologics, Chicago, IL) and maintained according to manufacturer's recommendations at 37 °C and 5% CO2 with complete endothelial cell medium supplemented with 6% fetal bovine serum. All experiments were performed between passages 3 and 8. Assays were batched by exposure to enhance consistency and comparability across samples. Obtained endothelial cells were treated 4 h in vitro with the enriched peptide fraction from MWCNT exposed or DM control mouse serum to assess the serum cumulative inflammatory potential as previously published.[60] In short, endothelial cells were serum starved overnight and incubated with culture media supplemented at a final concentration of 5% subject peptide fraction for 4 h and harvested. RNA was isolated using the RNeasy Mini Kit (QIAGEN, Germantown, MD) and reverse transcribed prior to quantitative real-time PCR. Expression of interleukin 6 (Il6), C-C motif chemokine ligand 2 (Ccl2), C-C motif chemokine ligand 5 (Ccl5), vascular cell adhesion molecule 1 (Vcam1), intracellular adhesion molecule 1 (Icam1), tumor necrosis factor alpha (Tnfa),

and transforming growth factor beta (Tgfb) (Applied Biosystems, Foster City, CA) were measured using the TaqmanR Gene Expression protocol (ThermoScientific, Waltham, MA) following the manufacturer's instructions. Relative gene expression normalized to the endogenous control TATA-Box Binding Protein gene was analyzed using the 2−ΔΔCT method.

Myography vascular function assay

Analysis was performed as described previously.[7] Briefly, 2 mm segments of thoracic aorta rings were isolated from naïve C57BL/6 J mice, cleaned of connective tissue and mounted in a 4-chamber multi-wire myograph (610 M; Danish Myo Technology A/S, Aarhus, Denmark) submerged within solutions continuously maintained at 37 °C and bubbled with 21% O2–5% CO2 in nitrogen. Naïve vessels were initially submerged in physiological saline solution (PSS): 4.7 mM KCl, 119.0 mM NaCl, 25.0 mM NaHCO3, 5.5 mM glucose, 1.2 mM MgSO4, 1.2 mM KH2PO4, 0.025 mM EDTA, 2.5 mM CaCl2 and equilibrated for 30 min. Vessel viability was then tested by assessing a contractile response to a high-concentration potassium chloride physiological saline solution (KPSS): 58.9 mM KCl, 64.9 mM NaCl, 25.0 mM NaHCO3, 5.5 mM glucose, 1.2 mM MgSO4, 1.2 mM KH2PO4, 0.025 mM EDTA, 2.5 mM CaCl2. Afterwards, all vessels were washed four times with PSS and equilibrated for 30 min. The naïve vessels were then treated and allowed to stabilize ex vivo in PSS spiked at 1% (v/v) with the serum peptide fraction derived from the animals previously exposed to MWCNT or DM in vivo. Then the cumulative concentration-response curve to acetylcholine (10− 9 to 10− 4 M) was acquired using LabChart software.

Electrical wound-healing angiogenesis assay

Mouse endothelial cells were plated at 2 × 105 cells/mL and grown to confluence on a 96-well 96W1E+ electrode plate coated with 0.01% poly-L-lysine for an Electric Cell-Substrate Impedance System (ECIS; Applied Biophysics, Troy, NY).[60] Transmembrane resistive impedance was recorded continuously (4 Hz) until establishment of tight intracellular contact. Synthetic TSP402–460 peptide or the serum peptide fraction derived from the animals previously exposed to MWCNT or DM in vivo were added to each well at 5% (v/v) in media. After a 4-h in vitro treatment, a 1 mA current pulse was passed through a central electrode on each well to instigate a wound. Angiogenesis regrowth towards the center of the well was then monitored as the recovery of transmembrane impedance. The ECIS assay was preferred to the physical scratch method, as the protein coating on the wells is unperturbed by the electrical stimulus. Results were reported as the average normalized impedance per hour as a percent of baseline impedance from the hour prior to treatment.

Exosome characterization

Serum exosomes were purified first by passing through a 0.22 μm Ultrafree MC centrifugal unit to eliminated larger-sized debris and apoptotic bodies and then by size-exclusion chromatography to resolve from lipovesicles and serum protein using a 5 mm × 10 cm column packed with Sephacryl S-500 HR media (GE Bio-Sciences, Uppsala, Sweden) at 0.2 mL/min in PBS buffer. The optimized exosome fraction was collected from 3 to 5 min and assessed using a Zetasizer Nano S90 (Malvern Panalytical, Malvern, UK). Exosome samples were also fixed in 4% paraformaldehyde in 0.15 M sodium cacodylate buffer 1:1 (v:v), a 10 μl drop was placed onto parafilm and covered with a formvar-coated grid. Mounted samples were rinsed with PBS and fixed again with 1% glutaraldehyde in 0.1 M sodium cacodylate. The sample was then rinsed and negative stained using 0.5% aqueous uranyl acetate and air dried overnight. A JEOL JEM-1230 transmission electron microscope with Gatan Orius SC1000 side-mount CCD camera was used for imaging.

Gene expression analysis examined for c-Jun regulatory targets

RNA was extracted from naïve endothelial cells, as described earlier for the serum cumulative inflammatory potential assay, after a 4-h in vitro treatment with serum collected 4-h after exposing mice in vivo to DM vehicle, 10 μg, and 40 μg MWCNT. Extracted RNA was analyzed using Affymetrix GeneChip Mouse 430 2.0 arrays according to the manufacturer's protocol and as described previously.[8] Briefly, 1 μg of total RNA was used to produce biotinylated cRNA, synthesized by in vitro transcription using the GeneChip IVT Labeling Kit (Affymetrix) and fragmented and hybridized to the Affymetrix GeneChip following the chip protocol. Arrays were scanned with an Affymetrix GeneChip Scanner 3000. Results meeting a minimal log change ratio of 0.5 from DM control and $p < 0.01$ were then selected if known as c-Jun regulatory targets.

Statistical analysis

Statistical analysis of log2-transformed mass spectral peptide data was performed in MultiExperimentViewer v4.9[73] using the one-way ANOVA function and the significance level corrected for multiple peptide measures to

a 5% FDR using the Benjamini-Hochberg method.[74] Statistically responsive peptides were assessed for intensity correlation across matched serum and BALF samples using linear regression analysis in SigmaPlot v13. MMP9 ELISA and vesicular size results were assessed using one-way ANOVA with Holm-Sidak post hoc or one-way ANOVA on Ranks (for results with unequal variance) with Dunnett's post hoc testing for multiple comparisons in SigmaPlot. Serum cumulative inflammatory potential assay results were assessed by two-way ANOVA with dose and denaturing as factors and Holm-Sidak post hoc testing in SigmaPlot. Myography and ECIS results were assessed by two-way ANOVA with dose as the first factor and acetylcholine concentration (myography) or time (ECIS) as the second factor followed by Holm-Sidak post hoc testing in SigmaPlot. Microarray results were analyzed using the Limma R package in Bioconductor v3.8, which uses linear regression models for each gene assessed for the Bayes moderated t-statistic and associated p-values, corrected for multiple testing using the Benjamini-Hockberg method. Data were plotted as the mean ± SE, with n denoting the number of biological replicates described per figure legend.

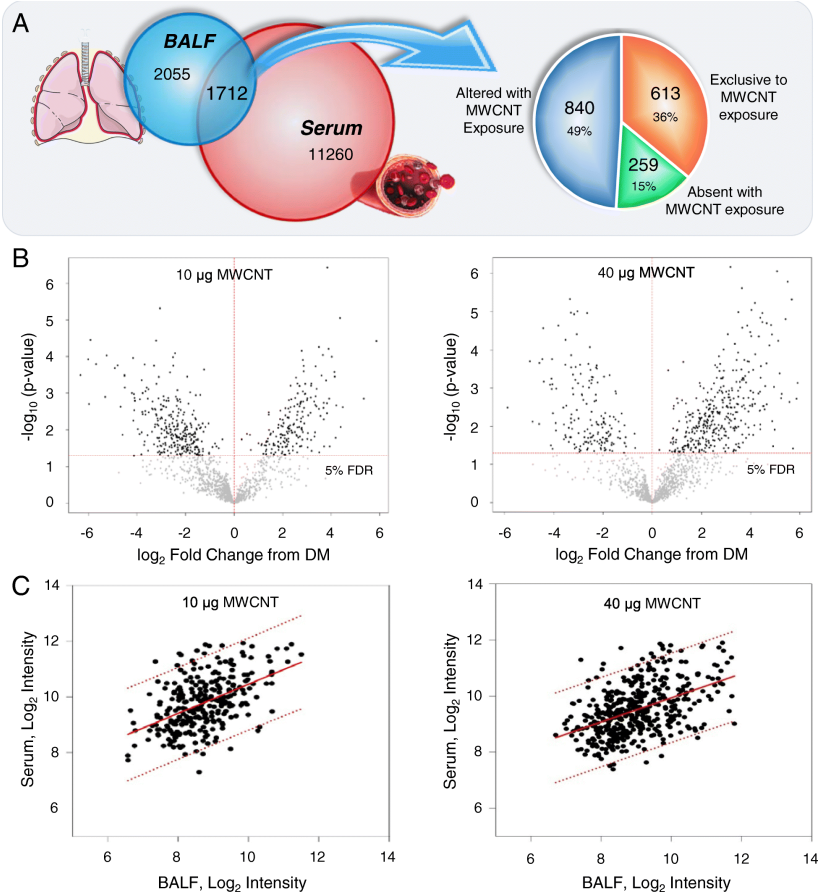

Figure 14. MWCNT-responsive peptidome exhibited correlatory abundance between BALF and serum. The complex molecular response 4-h after MWCNT exposure within enriched-peptide fractions was assessed by mass spectrometry in animal-paired BALF and serum specimens. a Overlapping factors (1712) included 613 measures detected exclusively or 259 lost entirely from fluids in response to MWCNT exposure relative to DM control treatment with the remainder found modulated by exposure. b Volcano plots depicting the fold-change and significance level between MWCNT exposed and DM control animals for measures from the enriched-peptide fraction found across BALF and serum, p adjusted to a 5% FDR. c Linear regression plots of mass spectral intensity measures between animal-paired BALF and serum specimens. Plotted are those peptide measures that reached the 5% FDR significance level. The regression line and 95% confidence interval are show as solid and dashed lines, respectively. All data were generated using matched BALF and serum from n = 6 replicate exposures per dose

RESULTS

MWCNT-induced peptides overlap between the lung and circulation

Enriched-peptide fractions from animal-matched serum and BALF specimens were isolated by size-fractionation and hydrophobic solid-phase extraction from proteinaceous and lipid components and assessed by data-independent mass spectrometry to identify cross-talk between the lung and circulation. As expected, the depth of detection was more limited for BALF (3767 reproducible measures), at 29% of that for serum (12,972 reproducible measures). The lavage procedure involves the rapid partition of the bronchoalveolar surface molecular mass into the lavage buffer for a dilute representation of the airway epithelial lining fluid, which limits recovery and assessment.[75] That said, 1712, or nearly half of all reproducible measures assessed in BALF were detected within serum, demonstrating substantial overlap between the two compartments (**Figure 14a**). Interestingly, more than half of the BALF-serum common measures (872 of the 1712) were exclusively detected either among replicate specimens from MWCNT or DM vehicle treatment groups, 613 (70%) of those solely detected after MWCNT exposure (i.e., not in any specimens from DM treated animals). Statistically, 841 of 1712 species were responsive to MWCNT treatment at a 5% FDR (**Figure 14b**). Of those, 567 species also demonstrated a significant abundance correlation between BALF and serum: 10 µg exposure, $R = 0.49$, $F = 84.7$, $p < 0.001$; 40 µg exposure $R = 0.48$, $F = 126.5$, $p < 0.001$ (**Figure 14c**). Thus, results here corroborated a robust molecular exchange between the lung and the circulation following MWCNT exposure allowing for further focused study of mediators of circulating systemic bioactivity in examining the identity of BALF-serum common factors as having more direct relevance to MWCNT-induced pulmonary pathobiology.

MWCNT-responsive peptides identified from matrix protease substrates

The fold-change response for the serum enriched-peptide fraction is illustrated across chromatographic and mass dimensions via 3D waterfall plots (**Figure 15a**). Evident is a predominant increase in the assessed factors following 10 µg or 40 µg treatment (colored yellow to orange). The mass distribution fell between 1000 and 7000 Da, which was consistent for peptides, and generally exclusive of masses for small molecule metabolites below 1000 Da and proteins above 7000 Da. The chromatographic retention profile reflected complete elution between 10 and 36% acetonitrile, which was confirmatory of an enriched-peptide fraction and effective lipid removal. **Figure 14b** illustrated a greater number of increased peptide with the 40 µg exposure relative to the 10 µg MWCNT. **Figure 15a** illustrates that the majority of additional peptides with 40 µg treatment are larger in mass, with greater density around 3 kDa and 6.5 kDa. As larger mass fragments are more likely to include complete binding motifs, they may convey broader bioactivity.

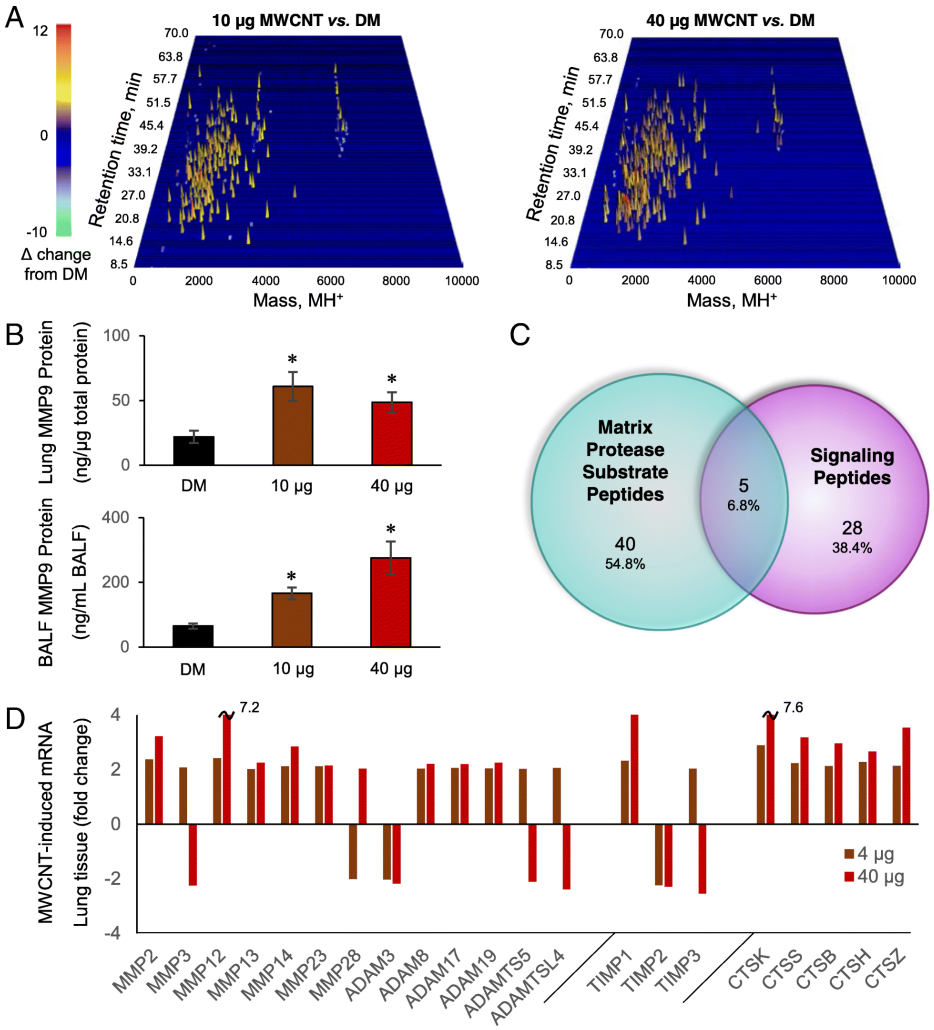

Figure 15. Circulating MWCNT-induced peptides relate to matrix protease activation. a Waterfall plots depicting the MWCNT-induced fold-change among responsive factors within the enriched peptide fraction plotted three-dimensionally against reversed-phase retention time and the charge-reduced protonated mass (MH+). b MMP9 protein abundance in animal-matched lung tissue and BALF 4-h after MWCNT exposure as assessed by ELISA and presented as the mean ± SE, n = 5 replicate mouse exposures per dose, *p < 0.05. c Venn diagram of identified MWCNT-responsive peptides in association with databases of matrix protease substrates and predicted secreted signaling motifs. d Gene expression changes in lung tissue across matrix proteineases of the MMP, ADAM and ADAMTS families, tissue inhibitors of metalloproteinases (TIMPs) and lysosomally-derived cathepsins (CTS) following a 4-h inhalation exposure to MWCNT. Results reported for proteases that exhibited a two-fold or greater response to MWCNT and reached significance at an FDR of 5% as assessed by Illumina BeadChip and presented at the mean response across n = 4 replicate mouse exposures per dose

The diversity of the peptidomic response suggests extensive proteolytic processing within the lung and subsequently in the circulation. Previously we demonstrated that MWCNT-induced vasodilatory deficits were dependent on MMP9.[7] An MMP9 elevation in lung ($F = 5.9$, $p = 0.013$) and BALF ($H = 11.6$, $p = 0.003$) support its potential involvement in peptide fragment generation (**Figure 15b**). Yet MMP9 cleavage alone is insufficient to explain the shear multiplicity of peptides produced in response to MWCNT exposure. We thus looked farther afield in identifying peptides related to known substrates broadly across matrix proteases, including MMPs, ADAMs, and ADAMTSs. Resources available from the MEROPS peptidase project of the European Bioinformatics Institute provided a concise source of known substrates for these proteases that could then be used to significantly reduce the sequence search space,[66] as beneficial to identifying endogenous peptide mass spectra.[76] Metalloproteases are further associated with extracellular signal-peptide release.[77] The SignalP resource from the Technical University of Denmark Bioinformatics unit extended our search capability to included predicted peptides of excreted proteins.[67] From these resources, 73 of the BALF-serum common measures found statistically responsive to MWCNT at one or both doses (10 µg or 40 µg) were identified (**Figure 15c** and Mostovenko et al., 2019[56]), relating the genesis of MWCNT induced peptides to known matrix

protease substrates and secreted proteins. To substantiate further involvement of additional proteases, we mined an existing lung tissue microarray dataset exhibiting the effects of inhaled Mitsui-7 MWCNT with four-hour deposited doses on par with those modeled here. Array analysis in lung tissue showed significant upregulation for a broad array of other MMPs, ADAMs and ADAMTSs with MWCNT exposure (**Figure 15d**). Furthermore, tissue inhibitors of metalloproteinases (TIMPs) were likewise modulated, with TIMP1 significantly increased at both doses, TIMP2 significantly decreased at both doses, and TIMP3 showing an opposing response between doses. Other proteases are also known to influence remodeling of the ECM after MWCNT exposure, to include lysosomal-released cathepsins.[78] Microarray data showed significant increased at both doses for cathepsins B, H, K, S and Z. Taken together, these data support involvement of multiple proteases, with likely promiscuous activation of one by another and tandem cleavage of common substrates, in generating the peptidomic response observed here.

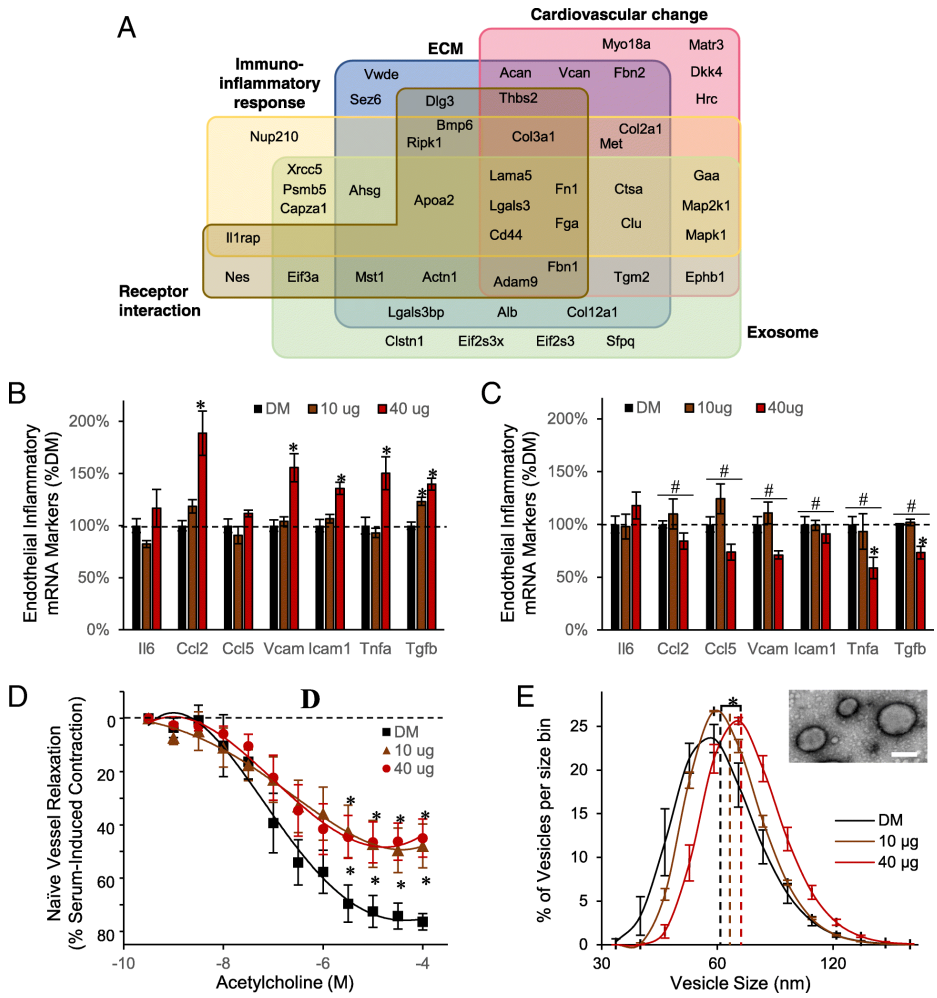

Figure 16. Functional relevance of the MWCNT-responsive peptidome. a Venn diagram reflecting functional associations among 73 identified peptides per ontology enrichment analysis. Groups denote the five most-enriched associations per biochemical, pathological, cellular and localization databases, with peptide-precursor protein symbols shown. Serum cumulative inflammatory potential assay results after treating endothelial cells for 4-h in vitro with b the enriched-peptide serum fraction and c after denaturing the peptide fraction. Presented as the mean ± SE, n = 6 serum peptide fractions from replicate mouse exposures per dose, #p < 0.05 for effect of denaturing; *p < 0.05 for effect of MWCNT. d Acetylcholine induced vascular relaxation assessed ex vivo using naïve aortic rings treated with the enriched-peptide serum fraction, expressed as a percent recovery towards the pre-contraction tension. Data are presented as the mean ± SE, n = 6 serum peptide fractions from replicate mouse exposures per dose, *p < 0.05. e The hydrodynamic vesicle size distribution for an exosome-enriched size-exclusion serum fraction, plotted as the mean ± SE for bins sized between 30 and 180 nm, n = 3 replicate exosomal serum extracts from n = 6 replicate mouse exposures per dose. Dashed lines denote the curve mean, *p < 0.05. Inset electron micrograph of the serum exosomes; scale bar = 100 nm

MWCNT-induced circulating peptidome contributes to cardiovascular endothelial responses

Bioinformatic functional enrichment analysis was performed to inform on the pathobiological relevance of the circulating peptidomic response to MWCNT. Results classified into five enriched associations (**Figure 16a** and Mostovenko et al., 2019[56]). The largest group of 31 peptides were associated with an extracellular matrix localization and functionally to extracellular matrix (ECM) organization. With ECM reorganization being a principle factor in cardiovascular disease and inflammatory lesion development, it was also fitting that many of the ECM-related measures were among the 27 peptides enriched in association with an abnormal cardiovascular phenotype and altered cardiovascular proliferative biological processes. The results also included 18 peptides reflecting relevance to cell-surface receptor interactions denoting signaling ligands within the peptidome. Peptide-receptor interactions are involved in numerous biological processes, including immune and associated inflammatory signaling, with 22 associated peptides. Lastly, 29 peptides were derived from known exosomal localized proteins, suggesting exosome involvement in systemic MWCNT responses. Collectively, the peptidomic fraction biochemically paralleled our prior published

inflammatory and vascular deficit outcomes induced in vivo and ex vivo using the present MWCNT exposure model.[7-9]

After establishing its pathobiological relevance, we then sought to assess the bioactive potential of the serum peptidomic fraction. The enriched peptide fraction was first assessed for its inflammatory potential on primary murine vascular endothelial cells, as previously reported for whole serum.[8] The assay assessed ex vivo endothelial induction across a battery of adhesion molecule and cytokine gene products linked with inflammatory-mediated immune responses. Naïve endothelial cells were treated in culture with the serum peptide fractions of MWCNT-exposed or DM control animals. As observed previously using whole serum from exposed animals,[8] the peptide-fraction alone induced significant increases in canonical inflammatory markers Ccl2, Vcam1, Icam1, and Tnfa, principally at the 40 µg MWCNT dose relative to DM control (**Figure 16b**). The magnitude of response was 189% ($p < 0.001$), 156% ($p < 0.001$), 136% ($p < 0.001$), and 150% ($p < 0.033$) of DM control levels for Ccl2, Vcam1, Icam1, and Tnfa, respectively. In contrast, Ccl5 showed no response to treatment. Tgfb and Il6 were additionally assessed in this study, relevant to the MWCNT peptidome's enriched association with immune response processes. Application of the serum peptide fraction induced significant dose-dependent increases in Tgfb expression: 123%, $p < 0.001$ at 10 µg; 140%, $p < 0.001$ at 40 µg. In contrast, Il6 levels were absent significant effects of treatment. To support that the inflammatory response was driven by peptide components within the enriched fraction, an aliquot was denatured by reduction and alkylation to disrupt peptide structure, buffer exchanged, and applied to naïve cerebrovascular endothelial cells. Notably, denaturing significantly reversed the peptide fraction's prior inflammatory potential: Ccl2 (40 µg, $p < 0.001$), Ccl5 (40 µg, $p = 0.004$), Vcam (40 µg, $p < 0.001$), Icam1 (40 µg, $p < 0.001$), Tnfa (40 µg, $p < 0.001$), and Tgfb (10 µg, $p = 0.002$; 40 µg, $p < 0.001$) (**Figure 16c**).

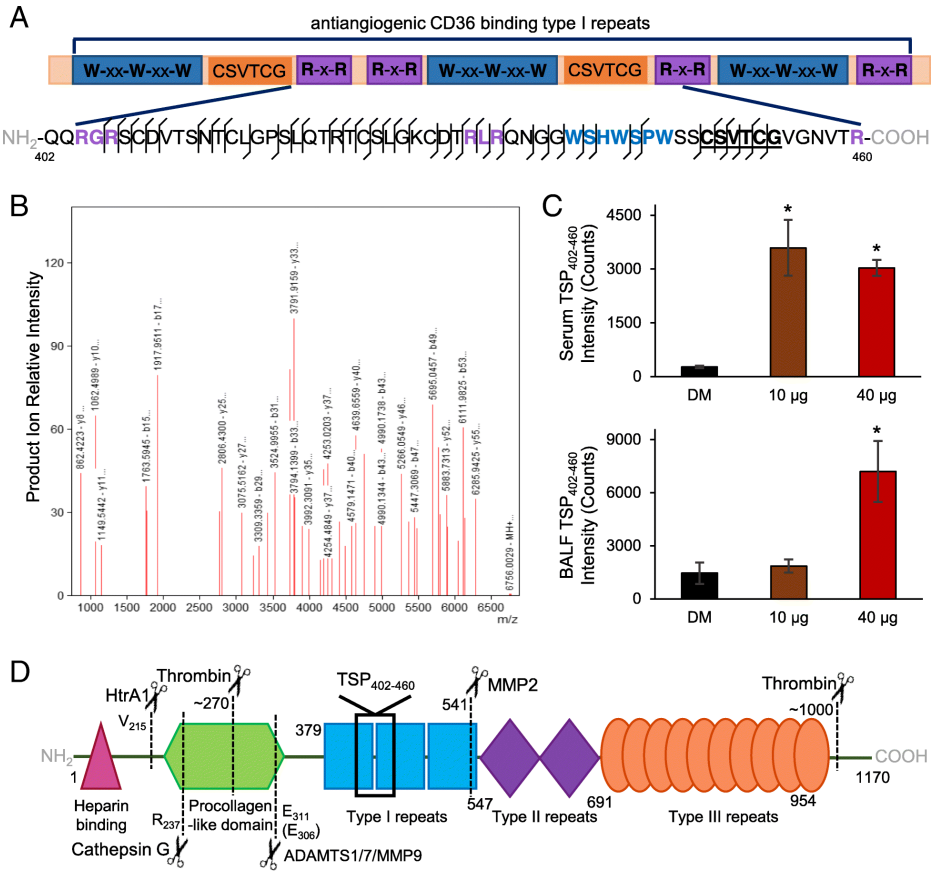

Figure 17. MWCNT-responsive thrombospondin fragment identified with CD36-modulatory motifs. a Among the identified peptides was a 59-mer thrombospondin fragment overlaping the second type-1 repeat domain (TSP402–460). Three established CD36 binding and modulatory motifs are color-coded and shown in bold within the peptide sequence. Matched mass spectral ion fragmentation sites are shown along the 59-mer sequence with a line angled to the left denoting a b-ion (left-to-right) a line angled to the right denoting a y-ion (right-to-left). b The TSP402–460 peptide's corresponding fragment ion mass spectrum with peaks labeled for their reduced mass (MH+) and b/y-ion designation. c Mass spectral ion intensity for the TSP402–460 peptide plotted as mean ± SE, n = 6 matched serum and BALF specimens from replicate mouse exposures per dose, *$p < 0.05$. d Proteolytic processing map for known thrombospondin cleavage sites with the protease and site given relative to functional domains

Next, the serum peptide fraction was assessed for its potential to induce vascular dysfunction as previously tested for whole serum using myography.[7] Naïve aortic rings treated with the serum peptide fraction from 10 µg and 40 µg dosed animals exhibited significant dysfunction ($F = 31.2$, $p < 0.001$, main effect of MWCNT exposure) in acetylcholine-mediated dilation (**Figure 16d**). The effect was dose-independent, reaching only 57% the dilation achieved with DM control at either MWCNT dose. As a percent of DM control, the peptide fraction induced the same magnitude deficit as whole serum treatment, which reach just 56% of DM control

relaxation at the 40 µg dose.[7] However, the response to the peptide fraction lacked an added deficit previously reported with whole serum at the 10 µg dose, which dilated to only 29% that reached with DM control serum.

MWCNT-responsive exosome-associated peptides coincide with serum exosomal shifts

As the MWCNT-responsive peptidome was significantly enriched in association with exosomes, we sought to next test an association of this change with a parallel increase in serum exosomes. An enriched exosomal fraction was purified by ultrafiltration followed by size-exclusion chromatography. The vesicle size distribution fell between 40 and 160 nm (**Figure 16e**) and excluded serum proteins that appear in later fractions between 6 and 20 nm. The measured vesicle distribution matched precisely that accepted for exosomes.[79] MWCNT exposure induced a dose-dependent shift to larger-sized serum-exosomal vesicles, reaching significance for the 40 µg dose (18.3% increase, $p < 0.001$): DM, 60.4 ± 1.0 nm; 10 µg, 64.7 ± 0.9 nm; 71.4 ± 0.4 nm. Furthermore, the area under the hydrodynamic-size curve increased with MWCNT exposure, relative to DM control, purporting a greater number of exosome-sized serum vesicles, which reach significance at the 40 µg dose (17.5% increase, $p = 0.0284$): DM, 924 ± 40.6; 10 µg, 974 ± 8.3; 40 µg, 1086 ± 26.1. The enriched vesicles were further assessed by transmission electron microscopy (**Figure 16e**), with their size and morphology consistent with that previously published for exosomes.[80]

Identified thrombospondin fragment relates peptidome relevance to vascular dysfunction

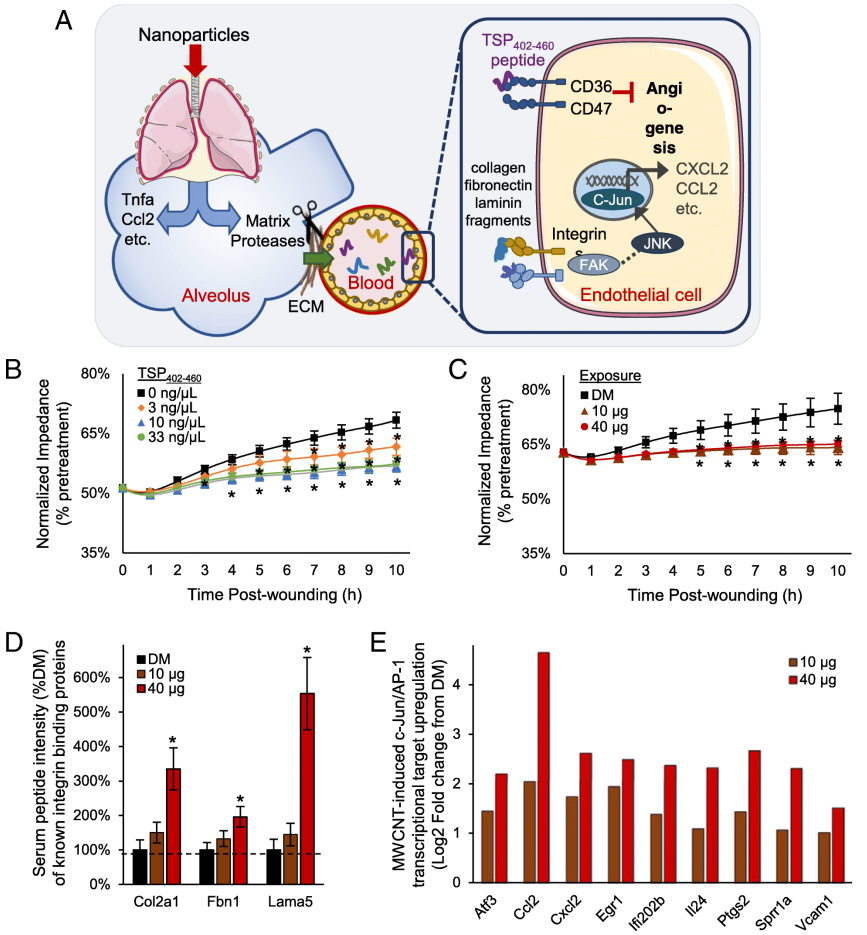

Figure 18. Peptide-mediated model of systemic bioactivation following pulmonary nanoparticle exposure. Results from this study support a proposed paradigm (a) by which nanoparticles in the lung activate matrix proteases, with a diversity of generated peptide products released into circulation with some acting as cell-surface receptor ligands that drive systemic vascular dysfunction and inflammation. The model depicts peptides products of thrombospondin and integrin-ligand proteins from the MWCNT-responsive peptidome triggering CD36 and integrin receptor signaling with downstream anti-angiogenic and inflammatory marker outcomes. b Following synthesis of the identified MWCNT-responsive TSP402–460 peptide, its anti-angiogenic properties were assessed using an electronic wound-healing assay after a 4-h treatment. c Likewise, the electronic wound-healing assay was used to assess the anti-angiogenic properties after a 4-h treatment with the serum peptide fraction from n = 6 MWCNT treated animals per dose. Electrical impedance values were plotted per hour for 10 h following wounding, with data centered and normalized as a percentage of pretreatment impedance and given as mean ± SE, n = 6 in vitro replicates, *p < 0.05. d Peptides identified from known integrin-binding proteins were dose-dependently increased, mass spectral intensity normalized as a % of DM vehicle control presented as mean ± SE, n = 6 replicate exposures per dose, *p < 0.05. e c-Jun transcriptional targets upregualted in endothelial cells treated 4-h in vitro with serum collected 4-h after MWCNT or DM control exposures. Mean log2 fold change results plotted, n = 4 replicate mouse exposures per dose, p < 0.01

The induction of endothelial-dependent vasodilatory deficits by serum factors from MWCNT exposed animals has recently been independently confirmed.[7,81] The two studies offer complementary mechanistic insight demonstrating the co-dependence between MMP9 activity and TSP-mediated CD36 signaling; yet, a molecular interconnection was not readily apparent. Included within the MWCNT-responsive peptidome reported here was a 59-mer fragment from a TSP2 type-1 domain between residues 402–460. Within TSP type-1 domains are three motifs that enable CD36 binding and modulation: R-x-R, W-xx-W-xx-W and CSVTCG motifs.[82,83] The identified TSP402–460 peptide contains all three motifs (**Figure 17a**), which was well characterized by the product ion spectra (**Figure 17b**). Significant increases in the TSP402–460 peptide were measured dose-independently within serum at the 10 µg ($p = 0.002$) and 40 µg (p

< 0.001) doses, but dose-dependently in BALF at the 40 μg dose (p = 0.002) relative to DM control (**Figure 17c**). The average serum TSP402–460 peptide concentration was then approximated at 24 nM and 20 nM in serum from 10 μg and 40 μg MWCNT-dosed animals, respectively, using the mean mass spectrometer response to a known peptide concentration. The similar concentration between the two MWCNT doses paralleled the comparable vascular deficit induced by the serum peptide fraction per myography (**Figure 16d**). Furthermore, the increased serum amount of the 59-mer peptide at the two MWCNT doses closely profiled MMP9 protein levels within lung tissue (**Figure 15b**). Yet known MMP9 cleavage of TSP between residues 306–307 sits well away from the TSP402–460 peptide identified here (**Figure 17d**), suggesting additional tandem cleavage events by other proteases. TSP is well known to be proteolyzed by other matrix-related enzymes such as MMPs 2 and 14, ADAMTSs 1 and 7, and cathepsin G.[84-87] Moreover, TSP is proteolyzed by immune-cell released and circulating enzymes, for example, elastases, thrombin, plasmin, and HtrA1.[88-91] The complement of established cleavage sites for these proteases (**Figure 17d**), however, are likewise nonspecific to the sequence of the TSP402–460 peptide. Recognizing that the full complement of TSP cleavage events, particularly with sequential processing by multiple proteases, cannot be known, we then looked to site prediction informatics. Using the feature-based tool PROSPER[92], we resolved that the c-terminal side of the TSP402–460 peptide is a probable neutrophil elastase cleavage site (cleavage probability score 1.11 > 0.8 cutoff for positive prediction at an 82.9% accuracy for elastase-2). While the full complement of proteolytic processing needed to yield this peptide is expectedly complex, its retained CD36 ligand characteristics exemplify the bioactive potential of the MWCNT-induced circulating peptidome.

Peptide-mediated model of systemic effects following pulmonary nanoparticle exposure

Cumulatively, findings here establish a complex serum peptidomic response acutely following exposure to MWCNT that conveys bioactivity. Included among the responsive factors are peptide fragments related to abnormal cardiovascular and inflammatory responses, exemplified by the identification of a TSP402–460 peptide with CD36 binding motifs. Results here support consideration of a new peptide-mediated model of systemic effects (**Figure 18a**) following nanoparticle exposure. Proposed is that a diverse assortment of matrix remodeling proteases activated following exposure induce peptide byproducts into circulation where they may be further modified yielding an expanded serum peptidomic complexity. The peptidomic response includes cell-surface receptor binding capacity that promotes extra-pulmonary effects. To validate the potential of this model, we synthesized the TSP402–460 peptide and applied it in a CD36/CD47-mediated endothelial cell in vitro wound healing angiogenesis assay (**Figure 18b**). Addition of the TSP402–460 peptide into the culture media produced a significant anti-angiogenic effect (F = 43.5, p < 0.001), impairing cell regrowth as measured by recovered membrane impedance. Relative to vehicle control, a 6% deficit reestablishing baseline impedance 10 h after wounding was observed at a 3 ng/μL dose (p = 0.002), a 22 nM concentration in media similar to that estimated in the serum of exposed animals. A 3-fold or greater increase in TSP402–460 concentration saturated the deficit at 12% (p < 0.001). In comparison, the serum peptide fraction from MWCNT exposed animals also significantly inhibited (F = 32.7, p < 0.001, main effect of dose) endothelial cell regrowth out to 10 h after wounding (**Figure 18c**). The induced deficit recovering baseline impedance was 9.5% (p < 0.001) relative to DM control, which fell between that induced at 3 and 10 ng/μL TSP402–460 peptide. These data establish the bioactive nature of the circulating TSP402–460 peptide that, at least in part, accounts for the anti-angiogenic capacity of the serum peptide fraction.

DISCUSSION

Looking beyond the TSP peptide, the MWCNT-responsive peptidome was enriched with other fragments of receptor-binding proteins (**Figure 16a**). A number of them were derived from known integrin binding collagens, fibronectin and laminins, offering additional potential in mediating observed bioactivity. The MWCNT-response among these peptides was dose-dependent (**Figure 18d**) similar to findings from the serum cumulative inflammatory potential assay (**Figure 16b**), which contrasted with the dose-independent increase in the TSP402–460 peptide and CD-36 dependent myography (**Figure 16d**) and wound healing (**Figure 18c**) findings. The MWCNT-responsive peptidome was also significantly enriched in association with interactions upstream of c-Jun transcription (FDR 0.0127) and integrins are known to induce c-Jun-mediated inflammatory factor transcription. Supporting the integrin-ligand potential of the MWCNT-responsive peptidome, in vitro treated endothelial cells exhibited significant dose-dependent upregulation of numerous c-Jun transcriptional products (**Figure 18e**) relative to DM control. Together, results here implicate integrin-ligand functionality of the MWCNT-responsive peptidome as an additional part of a broader combinatorial molecular response mediating systemic bioactivity after nanoparticle exposure.

Findings here substantiate proteolytic peptide involvement in mediating systemic consequences of nanoparticle exposure. A wide variety of inhaled xenobiotics upregulate matrix proteases and produce various systemic effects. Agents from titanium dioxide to diesel exhaust have been shown to induce extra-pulmonary inflammation and cardiovascular impairments much as reported here for MWCNT.[16,20,93] Indeed, many insoluble metal and engineered nanoparticles (Au, Ag, titanium dioxide, ultrafine carbon and other CNTs, etc.) induce pulmonary pathology that may be accompanied by proteolytic generation and release of bioactive peptides. Once in circulation, fragments such as the TSP402–460 peptide or those from integrin ligands induce cell-surface receptor mediated systemic stress and inflammation, driving particulate exposure's adjuvant role in promoting everything from cardiovascular to neurodegenerative diseases. Furthermore, the revealed existence of a pathological peptidomic response to nanoparticle exposure represents a highly diverse and dose-dependent molecular source of putative biomarkers that may provide greater specificity than previously available.[10] More thorough characterization of circulatory factors is warranted to assess the role of peptide byproducts mediating systemic disease following pulmonary insult to a broader array of occupational and environmental xenobiotic agents.

AIM 2.2. Transmission of MWCNT-induces seromic factors.

Nanoparticle-induced BBB dysfunction represents a significant concern given findings demonstrating a strong correlation between air pollution and neurodegenerative ramifications in adults [18,19,94] as well as neurodevelopmental abnormalities in children.[95,96] Many neuropathies have been linked with a compromised BBB, whereby the brain is opened to exogenous molecular factors that promotes neuroinflammation and potentially neuronal functionality. Thus, here we hypothesized that the peptidomic fraction induced within the circulation following MWCNT exposure would have access to the brain parenchyma and that observed neuroinflammation would be commiserate with neuronal perturbation. To test this hypothesis, we assessed correlating peptidomic perturbation within matched serum and cerebrospinal fluid (CSF) of MWCNT-exposed and control mice. The functional relevance of identified CSF peptides was then related back to cellular perturbation within the brain parenchyma.

MATERIALS AND METHODS

***Animals, exposure and sample collection*.** Specific pathogen-free male C57BL/6J mice (Jackson Laboratory, Bar Harbor, ME) were used for this work. Animals were housed at the National Institute for Occupational Safety and Health in an Association for Assessment and Accreditation of Lab Animal Care International approved animal facility. Animal care and use procedures were conducted in accordance with the US Public Health Service's Policy on Humane Care and Use of Laboratory Animals and the National Institutes of Health's Guide for the Care and Use of Laboratory Animals. Mice were housed in ventilated cages in a temperature and humidity-controlled environment with a 12-h light/dark cycle, while food and tap water were available *ad libitum*. Exposure to MWCNT-7 (Hodogaya, Japan) was performed using an established mouse model at doses found physiologically relevant to human occupational exposure.[13] Eight week old mice received 0 μg (n = 7, control), 10 μg (n = 6), or 40 μg (n = 6) of MWCNT-7 *via* oropharyngeal aspiration within dispersion media consisting of 0.6 mg/mL mouse serum albumin and 10 μg/mL 1,2-dipalmitoyl-sn-glycero-3-phosphocholine. The 10 μg dose in mouse approximated light handling for one month at a manufacturing facility with ambient MWCNT aerosol of 400 $\mu g/m^3$ while the 40 μg dose represented heavy handling or an accidental exposure. The MWCNT-7 was characterized to have an average diameter and length of 49 nm and 3.86 μm (geometric SD = 1.94), respectively, was >99% pure carbon, and was LPS negative. At 4 h post exposure, animals were anesthetized under 2.5% isoflurane and immobilized within a stereotaxic frame. A 100 μL capacity pulled glass tip was inserted by micromanipulator into the cisterna magna and allowed to collect > 20 μL of CSF for 20 min. Blood was then collected via cardiac punch, allowed to clot and separated to collect serum. Animals were then decapitated and brains removed, rinsed and snap frozen within 1 min. All materials were transferred to Virginia Commonwealth University on dry ice and stored at -80°C until use.

Endogenous peptide enrichment and mass spectral analysis. The peptidomic fraction from serum and CSF were generated as previously published.[56] Briefly, 40 μL of serum and 20 μL of CSF were clarified through a 0.22 μm Ultrafree-MC filtration unit (EMDMillipore, Billerica, MA). The filtrate was denatured with 20% acetonitrile and reduced with 18 mM TCEP with HALT cocktail (Thermo Scientific, Rockford, IL) added to 1x for protease and phosphatase inhibition. Cysteine reduction was maintained with 30 mM iodoacetamide alkylation. MicroCon YM-30 (EMDMillipore) centrifugal filter units were used to resolve the peptide fraction (~8 kDa upper limit), with a second collection spin performed after acidification with 0.4% formic acid to further disrupt peptide binding. Crude peptide fractions were then loaded (4 μL for serum and 8 μL for CSF) onto

Symmetry C18 trap column (Waters, Milford, MA) to remove lipids, reagents and salts. Peptides were resolved by gradient reversed-phase chromatography between 6% to 44% acetonitrile in water (0.1 % formic-acid) over 65 min using a 150mm×75 µm HSS T3 column at coupled 55ºC online with a Synapt G2-Si tandem mass spectrometer (Waters). Data were acquired with ion mobility-enabled data-independent acquisition (UDMSe) between 400 and 1800 m/z at 25,000 nominal resolution.[57] Raw spectral data were processed as previously described [56] using PLGS v3.0.3 software (Waters) for peak-picking, chromatographic peak area integration, and precursor-product ion alignment, and aligned across biological replicate were by retention time (±2 min), drift time (±5 bins), and ion mass (MH^+, ±12 ppm) in EndogeSeq. Data were then filtered to retain reproducible ion features (4+ replicate measures per group, n =6).

Immunofluorescent microscopy. Fresh-frozen brains were sagittal thin-sectioned (10 µm) in a cryostat and air dried prior to fixation with 4% paraformaldehyde within the right hemisphere at a depth of 1 mm from midline. Sections were blocked and permeabilized in 5% normal goat serum and 0.1% Triton X-100 for 1 h at room temperature. Sections were then probed at 4 °C overnight with primary antibodies in blocking buffer: vascular marker anti-rat ZO1 tight junction protein 1 (Developmental Studies Hybridoma Bank, R26.4C, 1:5), BBB permeation marker anti-rabbit albumin (Bioss, bs-2256R, 1:300), microglial marker anti-guinea pig IBA1 (Synaptic Systems, 234-004, 1:2000), astrocytic marker anti-chicken GFAP (Abcam, ab4674, 1:3000), glutamatergic synaptic marker anti-guinea pig Vglut1(Millipore, AB5905, 1:1000), and GABAergic synaptic marker anti-mouse Gad65 (Developmental Studies Hybridoma Bank, GAD-6, 1:5). Sections were then probed with corresponding AlexaFluor 488/568/680-conjugated goat secondary antibodies at room temperature for 2 h. Mounted sections were coverslipped in ProLong Diamond Antifade Mountant (Thermo Scientific). Slides were imaged via multichannel immunofluorescence with a Zeiss AxioImager M2 microscope with structured illumination for both widefield and optical sectioning (0.25-µm stack thickness). Image acquisition and processing were performed with Zeiss Zen 2.1 software, with 12 images collected per brain region across 3 sections per animal, and region of interest quantitative analysis was performed in Fiji.[97] Images were focused on penetrating cerebrovasculature with a vascular diameter > 10 µm as described previously.[8] A 100 µm diameter region of interest was then centered on the vessel for densitometry, with the vessel luminal area excluded. GFAP and IBA1 staining were then assessed for area fraction and mean fluorescence intensity within the region of interest with positive staining determined using the Otsu threshold algorithm, standardized across all sections for unbiased measurements.

Statistical and informatic analysis. Mass spectrometric peak area intensity data were median centered, imputed for left-censored data reproducibly falling below the limit of detection across at least 5 of 6 replicates per group, $\log_2$ transformed, and standardized to the average intensity across the 0 µg MWCNT control group, as previously described.[56] One-way ANOVA was performed in MultiExperimentViewer (v.4.9.0), corrected for multiple peptide measures using the Benjamini-Hochberg false discovery rate method to control type 1 error to 5%. Significant responsive peptide features were searched against targeted databases for matrix protease substrates and secretory proteins with results limited to a 5% false identification rate at the peptide level as published previously.[56] Significantly responsive CSF peptide features were aligned with corresponding serum features by retention time (±2 min), drift time (±5 bins), and ion mass (MH^+, ±12 ppm) to assess linear correlation in the measured peptide quantity across biofluids via the Pearson test in R studio (v1.1). Immunofluorescence microscopy measures were standardized to the average measure for the 0 µg MWCNT control group and assessed using one-way ANOVA with the Holm-Sidak multiple comparisons procedure for pairwise analysis within SigmaPlot (v14).

RESULTS

MWCNT inhalation exposure promotes a largely independent CSF-peptidomic response. We recently published on the highly diverse peptidomic response to MWCNT exposure across paired bronchoalveolar lavage fluid and serum.[56] There was a striking 45% overlap in peptide factors responsive in the lung and their detection in the circulation, with 51% of those features detected only with MWCNT treatment relative to 0 µg vehicle control treatment using the same mouse model as employed in the present study. These MWCNT-responsive peptides exhibited significant ($p<0.001$) quantitative correlation in their abundance between the lung and circulation at both the 10 µg and 40 µg doses. Moreover, the circulating peptide fraction was found to induce endothelial inflammation, inhibit angiogenesis, and promote vessel contractile deficits, emphasizing the bioactive nature of the MWCNT-induced peptidome and its role as an indirect mediator of vascular dysfunction. A similarly diverse circulating peptidome (6449 features) was reproducibly detected (n≥4) across serum

specimens in this study (**Figure 19A**). Of these circulating peptides, 1315 were detected only with (830, 63%) or without (485, 37%) MWCNT treatment, which was consistent with our prior report.

Here we assessed the peptidomic overlap between matched CSF and serum samples with 2226 reproducible (n≥4) features detected within the peptide-enriched CSF fraction. Unexpectedly, we only found an 8% overlap between the CSF and serum peptidomes with 658 common features (**Figure 19A**). Of those, just 4 (0.6%) exhibited significant within-animal correlation in CSF and serum levels, after correcting for multiple comparisons (**Figure 19B**), with far less overall peptidomic correlation between serum and CSF than found between lung lavage and serum. This was contrary to the present hypothesis, having posited that reported BBB dysfunction with this model[8] would have resulted in greater communication between serum and CSF.

In contrast to our expectation, 70% (1568) of the detected CSF factors were unique to CSF – not detected within serum replicates – pointing to the specificity of the CSF peptidome. ANOVA results indicated that 291 CSF-distinct peptide measures were significantly responsive to MWCNT exposure at a 5% FDR (**Figure 20A**), with 192 (66%) exhibiting a dose-independent response. Thus, while there was little cross-talk between the circulation and CSF, a neuropathological response to MWCNT exposure was evident by the significant influence on the CSF peptidome.

CSF-specific peptidomic response attributed to neuroinflammation and synaptic plasticity. We employed the tandem mass spectral data collected across the MWCNT-responsive CSF peptidome to identify sequences and inform on functional relevance. We identified 8 unique endogenous peptides (**Figure 20B**) from a targeted matrix protease (MMPs and ADAMs) substrate database.[56] Peptides from AFF1 (AF4/FMR2 family member 1), HOXA4 (homeobox protein Hox-A4), and STAM (signal transducing adapter molecule 1) were affected in a dose-independent manner. The AFF1 peptide decreased 87.2-fold at 10 µg and 101-fold at

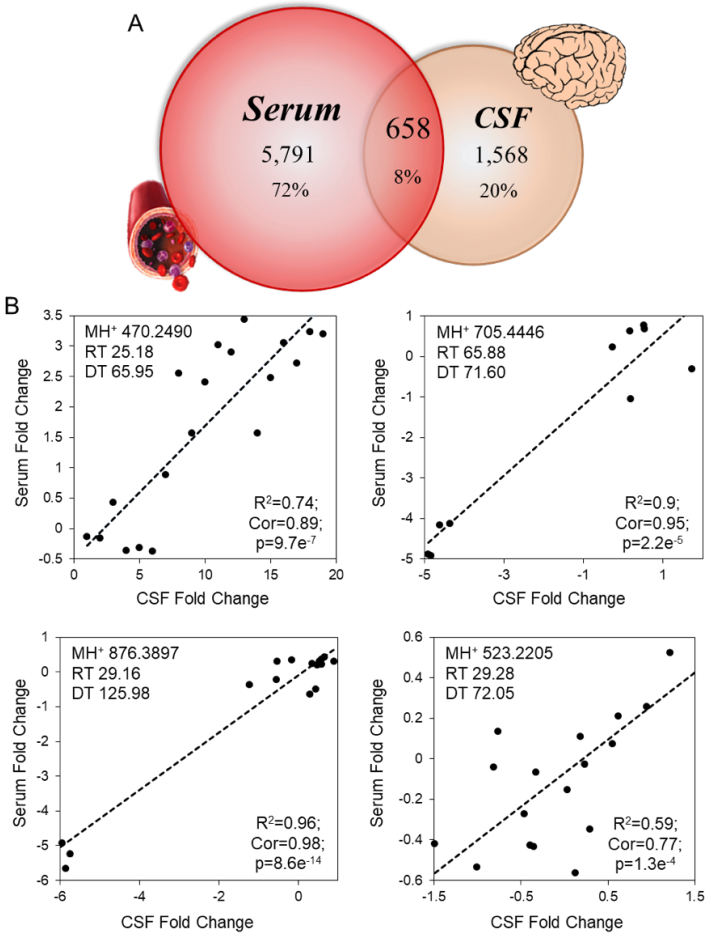

Figure 19. Limited correlation between serum and CSF peptidomic responses to pulmonary MWCNT exposure. Matched serum and CSF collected 4 h after MWCNT exposure was fractionated to enrich for endogenous peptides and analyzed by ion mobility-enabled data-independent mass spectrometry. (A) Overlap in reproducibly (n ≥ 4) detected peptide measures between serum and CSF, defined by a signature of common retention time (RT), ion mobility drift time (DT) and accurate mass measures (MH+). (B) The log(2) relative ion intensity plotted across serum and CSF measures for the four peptides found with significant linear correlation. The square of the Pearson product-moment coefficient (R^2), Pearson's correlation coefficient (Cor), and p-values are noted, n=6-7/grp.

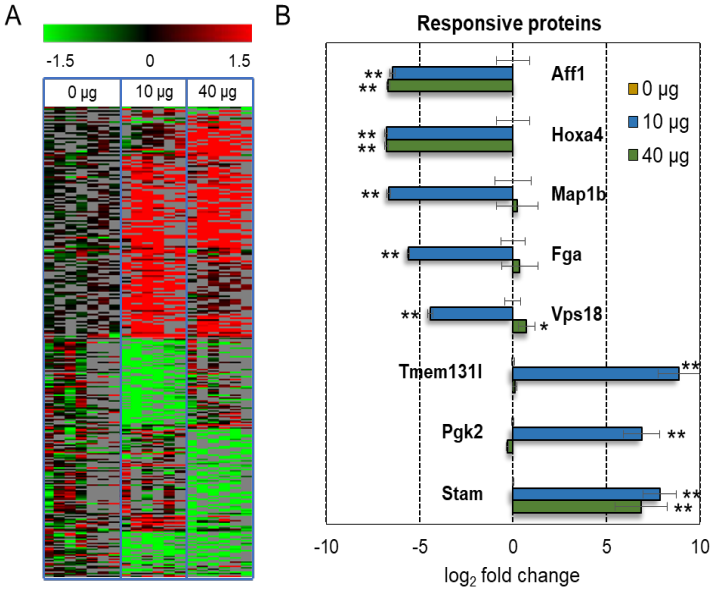

Figure 20. Significant CSF peptidomic response to pulmonary MWCNT exposure. CSF collected 4 h after MWCNT exposure was fractionated to enrich for endogenous peptides and analyzed by ion mobility-enabled data-independent mass spectrometry. (A) Heatmap representation of CSF peptide responses to 10 µg or 40 µg MWCNT exposures relative to the 0 µg control group. The log(2) relative ion intensity is colored per the shown scale. (B) The log(2) ion intensity relative to the 0 µg control group for identified peptides across 10 µg and 40 µg MWCNT exposures. Data are presented as mean ± SEM, n=6-7/grp. * p<0.05; ** p<0.001.

40 µg MWCNT. Similarly, the HOXA4 peptide was depleted 109-fold in both groups. In contrast, the STAM peptide significantly increased 231.8- and 115.6-fold, respectively between 10 µg and 40 µg exposures. Peptides to fibrinogen alpha chain (FGA, decreased 48.3-fold), microtubule-associated protein 1B (MAP1B, decreased 100.3-fold), phosphoglycerate kinase 2 (PGK2, increased 117.8-fold), transmembrane protein 131-like (TMEM131L, increased 476.8-fold), and vacuolar protein sorting-associated protein 18 (Vps18, decreased 21.7-fold) were all significantly affected following the low dose exposure while exhibited no change at 40 µg.

Next, we assessed published roles for each originating protein within the brain. A full 75% of the identified peptides originate from proteins have a distinct neurophysiological functions (**Table 1**). Functional annotations were assigned as proteins involved in: neuronal plasticity, AFF1, MAP1B and Vps18[98-103]; neuronal survival, Vsp18 and AFF1[104-107]; cell migration, Vsp18 and FGA; modulating endo-lysosomal machinery, STAM; and vascular remodeling, HOXA4[108]. Little is known about PGK2 and TMEM131L in the brain; however, their paralogues PGK1 and Tmem131 have been shown involved in neuronal stress resistance[109], glutamatergic

Protein ID	Protein Symbol	Protein Name	Peptide Sequence	Fold Change (10, 40)	Function in CNS	References
O88573	**AFF1**	AF4/FMR2 family member 1	GNAKPGKPQVKSDR	-6.45 -6.67	Promotes dendritic remodeling	(36, 37)
E9PV24	**FGA**	Fibrinogen alpha chain (fibrinopeptide A)	EDKGEFLSEGGGVR	-5.6 0.4	Marker of neuroinflammation, initiates astrogliosis/glial scar formation. Cell migration guidance	(67–70)
P06798	**HOXA4**	Homeobox protein Hox-A4	QSAPHLPAPNPHAARQP	-6.78 -6.77	Suppresses vascular remodeling	(46)
P14873	**MAP1B**	Microtubule-associated protein 1B	DTKMSISEGTVSDKSATP	-6.65 0.22	Affects axon branching, synaptic formation and maturation	(38–40, 86, 93)
P09041	**PGK2**	Phosphoglycerate kinase 2	MDEVVKATSNGCVTIIGGGDTATCCAKWGTEDK	6.88 -0.3	Mediates stress resistance, synaptic neurotransmission and early-onset of Parkinson's disease by attenuating ATP levels*	(47, 48, 94–96)
P70297	**STAM**	Signal transducing adapter molecule 1	LDICDKVGQSRTGPKD	7.86 6.85	Essential for neuronal cell survival *in vivo*	(43)
Q3U3D7	**TMEM131L**	Transmembrane protein 131-like	CQQLKSCSLGSDDALHLEMNIIVAVENSSKQ	8.9 0.1	Neuroinflammation**	(49, 50)
Q8R307	**Vps18**	Vacuolar protein sorting-associated protein 18 homolog	LYVLNEEGGPAPV	-4.44 0.73	Supports dendrite development of Pukinje cells, critical for neuron cell survival	(41, 42)

transmission[110] and neuroinflammation[111,112]. These findings inform on the overall relevance of the CSF-peptidomic response to MWCNT exposure, highlighting a connection with neuroinflammation, neuronal stress/survival and adapted plasticity, and portending a broader neurological consequence of exposure than previously reported.

Table 1. Identification of significantly responsive to MWCNT exposure peptide factors in CSF.

* - function and references reported for PGK1 (due to 90% sequence similarity)

** - function and references reported for Tmem131 (an important paralogue of TMEM131L)

MWCNT-induced neuroinflammatory glial activation is regionally dependent. In follow-up to the pro-inflammatory and cell stress/survival associated peptide factors, we evaluated glial reactivity proximal to albumin-permeated vasculature and assess regional selectivity between cortex, striatum and thalamus. As we reported earlier[8], there was a robust increase in astrocytic GFAP staining proximal to the vasculature (**Figure 21A**). Astrocytic process morphology was substantially dilated, as quantified by the GFAP+ area fraction within a 100 µm radius of the vessel lumen (**Figure 21B**). Correspondingly, the mean fluorescence intensity within the GFAP+ area was also increased (**Figure 21C**), with both assessments consistent with reactive astrocytosis. Moreover, astrocyte processes can be seen engorged with leaked albumin (yellow streaks within red-visualized processes, **Figure 21A**), showing scavenging by proximal astrocytes.

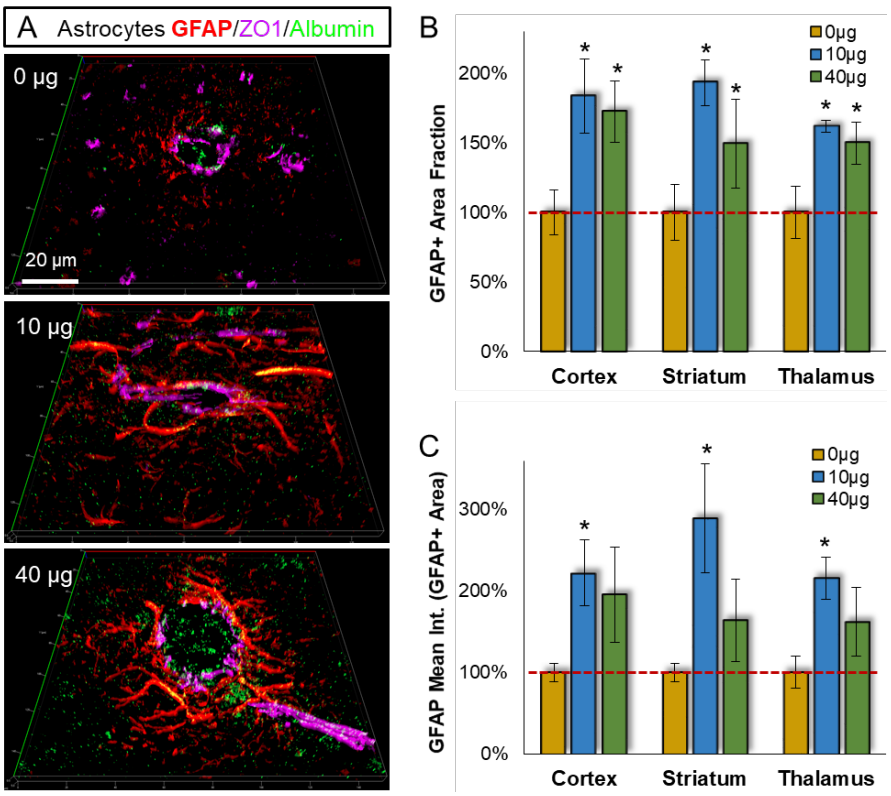

Figure 21. Pulmonary MWCNT exposure increased astrocyte reactivity across multiple brain regions. Brain tissues collected 4h after exposure were stained with the astrocyte marker GFAP (red), with counter DAPI staining for nuclei (blue) and ZO1 staining for cerebrovasculature (magenta). (A) Representative GFAP staining proximal to cerebrovasculature are shown from striatum. (B) The percent area within 100 µm of the ZO1 defined vessel wall was assessed across neocortex, striatum and thalamus, relative to the 0 µg control exposure group. (C) The fluorescent intensity of GFAP staining within 100 µm of the vessel wall was assessed relative to the 0 µg control exposure group within neocortex, striatum and thalamus. Data are presented as mean ± SEM, n=6/grp. * $p<0.05$; ** $p<0.001$. Scale bar = 20 µm.

Next, we assessed regional specificity of the astrocytotic response across MWCNT doses. While the GFAP+ area fraction increased significantly in all regions at the 10 µg dose, it was greatest in striatum (193%) > cortex (184%) > thalamus (162%), relative to the 0 µg MWCNT control group. The same trend was affirmed with the mean GFAP intensity measures, with the greatest increase in striatum (289%) > cortex (222%) > thalamus (216%). Comparatively, the astrocytotic response appeared to be less evident after the 40 µg dose across all brain regions, with the greatest GFAP+ area fraction response in cortex (172%) > thalamus (150%) > striatum (149%). A correlative trend was observed with mean GFAP intensity, however the results did not reach significance at the 40 µg dose. Assessing the morphological correlation of this dose-dependency (**Figure 21A**), we observed that reactive astrocytes were more tightly accumulated up next to the vascular lumen with the 40 µg dose, while at the lower 10 µg dose, there appeared to be a more wide-spread, less dense accumulation of reactive astrocytes that occupied a bit more of the area proximal to the leaking vessel (within 100 µm of the vessel wall).

Also observed was a significant increase in IBA1-associated microglial/macrophage reactivity surrounding leaking vessels (**Figure 22A**) that was also regionally selective. The IBA1+ area fraction increased consistently between regions and was greater at the higher dose, with the greatest response in striatum (166%/181%, respective to 10 µg/40 µg) > thalamus (88%/94%) > cortex (72%/80%) over the 0 µg control (**Figure 22B**). IBA1 mean fluorescence intensity measures followed the same profile between doses, greatest in striatum (323%/498%) > thalamus (243%/278%) > cortex (203%/273%) (**Figure 22C**). Morphologically, reactive microglia were more spread out from the leaking vessel at the 10 µg dose relative to the 40 µg of MWCNT. However, the intensity of IBA1 staining increased with dose, in contrast to the decreased GFAP staining, suggesting a more compact, IBA1-dense cellular morphology. Taken together, these data denote greater striatal susceptibility to neuroinflammation proximal to leaking cerebrovasculature, and a dose-dependency difference between astrocyte and microglial reactivity.

MWCNT-induced excitatory/inhibitory synaptic imbalance proximal to leaking cerebrovasculature. The CSF peptidomic response further suggested altered synaptic plasticity after MWCNT exposure. To test this possibility, we assessed an MWCNT-induced change in glutamatergic and GABAergic synaptic density using the selective markers Vglut1 and Gad65, respectively (**Figure 23**). Adjacent to the cerebrovasculature, there was a significant increase in Vglut1+ glutamatergic synaptic staining across all regions and at both doses relative to 0 µg MWCNT control (**Figure 23A**). The effect over control was strongest within the cortex (97%/83%, respective to 10 µg/40 µg) > striatum (80%/49%) > thalamus (51%/39%). Likewise, the effect of MWCNT on GABAergic inhibitory synaptic staining was most pronounced in cortex; however, Gad65+ staining was significantly decreased as opposed to the increase in Vglut1 (**Figure 23B**). The Gad65 decrease was more pronounced at the 10 µg than the 40 µg dose in cortex (68%/42%; 10µg/40µg) and striatum (58%/25%), while being the same for both doses in the thalamus (34%/34%). The increased density of Vglut1 appeared more localized against the vascular lumen at the 40 µg dose than at the 10 µg (**Figure 22C**), consistent with reactive astrocyte proximity to the vessel between doses. In contrast, there did not appear to be a difference in localization across GABAergic synapses, just a reduction in Gad65 accumulation on cell soma in the wider area within 100 µm of the vessel wall. Taken together, increased Vglut1 and decreased Gad65 indicated a pronounced elevation in the excitatory / inhibitory (E/I) balance with MWCNT exposure, which appeared more pronounced in the cortex > striatum > thalamus. Importantly, E/I imbalance is widely noted across behavioral and psychiatric disorders.

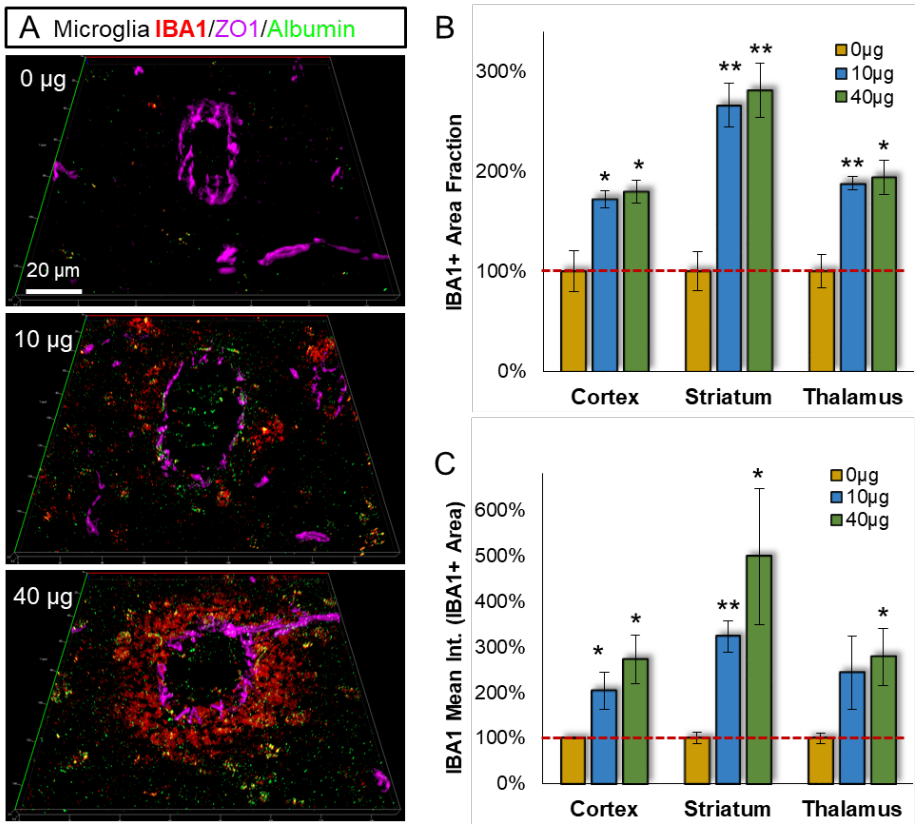

Figure 22. Pulmonary MWCNT exposure increased microglial reactivity across multiple brain regions. Brain tissues collected 4h after exposure were stained with the microglial/macrophage marker IBA1 (red), with counter DAPI staining for nuclei (blue) and ZO1 staining for cerebrovasculature (magenta). (A) Representative IBA1 staining proximal to cerebrovasculature are shown from striatum. (B) The percent area within 100 µm of the ZO1 defined vessel wall was assessed across neocortex, striatum and thalamus, relative to the 0 µg control exposure group. (C) The fluorescent intensity of IBA1 staining within 100 µm of the vessel wall was assessed relative to the 0 µg control exposure group within neocortex, striatum and thalamus. Data are presented as mean ± SEM, n=6/grp. * p<0.05; ** p<0.001. Scale bar = 20 µm.

DISCUSSION

While exposure to air pollutants has repeatedly shown an association with neurological outcomes, there remains uncertainly surrounding the mechanisms along the lung-brain axis.[113-116] Nanoparticle exposure in particular appears to compromise the BBB, whether by direct particle translocation or through indirect influences on the vascular wall and associated tight junctions[8,117-120]. We recently added that nanoparticle exposure generates proteolytic peptides that cross from the lung into circulation ad mediate systemic dysfunction of the vasculature.[56] Using mass spectrometry, a complex peptidomic response was observed that when isolated from the serum was able to induce endothelial inflammation, inhibit endothelial growth, and promote deficits in vascular tone. Exposure-mediated peptides comprised ligand functionality in the periphery, targeting cell-surface receptors. For example, we identified a 58-mer thrombospondin peptide that contained binding and modulating motifs, which we demonstrated to stimulate CD36-mediated cerebrovascular endothelial cell dysfunction. Moreover, the animals exposed to either 10 µg or 40 µg of MWCNT presented with frank BBB dysfunction, exhibiting albumin leakage and associated neuroinflammation.[8] Taken together,

we hypothesized in the present study that with a compromised BBB, MWCNT-induced bioactive peptides would cross from the circulation into the brain where they could promote dysfunction.

AIM 2.3. Engineer new software to enhance identification of endogenous biomolecules.

(i) We have succeeded in addressing this subaim, with a released version of the EndogeSeq platform that addresses the need for handling both quantitative and identification functions for peptidomic analysis. The package provides users with both a command line interface (CLI) and graphical user interface (GUI), depending on preference, to launch common functionality from the EndogeSeq processing engine. The GUI (**Figure 24A**) is preferential for most users who wish to use a standard windows-style interface, while the CLI allows more advanced users to employ batch scripting to serially execute an entire workflow with limited user intervention. The latest version at https://ottenslab.weebly.com/endogeseq.html will continued to be updated based on added functionality. The website also offers instructions for installing and use of the software. Note that this project was proposed for capability with the first commercial platform for data-independent analysis, Waters HDMSe data acquisition, which is preferential for reproducible quantification of all-ions above the limit of detection. With future funding, we hope to expand this platform to work with vendor-neutral data formats as they become standardized for data-independent workflows.

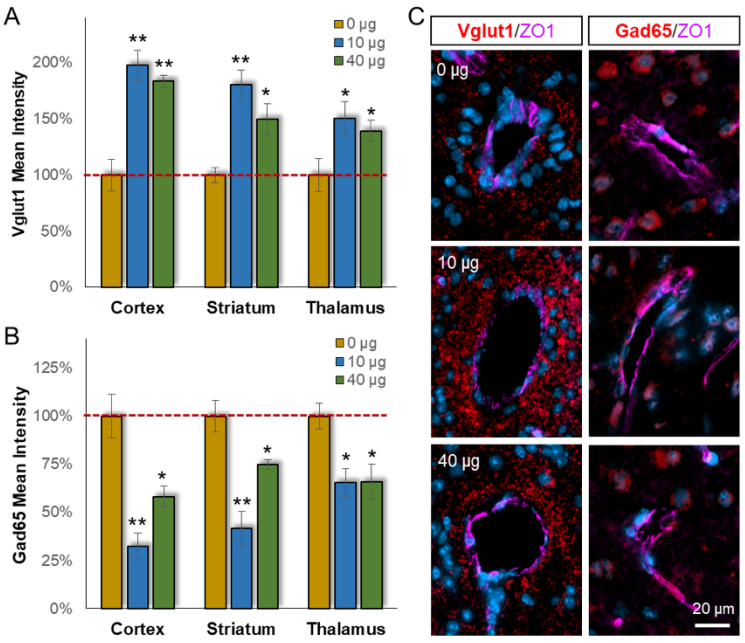

Figure 23. Pulmonary MWCNT exposure resulted in excitatory/inhibitory network imbalance. Brain tissues collected 4h after exposure were stained with either the excitatory synaptic marker Vglut1 or the inhibitory synaptic marker Gad65 (red), with counter DAPI staining for nuclei (blue) and ZO1 staining for cerebrovasculature (magenta). Densitometric analysis of (A) Vglut1 or (B) Gad65 fluorescent intensity within 100 µm of the vessel wall was assessed relative to the 0 µg control exposure group within neocortex, striatum and thalamus. (C) Representative Vglut1 and Gad65 staining proximal to cerebrovasculature are shown from striatum. Data are presented as mean ± SEM, n=6/grp. * p<0.05; ** p<0.001. Scale bar = 20 µm.

(ii) A second objective of this subaim was to optimize a scoring algorithm that was sensitive to detecting real endogenous peptides while minimizing false-positives that would limit overall performance. The rational here is that commercial software has been developed specifically for proteomic applications, where scoring is optimal in conditions where there are more than one peptide to a common protein and that those peptides are generally tryptic in nature. However, peptidomics lacks informatic constraints, challenging identification due to greater sequence-search space. We have improved our approach to address this goal by employing a mixture of known peptide sequences from JPT.com. With a library of 456 known sequences, we could better optimize scoring to discriminate real identifications from random or off-target identifications after spiking this mixture into a complex medium. Tabulating a series of metrics on each matched sequence to an ion event, we then used discriminant analysis (PLS-DA) to resolve the most discriminant

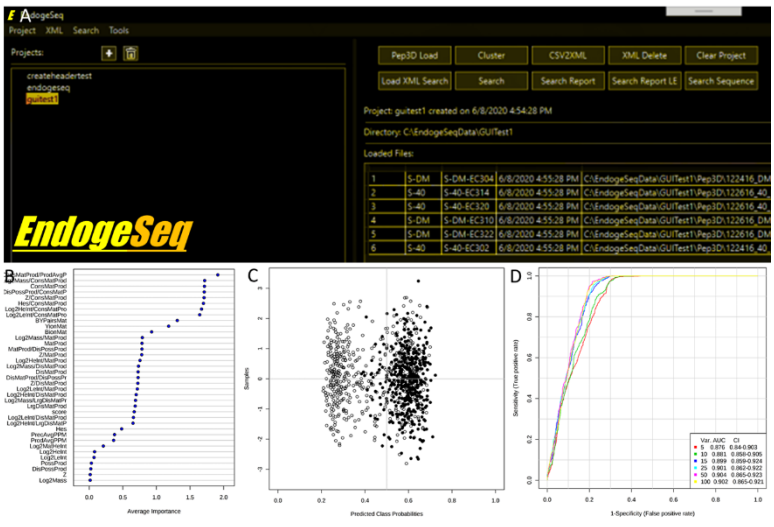

Figure 24. EndogeSeq Bioinformatics Software development. (A) The graphical interface for using EndogeSeq. (B) Scoring was optimized using PLS-DA discriminant analysis to identify variables that most effectively differentiated known peptides within a complex mixture. (C) Scoring models employing multiple variables provided for AUC measures above 0.87, with 80% specificity at 90% sensitivity to detect real features spiked into the sample.

variables (**Figure 24B**). In the end, we determined that a count of discrete matched product ions was best taken as a ratio to the total number of discrete possible products for a given peptide sequence. And that this ratio could then be normalized across ion events to the count of products observed for a given ion. This last step is particularly important for data-independent analysis, where there often are distractor product ions present due to stochastic product-to-precursor events. This compound variable was the major discriminant, which was aided by a second ratio that took the summed ion intensity for all matched products and divided that by the total product ion intensity for each ion event (i.e., an account of product ion intensity that was matched to the given sequence). Lastly, the sum of these two variables was corrected by the inverse of the mean product ion matching mass error, which generally was higher for false matches than for real detections. This score algorithm was found highly predictive of true positive identifications (**Figure 24C**) providing an AUC of 0.87 with five variables recognized and specificity of 80% at 90% sensitivity.

(iii) The last objective was to compare identification performance between EndogeSeq and other search engines. For this purpose we took advantage of the JPT SpikeMix being a set of known tryptic peptides that could be searched using conventional tryptic-specificity on our Waters PLGS software, which provided us with a control level of true positive identifications by which to assess the non-enzyme specific search performance of EndogeSeq and other software. As it turns out, EndogeSeq outperformed all other tested search engines, achieving 77% if true positive IDs at a 10% false-detection-rate, with the next best being the De-Novo search program Peaks (**Figure 25**). However, EndogeSeq performed best when we did not use its mass-tag functionality, which identified only 162 (48%) of possible true positives in the sample set. We initially proposed to use a mass-tag approach in order to reduce the sequence-search space based on this partial de-novo approach. We built the mass-tag functionality upon the available free-use software DirecTag from David Tabb's research group (Vanderbilt). While this function did reduce sequence search space, it also limited the number of ion events that could be searched because so few had discernable mass tags (easily resolved consecutive amino acid product masses). This inflated the true negative rate, which resulted in worse performance than the standard database search-functionality of EndogeSeq.

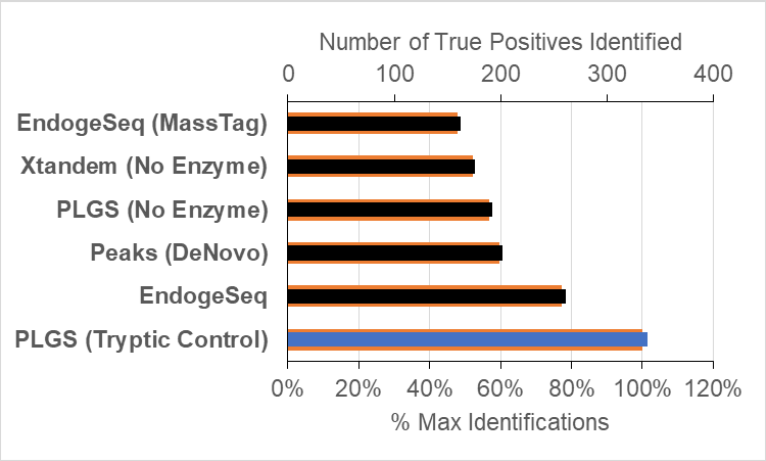

Figure 25. EndogeSeq Bioinformatics Software development. (A) The graphical interface for using EndogeSeq. (B) Scoring was optimized using PLS-DA discriminant analysis to identify variables that most effectively differentiated known peptides within a complex mixture. (C) Scoring models employing multiple variables provided for AUC measures above 0.87, with 80% specificity at 90% sensitivity to detect real features spiked into the sample.

(iv) We've added additional functionality to EndogeSeq that provides for a more effective workflow. Clustering functionality allows the user to provide a full study of samples from different groups and biological replicates, and then match ion events and tabulating their ion intensity effectively across all replicates. Then we've built into the workflow the ability to perform ion filtering and statistical analysis to reduce the number of ion events that need to be searched, which increases the speed of analysis and eliminates non-reproducing distracting ion events. Moreover, we utilize the clustering functionality to then average out the aligned product mass spectra, which effectively improves signal-to-noise.

AIM 3. Characterize MWCNT-induced inflammatory potential and seromic response in samples derived from an occupationally-exposed human cohort. Allied with an NIOSH cross-sectional epidemiologic and carbon nanotube/nanofiber (CNT/CNF) exposure assessment study, we assessed collected serum specimens for endothelial activation linked to CNT/CNF personal breathing zone measurements of elemental carbon, and examined a correlated induction of seromic factors for diagnostic model building.

Exceedingly few human outcomes studies have been conducted with respect to inhaled ENM and cardiovascular risks. We have previously explored the circulatory impacts of diesel emissions and nitrogen dioxide in controlled human studies in collaboration with the Human Studies Division of the Environmental Protection Agency. In these studies, serum was drawn prior to and after 2 h exposures to 100 μg PM/m^3 diesel and these serum samples were used to treat human coronary artery endothelial cells (hCAECs), which were

subsequently assayed for transcriptional changes. Vcam1, Il8, and Icam1 were shown to be upregulated by serum obtained after exposure to diesel, compared to pre-exposure or filtered air (sham) exposures (**Figure 26**). Microarray analysis of the hCAEC response revealed a clear link to NFkB and E2F activation cause by components of the serum following diesel exposure (**Figure 26**).

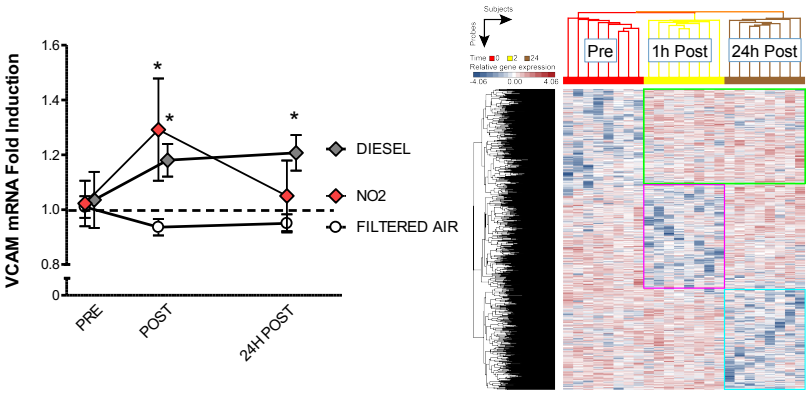

Figure 26. Basis of the Serum Cumulative Inflammatory Potential (SCIP) assay. Shown is VCAM-1 mRNA expression in hCAECs incubated for 24 hours with plasma from humans obtained before, immediately after, or 24 h after exposure (left).[1,2] Subjects were exposed for 2 h to 100 μg/m^3 diesel emissions or 500 ppb NO_2, compared to filtered air control exposures. N=7 per group with repeated measures for each exposure (diesel and filtered air). Asterisks denote significant difference from control ($p<0.05$) by 2-way ANOVA. Notably, both diesel and NO_2 induce early changes in the plasma, but the PM-containing diesel atmosphere causes a prolonged induction of circulating inflammatory potential. Similar findings were noted for ICAM and p-selectin, and microarray analysis is currently ongoing to more fully characterize these responses (right). Such inquiry revealed expected outcomes related to NFkB and TGF-β activation, but also novel pathways of WNT and FAS.

Subject Recruitment. Blood specimens were provided through collaboration with Dr. Mary Schubauer-Berigan from exposed workers. The source population was selected from facilities producing, using or distributing CNT or CNF at/above R&D scale in the U.S. Subjects were enumerated in a Phase I feasibility study and augmented during Phase II using several additional sources (*e.g.*, registrations with the US Environmental Protection Agency to manufacture or use CNT or CNF). Frozen serum samples (1 ml aliquots) were shipped to UNM de-identified and coded such that data generated in the present Aim can be incorporated into overall models of health outcome and risk assessment, along with many other conventional biomarkers (C-reactive protein, TIMP2, IL-6, etc).

Concurrent worker exposure assessment. In conjunction with biological fluid collection, detailed exposure assessment for each worker was performed. Individual full-shift personal breathing zone samples were collected to measure elemental carbon and quantitate exposure by developing structure counts methodologies. The current NIOSH REL for carbon nanotubes and nanofibers is based on the mass measurement of elemental carbon and represents the best measure for worker exposure. Prior to the beginning of this study, no biological outcomes with paired exposure assessment had been published in workers handling CNT/CNF.

AIM 3.1. Characterize MWCNT-induced inflammatory potential and seromic response in samples derived from an occupationally-exposed human cohort.

Determine bioactivity of serum in endothelial biosensor assays. In year 1, we received approval to use the serum samples and had an MOU in place with our colleagues at NIOSH in Cincinnati. In year 2 we received serum samples and begun treatments of serum on endothelial cells in culture. Serum was obtained from a cohort of 106 subjects with data linked to CNT/CNF personal breathing zone measurements of elemental carbon (courtesy of Mary Schubauer-Berigan and Matthew Dahm). In year 3 we completed treatments of serum on endothelial cells in culture, using both human coronary artery endothelial cells (HCAECs) and human umbilical vein endothelial cells (HUVECs). Briefly, cells were incubated with 2.5% serum vol/vol in media for 4h, after which cells were harvested for RNA isolation and quantitative polymerase chain reaction measures of transcripts (Il6, Ccl2, Vcam1, Icam1, Tnfa, Tgfb). We evaluated the correlated induction of seromic factors to build a blood diagnostic of occupational ENM exposure. In year 4, we began developing multivariate strategies to address the association between exposure metrics and outcomes, under consulation with the director of the UNM Clinical and Translational Science Center's Biostatistics, Epidemiology and Research Design Core, Dr. Yiliang Zhu.

Genes assessed in HCAECs treated with subjects' serum included Il6, Ccl2, Tnfα, Tgfβ, Vcam1 and Icam1. Multiple regression analyses of qPCR data from factory worker serum-exposed HCAEC, assessing correlations of significant primary (SWCNT, MWCNT and CNF) and secondary (Solvent and Polymers, Acids and Dust) exposure variables, revealed coefficients with a mix of positive and inverse correlations ranging from -0.63 to 0.08 in IL-6 and -0.04 in Ccl2. Other genes assessed exhibited no significant primary variable associations with a primary or secondary exposure variable. Il6 was significantly associated with primary CNF past exposure duration ($p = 0.0003$), solvent past (-0.07; $p = 0.2418$) and current (0.08; $p = 0.2727$) exposure and polymers, acids and dust current (-0.10; $p = 0.1857$) exposures (**Table 2**).

After adjusting from confounding factors, individuals with at least some college education showed positive associations with significant primary and secondary variables. Lifestyle factor current alcohol usage was correlated with inflammatory serum potential from primary and secondary particle exposure. Smoking was also significantly associated with Il6 gene expression, with those workers who never smoked being inversely associated with inflammatory potential. Former and current smokers were positively associated. Considering health data from factory worker group, waist circumference below 102 cm was negatively associated with an inflammatory activation, while waist circumference above 112 cm was positively associated (0.16; p = 0.2649). Serum from workers who responded in the affirmative to having a current cold and suffering from hypertension and respiratory allergies were negatively associated with gene expression. Hypertension medication use was positively correlated with Il6 expression.

	EXPOSURE METRIC or COVARIATE	GENE EXPRESSION CHANGE (p-value)		EXPOSURE METRIC or COVARIATE	GENE EXPRESSION CHANGE (p-value)
IL-6	**Exposures**		CCL2	**Exposures**	
	CNF_Past	-0.63 (0.0003)		*log(EC_RC*current job duration)*	-0.04 (0.0289)
	Solvent_Current	0.08 (0.2727)		**Lifestyle**	
	Solvent_Past	-0.07 (0.2418)		*Alcohol_cur*	-0.17 (0.0631)
	Polymers, Acids, Dust Current	-0.10 (0.1857)		*SmokingFormer*	0.19 (0.1940)
	Education			*SmokingNever*	0.06 (0.6511)
	Education2: Some college	0.06 (0.6095)		**Health Metrics**	
	Education3: College graduate	0.20 (0.0787)		*BMI_cat2: 25-<30*	-0.09 (0.4290)
	Education4: Postgraduate	0.30 (0.0105)		*BMI_cat3: 30-<35*	-0.04 (0.8243)
	Lifestyle			*BMI_cat4: >=35*	-0.18 (0.5255)
	Alcohol_cur	-0.08 (0.2642)		*Waist_cat_cm2: >80 to 88*	-0.14 (0.3199)
	SmokingFormer	0.01 (0.8959)		*Waist_cat_cm3: >88 to 95*	0.01 (0.9305)
	SmokingNever	-0.10 (0.3297)		*Waist_cat_cm4: >95 to 102*	-0.05 (0.7681)
	Health Metrics			*Waist_cat_cm5: >102 to 112*	-0.06 (0.7714)
	Waist_cat_cm2: >80 to 88	-0.10 (0.3409)		*Waist_cat_cm6: >112*	0.21 (0.5289)
	Waist_cat_cm3: >88 to 95	-0.09 (0.3622)		**Demographics**	
	Waist_cat_cm4: >95 to 102	-0.03 (0.8005)		*Age_Cat2: 25-<35*	0.15 (0.4537)
	Waist_cat_cm5: >102 to 112	-0.12 (0.2976)		*Age_Cat3: 35-<45*	0.21 (0.3469)
	Waist_cat_cm6: >112	0.16 (0.2649)		*Age_Cat4: 45-<55*	0.19 (0.3855)
	Current_cold	-0.09 (0.3840)		*Age_Cat5: 55-<65*	0.13 (0.5658)
	Hypertension	-0.08 (0.4260)		*Age_Cat6: >=65*	0.07 (0.7901)
	Resp_Allergy	-0.14 (0.0329)		*Sex1 - Female*	-0.19 (0.0924)
	hypertension_med	0.31 (0.0265)			
	Demographics				
	Age_Cat2: 25-<35	-0.24 (0.1311)			
	Age_Cat3: 35-<45	-0.17 (0.3399)			
	Age_Cat4: 45-<55	-0.21 (0.2054)			
	Age_Cat5: 55-<65	-0.27 (0.1183)			
	Age_Cat6: >=65	-0.35 (0.0950)			

Table 2. Results of multi-linear regression modeling of HCAEC inflammatory gene expression from serum cumulative inflammatory potential assay of human serum on endothelial cells in culture. Shown are associations with exposure measures and covariates from mulivariate regression modeling.

Ccl2 gene expression of HCAEC responding to nanomaterials serum showed an inverse association with primary metric respirable elemental carbon exposure (RC_EC) current exposure duration (p = 0.0289). No secondary exposure variable was associated with Ccl2 gene expression. Confounders of lifestyle, health metrics and age and sex demographics were associated with the RC_EC primary exposure. Current alcohol use was inversely correlated with Ccl2 gene expression and both non- and former- smokers showed positive correlation with Ccl2 exposure (0.06; 0.6511 and 0.19; p = 0.1940; respectively). Health assessment associated with primary exposure was both body mass index (BMI) and waist circumference. BMI indices 25 and higher being inversely correlated. Waist circumference showed mixed correlation with lowest recorded

being inversely correlated and highest recorded being positively correlated (0.21; p = 0.5289) with gene expression. Age association were positively correlated for individuals 25 and older. Serum from female workers was inversely correlated with a positive inflammatory response (-0.19; p = 0.0924).

We also used HUVECs for the *in vitro* assessment of nanomaterials factory worker serum inflammatory potential. Resultant qPCR data was subjected to multiple regression analyses for correlations of significant primary (SWCNT, MWCNT and CNF) and secondary (Solvent and Polymers, Acids and Dust) exposures, as well as associations of demographic, lifestyle, and health confounders. Tnfα and Tgfβ genes were the only genes with significant associations with primary exposure variables (**Table 3**). Coefficients showed inverse associations with primary variables and positive associations with secondary exposure variables (Solvent exposure). Other genes assessed exhibited no significant primary variable associations with a primary or secondary exposure variable. Tnfα was associated with the combined primary variable of respirable elemental carbon, inhalable elemental carbon and TEM (RC, IC, TEM) current exposure duration (p = 0.0019) and secondary exposure variable current solvent (p = 0.0057). Education was positively correlated with gene expression for workers with at least some college education; given the increased exposure risk for engineers with higher levels of education, this is not unexpected. Tnfa was positively correlated with the incidence of hypertension and inversely correlated with the use of hypertension medications.

	EXPOSURE METRIC or COVARIATE	GENE EXPRESSION CHANGE (p-value)
TNF-α	**Exposures**	
	*log((RC+IC+TEM)*current job duration))*	-0.17 (0.0019)
	Solvent_Current	0.72 (0.0057)
	Education	
	Education2: Some college	0.30 (0.4907)
	Education3: College graduate	0.38 (0.3369)
	Education4: Postgraduate	0.71 (0.0701)
	Health Metrics	
	BMI_cat2: 25-<30	0.51 (0.1263)
	BMI_cat3: 30-<35	0.02 (0.9666)
	BMI_cat4: >=35	-0.88 (0.2500)
	Waist_cat_cm2: >80 to 88	0.13 (0.7503)
	Waist_cat_cm3: >88 to 95	0.05 (0.9176)
	Waist_cat_cm4: >95 to 102	-0.62 (0.2267)
	Waist_cat_cm5: >102 to 112	0.59 (0.3322)
	Waist_cat_cm6: >112	0.42 (0.6536)
	Hypertension	0.96 (0.0085)
	hypertension_med	-1.73 (0.0014)
	Demographics	
	Age_Cat2: 25-<35	-0.42 (0.4671)
	Age_Cat3: 35-<45	-0.66 (0.2976)
	Age_Cat4: 45-<55	-0.02 (0.9706)
	Age_Cat5: 55-<65	1.02 (0.1031)
	Age_Cat6: >=65	-0.21 (0.7988)
	Sex1 - Female	0.41 (0.1988)
	Race1 - Multi,Black,AIAN,Hisp	-0.04 (0.9164)
	Race2 - Asian	0.69 (0.1199)

	EXPOSURE METRIC or COVARIATE	GENE EXPRESSION CHANGE (p-value)
TGF-β	**Exposures**	
	*log(EC_IC_avg * CurExpDur)*	-0.03 (0.0082)
	Solvent Current	0.16 (0.0565)
	Education	
	Education2: Some college	0.12 (0.4181)
	Education3: College graduate	0.07 (0.5966)
	Education4: Postgraduate	0.13 (0.3101)
	Health Metrics	
	BMI_cat2: 25-<30	0.06 (0.5744)
	BMI_cat3: 30-<35	0.01 (0.9577)
	BMI_cat4: >=35	-0.33 (0.2009)
	Waist_cat_cm2: >80 to 88	0.06 (0.6393)
	Waist_cat_cm3: >88 to 95	0.21 (0.1696)
	Waist_cat_cm4: >95 to 102	-0.12 (0.4839)
	Waist_cat_cm5: >102 to 112	0.20 (0.3175)
	Waist_cat_cm6: >112	0.16 (0.6191)
	Current_cold	-0.29 (0.0337)
	Asthma_bronchitis_emphysema	0.21 (0.0397)
	Hypertension	0.22 (0.0721)
	hypertension_med	-0.20 (0.2639)
	Demographics	
	Age_Cat2: 25-<35	-0.10 (0.6303)
	Age_Cat3: 35-<45	-0.14 (0.5049)
	Age_Cat4: 45-<55	-0.22 (0.2763)
	Age_Cat5: 55-<65	-0.09 (0.6491)
	Age_Cat6: >=65	-0.33 (0.2299)
	Sex1 - Female	0.14 (0.1813)
	Race1 - Multi,Black,AIAN,Hisp	-0.20 (0.1316)
	Race2 - Asian	0.29 (0.0508)

Table 3. Summary of Significant Associations of Primary Exposure Variables with Inflammatory Gene Expression in human umbilical vein endothelial cells (HUVECs).

Tgfβ from HUVECs was inversely associated with the inhalable elemental carbon (EC_IC) current exposure category (p = 0.0082) and positively associated with current solvent secondary exposures (0.16; p = 0.0565). Education was positively correlated for all workers with at least some college education. BMI below 35 showed a positive correlation with primary exposure, while BMI higher than 35 was inversely associated. Waist circumference 95 cm and below, as well as 102 and above were positively associated with a TGF-β gene

expression. Only waist circumference between 95 and 102 cm displayed an inverse association with TGF-β. Workers with health affirmative questionnaire responses for current cold and hypertension medication use showed inverse correlations with gene expression, while asthma/bronchitis/emphysema and hypertension were positively associated.

Overall, the findings from the serum cumulative inflammatory potential assays in both HCAECs and HUVECs were modest. We have never previously so deeply interrogated the data with multivariate modeling to observe such limited effects, even with a small epidemiological cohort study.[121] Additionally, recent studies with colleagues in China found that this in vitro serum inflammatory potential assay behaved predictably in a cohort of workers exposed to much higher levels of carbon nanoparticles (657 μg/m^3).[122,123]

Thus, we conclude that the modest effects seen in the present study, where two different cell types were used as an experimental redundancy, and advanced multivariate modeling was applied to identify relationships between exposure metrics and inflammatory potential, are largely due to tight occupational controls in the US-based cohort. With most personal breathing zone measures below 10 μg/m^3,[5] we conclude that this cohort was largely well-protected. However, a few subjects did have substantial exposures, and we conducted further inquiries to better address this issue

AIM 3.2. Peptidomic Assessment of Serum from Highly-Exposed Subjects. In Year 3, we performed a pilot experiment assessing the nanomaterial-exposure biomarker potential of circulating serum peptides using a selected cohort of n=8 high exposed subjects based on at least one elemental carbon (EC) exposure metric graded ≥5 (exposure duration >6 years; respirable EC >0.25 μg/cm^3; inhalable EC >0.5 μg/cm^3; TEM EC deposition >0.1 μg/cm^3) and n=8 low exposed subjects based on no EC metrics graded above 3 (respirable EC <0.25 μg/cm^3; inhalable EC <0.15 μg/cm^3; TEM EC deposition <0.02 μg/cm^3). Subjects were excluded from consideration if they were current smokers, had a cold or lung ailment, or were on nonsteroidal anti-inflammatory drugs. The sampled cohort over-represented female subjects at 37.5% relative to 22% in the total population. Samples were processed blind to treatment and analyzed in a sequential random order using reversed-phase capillary chromatographic separation online with a hybrid ion-mobility tandem mass spectrometer using data independent acquisition. 883 highly reproducible (75% replication) peptide measures were extracted, with 292 (**Figure 27A**) showing a significant effect of nanomaterial exposure (FDR 5%, q-value to correct for multiple measures). Based on these significant peptide measures, subjects tightly clustered into two distinct groups with non-supervised principal component analysis (**Figure 27B**), with one outlying high-exposure subject due to poor peptide coverage (poor data quality, **Figure 27C**). A majority of the increased peptide measures were consistently detected across the remaining 7 subjects, with 58% of variance explained by the first principal component.

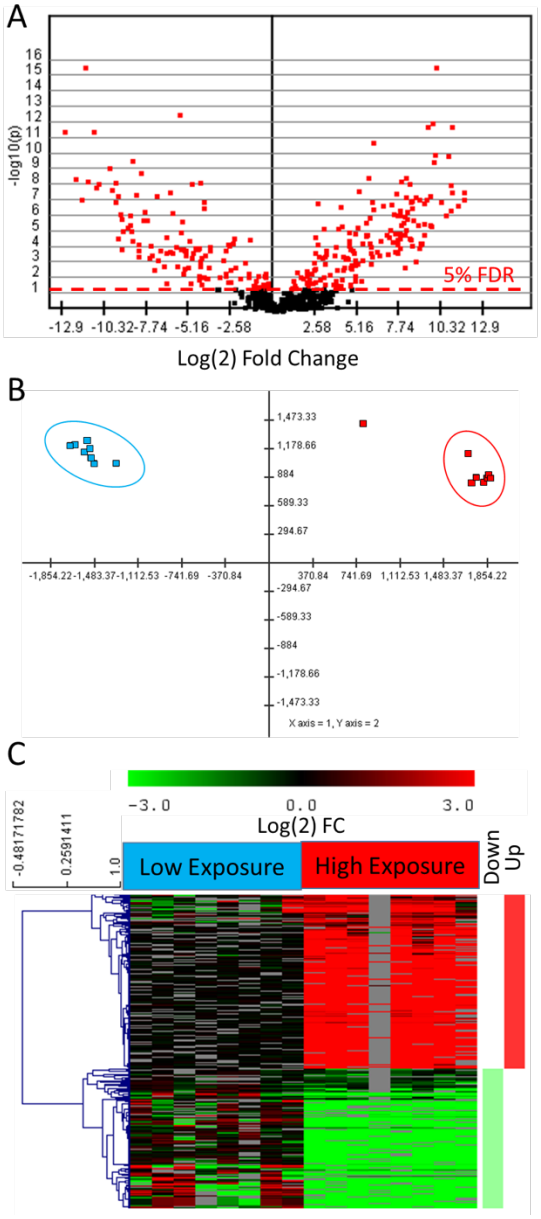

Figure 27. Peptidomic profile in serum distinguishes worker exposure to higher amounts of nanomaterial. (A) Volcano plot depicting 292 significantly (red) shifted peptide measures within serum of workers exposed to higher amounts of nanomaterial during the study period that had a minimum of a six-year history of exposure. (B) Peptidomic profile highly biased a distinction between those with high and low nanomaterial exposure in an unsupervised principal component analysis. (C) Among significant peptides a majority showed a 6-fold or greater abundance in high-exposure subjects, as illustrated here by a heatmap projection, a finding that was reproducibly detected across the cohort.

We leveraged our pilot study to further optimize the chromatography and m/z settings for analysis. As well, we increased power by identifying additional subjects to include in the proposed case-control study. Twelve individuals with an inhalable EC measure > 0.5 μg/cm3 (inhalable EC mean 8.71±5.40 μg/cm3; respirable EC

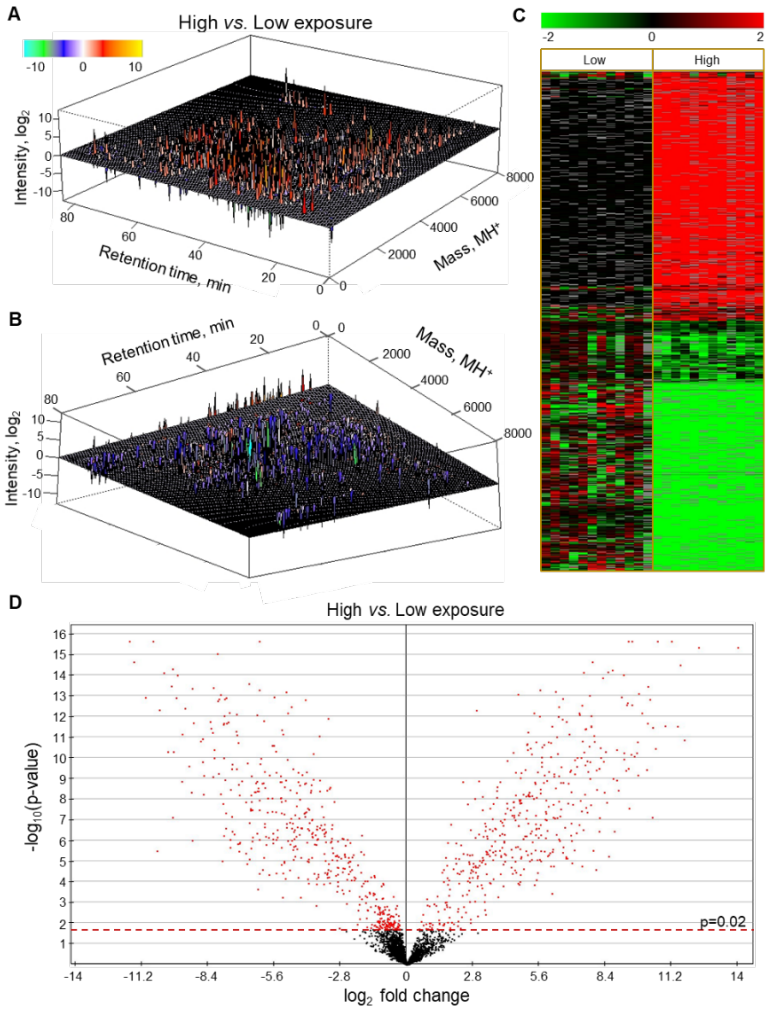

Figure 28. The carbon nanomaterial-exposure discriminant circulating peptidome among manufacturing workers. Between the two worker populations, the serum peptidomic fraction exhibited both significantly (A) increased (view from above, ion intensity markers point up) and (B) decreased (view from below, ion intensity markers point down) molecular abundance as illustrated here by perspective plots against distinct mass and chromatographic retention time measures. In total, 934 significantly responsive peptide factors were determined with a high-level of reproducibility across subjects (≥75% reproducibility across workers) as illustrated (C) by the heatmap (intensity per subject, with a color scale of the log(2) fold change from the mean measure across the Low EC group) and (D) volcano plots (log(2) fold change in peptide measure between High and Low EC groups plotted against the statistical p value, cutoff at a 5% false discovery rate).

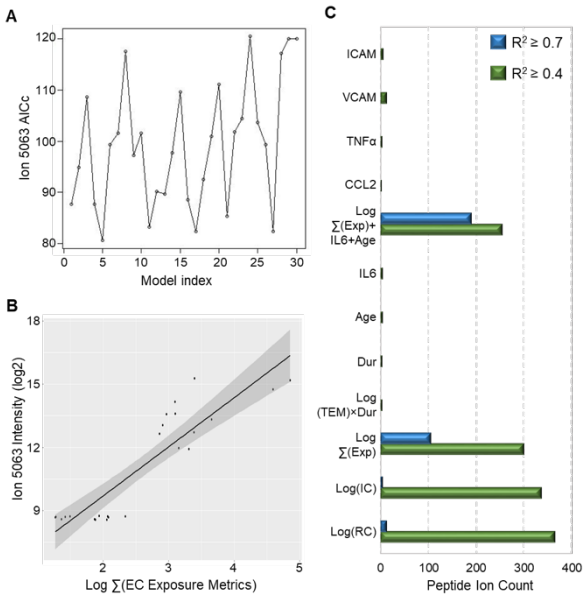

Figure 29. Model quality assessed against discriminant serum peptidomic features. Model results were assessed for out-of-sample predictive error using the corrected Akaika information criterion (AICc), which estimates the information loss of each model (lower AICc is better), (A) exemplified here for peptide ion 5063 (a subset of 30 models illustrated, for full 237 models representation see Supplementary figure 1), (B) following linear regression (Shapiro). Model quality was then assessed (C) by a higher number of peptide ions demonstrating a minimum AICc for that model after filtering by R2 values for each ions correlation. Simpler models with exposure metrics are preferred over more complex, multivariate models, since AIC estimation penalizes models with a greater number of variables; thus, the model built with the Log ∑(EC Exposure Metrics) was selected, which accounts for EC exposure based on the combination of respirable and inhalable ambient levels and the concentration of EC species detected in the sputum.

mean 1.56±0.96 µg/cm3) were selected as a high exposure group, while twelve workers with inhalable EC measures < 0.1 µg/cm3 (inhalable EC mean 0.05±0.01 µg/cm3; respirable EC mean 0.02±0.01 µg/cm3) were assigned as a low exposure group. Subjects were excluded from consideration if they were active smokers, had known respiratory (include colds) disease, or were on nonsteroidal anti-inflammatory drugs. Samples were analyzed using data-independent analysis and processed via EndogeSeq software to align ion events across biological replicates based on common accurate mass, retention time and drift time measures. We detected 11,546 reproducible features in the enriched peptide serum fraction that were reproducible across 50% or more subjects, of which 2,726 were significantly different between groups. Given the complexity, we restricted further analysis to those peptide measures that were detected in 75% or more subjects, with consistency of detection being useful for diagnostic discrimination. In total, 934 significantly distinctive measures were detected at this high-level of reproducibility (**Figure 28**). These features were distributed uniformly across retention time (10 – 36% acetonitrile) and mass (between 1000 to 8000 Da). These findings demonstrate that there is a highly complex circulating peptidome within the serum and that it is significantly responsive to higher-levels of carbon nanotube / nanofiber (CNT/F) in occupational exposures. We can see the positive impact of sampling across more subjects in provide greater depth of coverage on the responsive serum peptidome in comparing results between **Figures 27** and **28**.

The next step was to assess the CNT/F exposure and demographic variables that best explained the observed peptide variability across subjects. We utilized linear regression and the Akaike information criterion (AICc) to consider measures of inhalable and respirable elemental carbon and electron micrograph-counted CNT/F structures as the three personal breathing zone metrics. Covariates considered included metrics such as subject age, gender, and duration of past exposure. In addition, we also included measures from the serum cumulative inflammatory potential assay, mentioned above in Aim 3.1. The lowest AIC scores appeared for models containing the summation of all three exposure metrics (log transformed to achieve normality), including models 5 and 10 (**Figure 29A**). These models exhibited the greatest degree of linear correlation across the peptidome, with over 100 peptides exhibiting an $R^2 > 0.7$ (**Figure 29B,C**). While model 10 was exclusively the summated set of exposure metrics, model 5 also added subject age and IL6 induction within the SCIP assay. However, the AICc method is known to exhibit model over-fitting when using a greater number of variables, so we opted to use the simpler model 10 for further development.

We next employed partial least squares discriminant analysis (PLSDA) to prioritize the most discriminatory peptide measures between high-exposed and low-exposed subjects (**Figure 30A**). Variable importance scores (VIP) ranked those peptides features (**Figure 30B**). Given how distinctive the top ranked peptides were per group, analyses showed an AUC of 1, with perfect discriminatory performance across model subjects. Thus, we then subdivided subjects into training and validation cohorts to investigate model predictive performance. In validation set of 6 subjects per group, cross-validation testing using the leave-one-out approach again demonstrated perfect discrimination (**Figure 31B**), underlining the capacity of the serum peptidome to differentiate among those with occupational CNT/F exposure, recalling that these peptides were linearly correlated across subject exposure. Moreover, we verified that the PLSDA performance was not compromised by over-fitting by observing complete separation of the two subject cohorts using unsupervised principal component analysis (PCA) (**Figure 31A**).

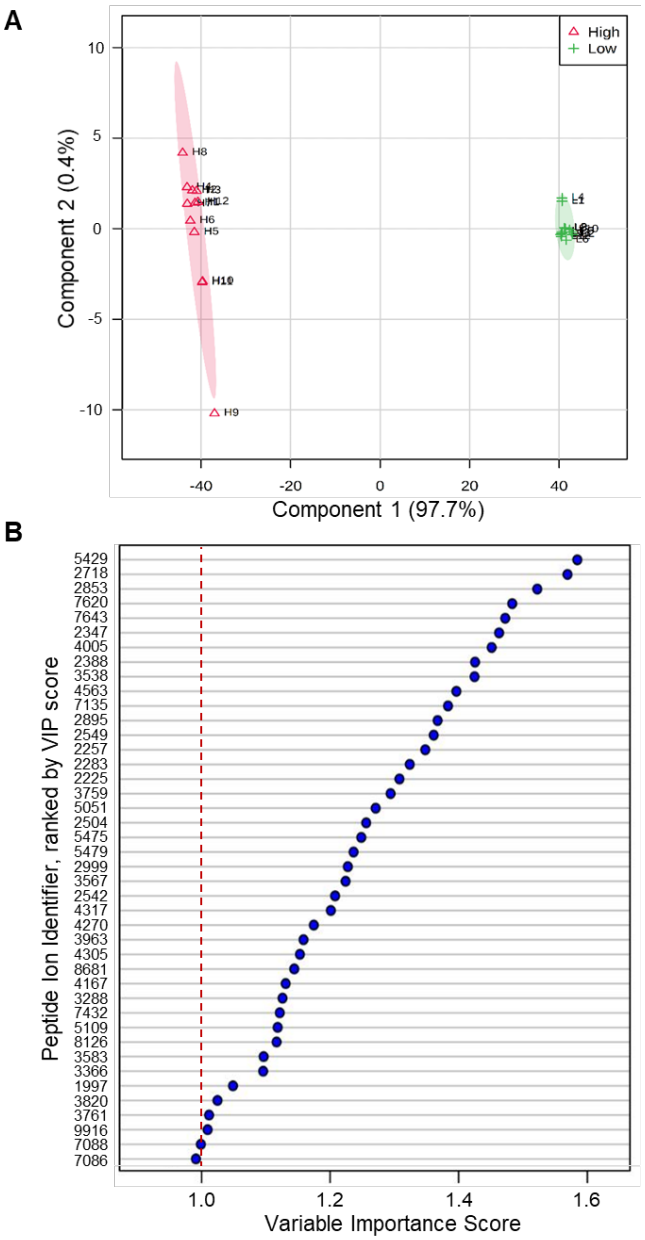

Figure 30. Discriminant peptide ion selection for biomarker model refinement. Partial least square discriminant analysis (PLS-DA) was employed to select the most predictive peptide ion features to (A) resolve the High EC and Low EC exposure groups based on the select 104 factors with R2>0.7 with Log ∑(EC Exposure Metrics). The contribution of each peptide ion to the PLS-DA model is then calculated as a weighted sum to the squared correlations, (B) producing a variable importance in projection score that can be used to rank ion features. (C) The top five scoring peptide ion features are quantitatively selective of samples in the High EC or Low EC exposure groups.

We next employed EndogeSeq for identification of the discriminatory peptides, focusing on the 41 top ranked (VIP score >1.0) out of the 104 that exhibited linear correlation with R^2>0.7. We were able to identify 27 sequences from 20 parent proteins. Eight of these were fragments of fibrinogen A, with 7 being variants of fibrinopeptide A. The remainder were related to vascular dysfunction, pulmonary injury, altered translation and autophagy/endocytosis processes (**Figure 32**), all of which fit with pathological outcomes found in modeled CNT/F exposure.

In conclusion, while health effects among CNT/F workers have yet to be clearly demonstrated, these findings reveal that there is a robust and highly discriminatory shift within the circulating peptidome that is linearly correlated with the log of personal breathing zone metrics of exposure. Moreover, the identified peptides reflect pathobiology that is consistent with negative pulmonary and vascular outcomes observed in modeled CNT/F

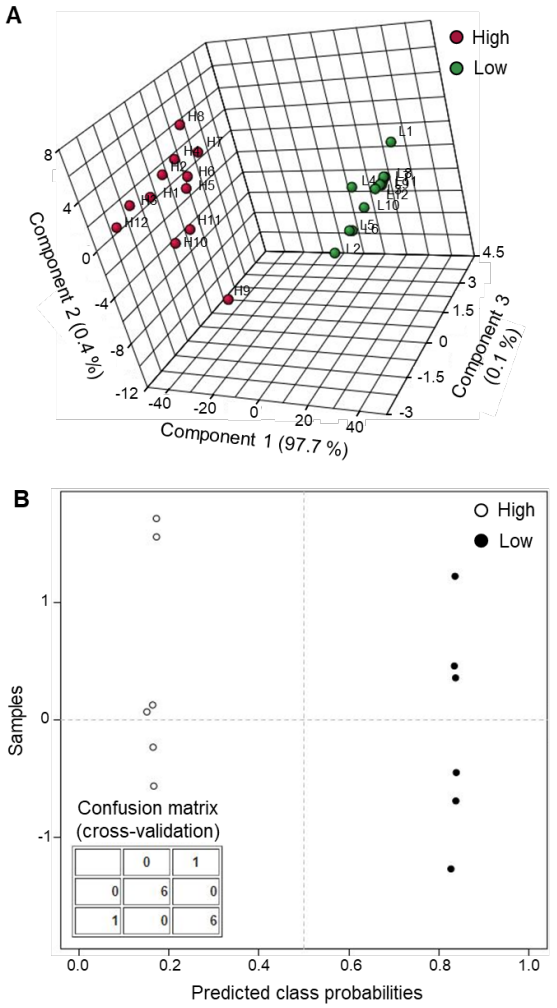

Figure 31. Validation of the peptide-ion serum biomarker model of carbon nanomaterial exposure. As a check against overfitting of the PLS-DA model, the originating peptide ion data were evaluated using unsupervised principal component analysis, an orthogonal means of assessing the structure of the data. (A) A three dimensional projection of each worker's serum peptidomic signature is shown with the first principal component explaining 97.7% of sample variance and distinctly resolving High EC from Low EC groups. Model evaluation on a separate subset of six High EC and six Low EC exposure worker samples was performed, with (B) perfect predictive performance as shown in this predictive class probability plot and confusion matrix.

exposure. These data support further development of peptide biomarkers for monitoring *in vivo* responses to CNT/F exposure among workers and the use of such diagnostics in longitudinal observational studies.

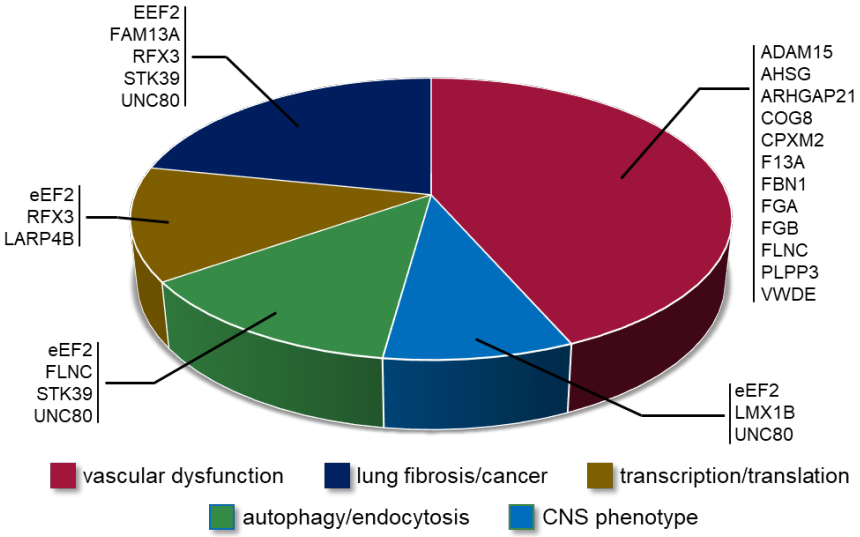

Figure 32. Select discriminant peptide factors with VIP > 1 were searched against human protein database for sequence assignment. All identified proteins were annotated and characterized into functional groups based on their biological role confirmed in literature.

PUBLICATIONS

Manuscripts (Accepted & Under Review)

1. Aragon M, Topper L, Tyler CR, Sanchez BN, Zychowski KE, Young T, Herbert G, Hall P, Erdely A, Eye T, Zeidler-Erdely P, Ottens AK, Campen MJ. Serum-Borne Bioactivity Caused by Pulmonary Multiwalled Carbon Nanotube Exposure Induces Neuroinflammation Via Blood Brain Barrier Impairment. Proc Natl Acad Sci USA, 114(10):E1968-E1976, 2017. PMID: 28223486
2. Mostovenko E, Young T, Muldoon PP, Canal CG, Vucetic A, Erdely A, Campen MJ, Ottens AK. Proteolytic Peptide Products as Drivers of Systemic Functional Deficits Evoked by Pulmonary Nanomaterial Exposure. Particle and Fiber Toxicology. PMID: 31142334
3. Young TL, Zychowski KE, Denson JL, and Campen MJ. Blood-brain barrier at the interface of air pollution-associated neurotoxicity and neuroinflammation. In Advances in Neurotoxicology, vol. 3, Aschner M and Costa L, eds. 2018.
4. Mostovenko E, Saunders SA, Muldoon PP, Bishop L, Campen MJ, Erdely A, Ottens AK. Carbon Nanotube Exposure Triggers a Cerebral Peptidomic Response: Barrier Compromise, Neuroinflammation and a Hyperexcited State. Under Review, Toxicological Sciences, TOXSCI-20-0612.

Manuscripts (in preparation)

5. Young TL, Sanchez B, Herbert G, Lucas S, Ottens AK, Erdely A, Campen MJ. Time Course Relationships Between Airway Inflammation and Systemic Vascular Responses Following Pulmonary Multiwall Carbon Nanotube Exposures. In preparation for submission to Inhalation Toxicology.
6. Young T, Begay JG, Lucas S, Herbert G, Zychowski K, Hunter R, Salazar R, Mostovenko E, Wang T, Erdely A, Ottens AK, Campen MJ. Role of matrix metalloproteinases in multiwalled carbon nanotube-mediated pulmonary and systemic inflammatory activation. In preparation for submission to Particle and Fibre Toxicology.
7. Young TL, Dahm M, Schubauer-Berigan M, Erdely A, Ottens AK, Campen MJ, and Zhu Y. Associations between occupational exposures to carbon nanomaterials and circulating inflammatory potential. In preparation for J Expo Sci Environ Epid.
8. Canal CG, Mostovenko E, Young T, Sayyad M, Koblinski J, Erdely A, Campen MJ, Ottens AK. Exosomes as Systemic Mediators of Nanotube Induced Neuroinflammation. In preparation for Mol. Cell. Proteomics.
9. Mostovenko E, Canal CG, Young TL, Erdely A, Campen MJ, Ottens AK. Indirect Mediators of Systemic Health Outcomes Following Nanoparticle Exposure. In preparation for Pharmacology and Therapeutics.
10. Mostovenko E, Dahm MM, Schubauer-Berigan MK, Erdely A, Young TL, Campen MJ, Ottens AK. Serum Peptidome as Diagnostic Markers of Occupational Carbon Nanomaterial Inhalation Exposure. In preparation for Particle and Fibre Toxicology.

Press-Releases

1. Small LM, Keeping our factory workers safe, VCU News, news.vcu.edu/research. Accessed 6 March 2017.
2. Haederle M, UNM researcher explains how air pollution could cause neurological diseases. UNM Newsbeat. http://hscnews.unm.edu/news/. Accessed 2 March 2017.

Abstracts

1. Saunders SA, Carter D, Muldoon PP, Campen MJ, Erdely A, Ottens AK. Effects of occupational nanomaterial exposure on the blood brain barrier. American Society for Biochemistry and Molecular Biology, Virginia Chapter, Undergraduate Research Conference, October, 2016.
2. Ottens AK, Muldoon PP, Vucetic A, Carter DR, Tenzer S, Campen MJ, Erdely AD. Data-independent mass spectrometry for development of occupational nanomaterial exposure biomarkers. American Society for Mass Spectrometry Conference on Mass Spectrometry and Allied Topics, June 2016.
3. Mostovenko E, Muldoon PP, Vucetic A, Campen MJ, Erdely A, Ottens AK. Mass spectrometry development of occupational nanomaterial exposure biomarkers. Society of Toxicology Annual Conference, March, 2017.

4. Ottens AK. Discriminatory circulating peptides from different inhalation exposures—biomarker and cerebrovascular implications. Society of Toxicology Annual Conference, March, 2017.
5. Saunders SA, Carter D, Muldoon PP, Campen MJ, Erdely A, Ottens AK. Effects of occupational nanomaterial exposure on the blood brain barrier. Society of Toxicology Annual Conference, March, 2017.
6. Young T, Sanchez B, Tyler C, Aragon M, Ottens A, Erdely A, Campen M. Role of matrix metalloproteinases (MMPs) in multi-walled carbon nanotube (MWCNT) exposure-induced inflammatory responses. Society of Toxicology Annual Conference, March, 2017.
7. *Saunders SA, Muldoon PP, Pilaka P, Campen MJ, Ottens AK. The effects of occupational nanomaterial exposure on the blood-brain barrier. Annual Biomedical Research Conference for Minority Students, October 2017.
8. *Young TL, Herbert G, Lucas S, Sanchez B, Ottens A, Erdely A, Campen M. Time Course Relationships Between Airway Inflammation, Circulating Exosome Formation, and Systemic Vascular Responses Following Pulmonary Multiwall Carbon Nanotube Exposures. Society of Toxicology Annual Conference, San Antonio Texas, March 2018.
9. *Mostovenko E, Young T, Muldoon PP, Vucetic A, Campen MJ, Ottens AK. Bioactive peptidome as a driver of systemic functional deficits evoked by inhalation of multi-walled carbon nanotubes. 66th American Society for Mass Spectrometry Conference on Mass Spectrometry and Allied Topics, June, 2018.
10. *Mostovenko E, Muldoon PP, Vucetic A, Campen MJ, Ottens AK. Mass Spectrometry Development of Occupational Nanomaterial Exposure Biomarkers. Annual Symposium of the Society for Neuroscience Virginia Chapter, March, 2018.
11. *Young TL, Herbert G, Lucas S, Ottens A, Erdely A, Campen M. The Role of Thrombospondin Type 1 Repeat (TSR) Domain in Multiwalled Carbon Nanotube–Induced Endothelial Dysfunction and Inflammation. International Union of Toxicology, Hawaii, July 17, 2019
12. *Mostovenko E, Saunders SA, Vucetic A, Fraser K, Campen MJ, Erdely A, Ottens AK. Effects of repeated nanomaterial exposure and recovery on circulating mediators and neurotoxicity. Society of Toxicology Annual Conference, March 2019.
13. *Canal CG, Mostovenko E, Young T, Sayyad M, Koblinski J, Erdely A, Campen MJ, Ottens AK. Exosomes as a systemic mediator of nanotube induced dysfunction. Society of Toxicology Annual Conference, March 2019.
14. *Young TL, Herbert G, Lucas S, Sanchez B, Begay J, Ottens AK, Erdely A, Campen MJ. Effects of multi-walled carbon nanotube exposure on brain oxidative stress and inflammation in C57BL/6 mice. Society of Toxicology Annual Conference, March 2019.
15. *Canal CG, Mostovenko E, Young T, Sayyad M, Koblinski J, Erdely A, Campen MJ, Ottens AK. Exosomes as Systemic Mediators of Nanotube-Induced Neurotoxicity. 68th American Society for Mass Spectrometry Conference on Mass Spectrometry and Allied Topics, June, 2020.
16. Mostovenko E, Young TL, Fraser K, Campen MJ, Erdely A, Ottens AK. Effects of Endogenous Peptide Factors on the Integrity of Blood-Brain Barrier Following Carbon Nanotube Exposure. 68th American Society for Mass Spectrometry Conference on Mass Spectrometry and Allied Topics, June, 2020.

Seminars and Invited Talks

1. Campen MJ. “Air Pollution and Health Effects Beyond the Lung: Traveling Sterile Inflammation” Infectious Disease and Inflammation Program, University of New Mexico School of Medicine, May 2016.
2. Campen MJ. “Inhalation of particulates and gases and systemic inflammatory effects: Modification of circulating components promotes cerebrovascular endothelial inflammation and dysfunction.” Japanese Society of Toxicology Annual Conference, Nagoya, Japan, June 2016.
3. Ottens AK. “Omic Mass Spectrometry for Researching Health Outcomes from Environmental Exposures” Department of Chemistry, University of Belgrade, Belgrade, Serbia June 2016
4. Campen MJ. “Circulating Inflammatory Bioactivity Resulting from Environmental Exposures” National Institute of Occupational Health Sciences, Cincinnati, OH, July 19th, 2016.
5. Ottens AK. “Occupational Nanomaterial Exposure Biomarkers: Peptide Byproducts of Pulmonary Pathobiology” National Institute of Occupational Health Sciences, Cincinnati, OH, July 19th, 2016.
6. Campen MJ. “Vascular Toxicity from Inhaled Toxins: Refining our understanding of “indirect” effects”, Division of Cardiology, University of Louisville, October 24, 2016.

7. Campen MJ. “Air Pollution and Health Effects beyond the Lung: Traveling Sterile Inflammation”, Nationwide Children’s Hospital, Columbus, OH, September 14, 2017.
8. *Campen MJ. "Neurovascular effects of inhaled toxicants", MJ Campen, Zhejiang Chinese Medical University, Hangzhou, China, March 26, 2018.
9. Ottens AK. “Hunting Circulating Mediators of Systemic Vascular Dysfunction after Carbon Nanotube Exposure”, AK Ottens, Annual Symposium of the US Human Proteome Organization, Minneapolis, MN, March 12, 2018.
10. Campen MJ. “Inhaled Toxicants and Neuroinflammation: Connecting the Dots”, MJ Campen, Department of Internal Medicine, College of Medicine, University of Arizona-Phoenix, AZ, February 23, 2018.
11. Ottens AK. “Pulmonary Nanotube Exposure Induces Proteolytic Byproducts and Neuroinflammation Consequences”, NTRC section, The National Institute for Occupational Safety and Health, Morgantown, WV, January 10, 2018.
12. Ottens AK. “Hunting Circulating Mediators of Systemic Vascular Dysfunction: a Look after Carbon Nanotube Exposure”, Invited talk, U.S. Human Proteome Organization, Minneapolis, MN, March 12, 2018.
13. Campen MJ. “Neuroinflammatory Consequences of Inhaled Pollutants: Role of Circulating Factors”, Cardiology Grand Rounds, University of California at Los Angeles, December 7, 2018.
14. Campen MJ. “Pulmonary-derived circulating factors promote cerebrovascular inflammatory mechanisms following inhalation of particles and gases” Keynote lecture for International Particle Toxicology Conference, Salzburg, Austria, September 12, 2019.
15. Ottens AK. “Ion mobility and data independent acquisition in peptidomic research” Invited seminar HRMS and Ion Mobility: From Research to Routine, Mass Spectrometry Applications Day, Beverly, MA, August 29, 2019.
16. Campen MJ. “Circulating Molecular Shrapnel: Identifying links between inhaled toxicants and neurological outcomes”, Michigan State University Institute for Integrative Toxicology Seminar Series, January 11, 2019.
17. Campen MJ. “From Cardiovascular Disease, to Fetal Effects, to Neurological Outcomes: Can Air Pollution Really Cause Everything?” University of Connecticut Toxicology Scholars Colloquium Seminar, April 6, 2020.
18. Campen MJ. “Air Pollution Impacts on Diverse Vascular Beds: Brain and Placenta as Targets” Case Western University Cardiovascular Research Institute’s Seminar Series, November 17, 2020.
19. Ottens AK. “The Circulating Peptidome: A Mediator and Diagnostic Window into Systemic Toxicity”, Department of Pharmacology and Toxicology Seminar Series, Virginia Commonwealth University, Richmond, VA, November 17, 2020.

OTHER REQUIRED INFORMATION

1. Include the Cumulative Inclusion Enrollment Table: This study utilized samples from a previously collected occupational cohort. We had no input on the recruitment strategy by our colleagues at NIOSH and, thus, accepted the samples as provided.

TARGETED/PLANNED ENROLLMENT: Number of Subjects			
Ethnic Category	**Females**	**Males**	**Total**
Hispanic or Latino			
Not Hispanic or Latino			
Ethnic Category: Total of All Subjects *			
Racial Categories			
American Indian/Alaska Native			
Asian	2	8	10
Native Hawaiian or Other Pacific Islander			
Black or African American	1	10	11
White	20	67	87
Racial Categories: Total of All Subjects *	23	85	108

2. Inclusion of gender and minority study subjects: This study utilized samples from a previously collected occupational cohort. We had no input on the recruitment strategy by our colleagues at NIOSH and, thus, accepted the samples as provided. Our understanding was that there was no intentional bias in the recruitment, in terms of gender or ethnicity, thus the cohort will ultimately represent the affected occupational community, with some bias incurred by self-selection.

3. Inclusion of Children: This study used serum from an occupationally-exposed cohort, thus children were not included.

4. Materials available for other investigators:
   a. EndogeSeq: This award supported the developing of EndogeSeq, a software program for bioinformatics processing of peptidomic data. This software works with data-independent mode mass spectrometry data generated on Waters time-of-flight instruments. Raw data are first peak-picked using standard Waters PLGS software. Resulting XML datafiles are then read into EndogeSeq where ion events are aligned across biological replicates and prepared for statistical analysis of peptide quantities. Selected peptide data are then processed against EndogeSeq's search engine to identify peptide sequences. The software and instructions for installation and use are available for non-profit research purposes at: https://ottenslab.weebly.com/endogeseq.html

REFERENCES

1 Schisler, J. C. *et al.* Endothelial inflammatory transcriptional responses to an altered plasma exposome following inhalation of diesel emissions. *Inhal Toxicol* **27**, 272-280, doi:10.3109/08958378.2015.1030481 (2015).

2 Channell, M. M., Paffett, M. L., Devlin, R. B., Madden, M. C. & Campen, M. J. Circulating factors induce coronary endothelial cell activation following exposure to inhaled diesel exhaust and nitrogen dioxide in humans: evidence from a novel translational in vitro model. *Toxicol Sci* **127**, 179-186, doi:10.1093/toxsci/kfs084 (2012).

3 Eatemadi, A. *et al.* Carbon nanotubes: properties, synthesis, purification, and medical applications. *Nanoscale Res Lett* **9**, 393, doi:10.1186/1556-276X-9-393 (2014).

4 Pattan, G. & Kaul, G. Health hazards associated with nanomaterials. *Toxicol Ind Health* **30**, 499-519, doi:10.1177/0748233712459900 (2014).

5 Dahm, M. M. *et al.* Carbon Nanotube and Nanofiber Exposure Assessments: An Analysis of 14 Site Visits. *Ann Occup Hyg* **59**, 705-723, doi:10.1093/annhyg/mev020 (2015).

6 Landsiedel, R. *et al.* Inhalation studies for the safety assessment of nanomaterials: status quo and the way forward. *Wiley interdisciplinary reviews. Nanomedicine and nanobiotechnology* **4**, 399-413, doi:10.1002/wnan.1173 (2012).

7 Aragon, M. *et al.* MMP-9-Dependent Serum-Borne Bioactivity Caused by Multiwalled Carbon Nanotube Exposure Induces Vascular Dysfunction via the CD36 Scavenger Receptor. *Toxicol Sci* **150**, 488-498, doi:10.1093/toxsci/kfw015 (2016).

8 Aragon, M. J. *et al.* Serum-borne bioactivity caused by pulmonary multiwalled carbon nanotubes induces neuroinflammation via blood-brain barrier impairment. *Proc Natl Acad Sci U S A* **114**, E1968-E1976, doi:10.1073/pnas.1616070114 (2017).

9 Erdely, A. *et al.* Cross-talk between lung and systemic circulation during carbon nanotube respiratory exposure. Potential biomarkers. *Nano letters* **9**, 36-43, doi:10.1021/nl801828z (2009).

10 Erdely, A. *et al.* Identification of systemic markers from a pulmonary carbon nanotube exposure. *Journal of occupational and environmental medicine / American College of Occupational and Environmental Medicine* **53**, S80-86, doi:10.1097/JOM.0b013e31821ad724 (2011).

11 Lam, C. W., James, J. T., McCluskey, R., Arepalli, S. & Hunter, R. L. A review of carbon nanotube toxicity and assessment of potential occupational and environmental health risks. *Critical reviews in toxicology* **36**, 189-217 (2006).

12 Mitchell, L. A. *et al.* Pulmonary and systemic immune response to inhaled multiwalled carbon nanotubes. *Toxicol Sci* **100**, 203-214, doi:10.1093/toxsci/kfm196 (2007).

13 Porter, D. W. *et al.* Mouse pulmonary dose- and time course-responses induced by exposure to multi-walled carbon nanotubes. *Toxicology* **269**, 136-147, doi:10.1016/j.tox.2009.10.017 (2010).

14 Shvedova, A. A., Pietroiusti, A., Fadeel, B. & Kagan, V. E. Mechanisms of carbon nanotube-induced toxicity: focus on oxidative stress. *Toxicol Appl Pharmacol* **261**, 121-133, doi:10.1016/j.taap.2012.03.023 (2012).

15 Aragon, M. J. *et al.* Inflammatory and Vasoactive Effects of Serum Following Inhalation of Varied Complex Mixtures. *Cardiovasc Toxicol* **16**, 163-171, doi:10.1007/s12012-015-9325-z (2016).

16 Lund, A. K. *et al.* The oxidized low-density lipoprotein receptor mediates vascular effects of inhaled vehicle emissions. *Am J Respir Crit Care Med* **184**, 82-91, doi:10.1164/rccm.201012-1967OC (2011).

17 Robertson, S. *et al.* CD36 mediates endothelial dysfunction downstream of circulating factors induced by O3 exposure. *Toxicol Sci* **134**, 304-311, doi:10.1093/toxsci/kft107 (2013).

18 Block, M. L. & Calderon-Garciduenas, L. Air pollution: mechanisms of neuroinflammation and CNS disease. *Trends Neurosci* **32**, 506-516, doi:10.1016/j.tins.2009.05.009 (2009).

19 Block, M. L. *et al.* The outdoor air pollution and brain health workshop. *Neurotoxicology* **33**, 972-984, doi:10.1016/j.neuro.2012.08.014 (2012).

20 Mumaw, C. L. *et al.* Microglial priming through the lung-brain axis: the role of air pollution-induced circulating factors. *FASEB J* **30**, 1880-1891, doi:10.1096/fj.201500047 (2016).

21 Schubauer-Berigan, M. K., Dahm, M. M. & Yencken, M. S. Engineered carbonaceous nanomaterials manufacturers in the United States: workforce size, characteristics, and feasibility of epidemiologic studies. *Journal of occupational and environmental medicine / American College of Occupational and Environmental Medicine* **53**, S62-67, doi:10.1097/JOM.0b013e31821b1e2c (2011).

22 Bai, N. & van Eeden, S. F. Systemic and vascular effects of circulating diesel exhaust particulate matter. *Inhal Toxicol* **25**, 725-734, doi:10.3109/08958378.2013.844749 (2013).
23 Folkmann, J. K., Vesterdal, L. K., Sheykhzade, M., Loft, S. & Moller, P. Endothelial dysfunction in normal and prediabetic rats with metabolic syndrome exposed by oral gavage to carbon black nanoparticles. *Toxicol Sci* **129**, 98-107, doi:10.1093/toxsci/kfs180 (2012).
24 Ge, C. *et al.* Binding of blood proteins to carbon nanotubes reduces cytotoxicity. *Proc Natl Acad Sci U S A* **108**, 16968-16973, doi:10.1073/pnas.1105270108 (2011).
25 Han, S. G., Newsome, B. & Hennig, B. Titanium dioxide nanoparticles increase inflammatory responses in vascular endothelial cells. *Toxicology* **306**, 1-8, doi:10.1016/j.tox.2013.01.014 (2013).
26 Duan, J. *et al.* Toxic effect of silica nanoparticles on endothelial cells through DNA damage response via Chk1-dependent G2/M checkpoint. *PLoS One* **8**, e62087, doi:10.1371/journal.pone.0062087 (2013).
27 Nawrot, T. S., Perez, L., Kunzli, N., Munters, E. & Nemery, B. Public health importance of triggers of myocardial infarction: a comparative risk assessment. *Lancet* **377**, 732-740, doi:10.1016/S0140-6736(10)62296-9 (2011).
28 Peters, A. & Pope, C. A., 3rd. Cardiopulmonary mortality and air pollution. *Lancet* **360**, 1184-1185, doi:10.1016/S0140-6736(02)11289-X (2002).
29 Pope, C. A., 3rd *et al.* Cardiovascular mortality and long-term exposure to particulate air pollution: epidemiological evidence of general pathophysiological pathways of disease. *Circulation* **109**, 71-77, doi:10.1161/01.CIR.0000108927.80044.7F (2004).
30 Gojova, A. & Barakat, A. I. Vascular endothelial wound closure under shear stress: role of membrane fluidity and flow-sensitive ion channels. *J Appl Physiol (1985)* **98**, 2355-2362, doi:10.1152/japplphysiol.01136.2004 (2005).
31 Li, Z. *et al.* Cardiovascular effects of pulmonary exposure to single-wall carbon nanotubes. *Environ Health Perspect* **115**, 377-382, doi:10.1289/ehp.9688 (2007).
32 Niwa, Y., Hiura, Y., Murayama, T., Yokode, M. & Iwai, N. Nano-sized carbon black exposure exacerbates atherosclerosis in LDL-receptor knockout mice. *Circulation journal : official journal of the Japanese Circulation Society* **71**, 1157-1161 (2007).
33 Nurkiewicz, T. R. *et al.* Systemic microvascular dysfunction and inflammation after pulmonary particulate matter exposure. *Environ Health Perspect* **114**, 412-419 (2006).
34 Simeonova, P. P. & Erdely, A. Engineered nanoparticle respiratory exposure and potential risks for cardiovascular toxicity: predictive tests and biomarkers. *Inhal Toxicol* **21 Suppl 1**, 68-73, doi:10.1080/08958370902942566 (2009).
35 Shvedova, A. A. *et al.* Inhalation vs. aspiration of single-walled carbon nanotubes in C57BL/6 mice: inflammation, fibrosis, oxidative stress, and mutagenesis. *American journal of physiology. Lung cellular and molecular physiology* **295**, L552-565, doi:10.1152/ajplung.90287.2008 (2008).
36 Nurkiewicz, T. R. *et al.* Nanoparticle inhalation augments particle-dependent systemic microvascular dysfunction. *Part Fibre Toxicol* **5**, 1, doi:10.1186/1743-8977-5-1 (2008).
37 Sriram, K. *et al.* Mitochondrial dysfunction and loss of Parkinson's disease-linked proteins contribute to neurotoxicity of manganese-containing welding fumes. *FASEB J* **24**, 4989-5002, doi:10.1096/fj.10-163964 (2010).
38 Ze, Y. *et al.* TiO2 nanoparticles induced hippocampal neuroinflammation in mice. *PLoS One* **9**, e92230, doi:10.1371/journal.pone.0092230 (2014).
39 Levesque, S. *et al.* Diesel exhaust activates and primes microglia: air pollution, neuroinflammation, and regulation of dopaminergic neurotoxicity. *Environ Health Perspect* **119**, 1149-1155, doi:10.1289/ehp.1002986 (2011).
40 Lasagna-Reeves, C. *et al.* Bioaccumulation and toxicity of gold nanoparticles after repeated administration in mice. *Biochemical and biophysical research communications* **393**, 649-655, doi:10.1016/j.bbrc.2010.02.046 (2010).
41 Mercer, R. R. *et al.* Extrapulmonary transport of MWCNT following inhalation exposure. *Part Fibre Toxicol* **10**, 38, doi:10.1186/1743-8977-10-38 (2013).
42 Stott, W. T., Dryzga, M. D. & Ramsey, J. C. Blood-flow distribution in the mouse. *Journal of applied toxicology : JAT* **3**, 310-312 (1983).
43 Agarwal, B. *et al.* Resveratrol for primary prevention of atherosclerosis: clinical trial evidence for improved gene expression in vascular endothelium. *Int J Cardiol* **166**, 246-248, doi:10.1016/j.ijcard.2012.09.027 (2013).

44 Pryor, W. A. & Lightsey, J. W. Mechanisms of nitrogen dioxide reactions: initiation of lipid peroxidation and the production of nitrous Acid. *Science* **214**, 435-437, doi:10.1126/science.214.4519.435 (1981).
45 Postlethwait, E. M., Langford, S. D. & Bidani, A. Reactive absorption of nitrogen dioxide by pulmonary epithelial lining fluid. *J Appl Physiol (1985)* **69**, 523-531 (1990).
46 Ottens, A. K. *et al.* Post-acute brain injury urinary signature: a new resource for molecular diagnostics. *Journal of neurotrauma* **31**, 782-788, doi:10.1089/neu.2013.3116 (2014).
47 Soteriades, E. S., Smith, D. L., Tsismenakis, A. J., Baur, D. M. & Kales, S. N. Cardiovascular disease in US firefighters: a systematic review. *Cardiology in review* **19**, 202-215, doi:10.1097/CRD.0b013e318215c105 (2011).
48 Bjor, B. *et al.* Fifty-year follow-up of mortality among a cohort of iron-ore miners in Sweden, with specific reference to myocardial infarction mortality. *Occupational and environmental medicine* **66**, 264-268, doi:10.1136/oem.2008.040147 (2009).
49 Ibfelt, E., Bonde, J. P. & Hansen, J. Exposure to metal welding fume particles and risk for cardiovascular disease in Denmark: a prospective cohort study. *Occupational and environmental medicine* **67**, 772-777, doi:10.1136/oem.2009.051086 (2010).
50 Suadicani, P., Hein, H. O. & Gyntelberg, F. Strong mediators of social inequalities in risk of ischaemic heart disease: a six-year follow-up in the Copenhagen Male Study. *International journal of epidemiology* **26**, 516-522 (1997).
51 Wiebert, P. *et al.* Occupational exposure to particles and incidence of acute myocardial infarction and other ischaemic heart disease. *Occupational and environmental medicine* **69**, 651-657, doi:10.1136/oemed-2011-100285 (2012).
52 Campen, M., Robertson, S., Lund, A., Lucero, J. & McDonald, J. Engine exhaust particulate and gas phase contributions to vascular toxicity. *Inhal Toxicol* **26**, 353-360, doi:10.3109/08958378.2014.897776 (2014).
53 Zeidler-Erdely, P. C., Kashon, M. L., Li, S. & Antonini, J. M. Response of the mouse lung transcriptome to welding fume: effects of stainless and mild steel fumes on lung gene expression in A/J and C57BL/6J mice. *Respiratory research* **11**, 70, doi:10.1186/1465-9921-11-70 (2010).
54 Erdely, A. *et al.* Inhalation exposure of gas-metal arc stainless steel welding fume increased atherosclerotic lesions in apolipoprotein E knockout mice. *Toxicology letters* **204**, 12-16, doi:10.1016/j.toxlet.2011.03.030 (2011).
55 Porter, D. W. *et al.* Acute pulmonary dose-responses to inhaled multi-walled carbon nanotubes. *Nanotoxicology* **7**, 1179-1194, doi:10.3109/17435390.2012.719649 (2013).
56 Mostovenko, E. *et al.* Nanoparticle exposure driven circulating bioactive peptidome causes systemic inflammation and vascular dysfunction. *Part Fibre Toxicol* **16**, 20, doi:10.1186/s12989-019-0304-6 (2019).
57 Distler, U., Kuharev, J., Navarro, P. & Tenzer, S. Label-free quantification in ion mobility-enhanced data-independent acquisition proteomics. *Nat Protoc* **11**, 795-812, doi:10.1038/nprot.2016.042 (2016).
58 Cortes, D. F., Landis, M. K. & Ottens, A. K. High-capacity peptide-centric platform to decode the proteomic response to brain injury. *Electrophoresis* **33**, 3712-3719, doi:10.1002/elps.201200341 (2012).
59 Cung, H. *et al.* Characterization of a novel endothelial biosensor assay reveals increased cumulative serum inflammatory potential in stabilized coronary artery disease patients. *J Transl Med* **13**, 99, doi:10.1186/s12967-015-0457-5 (2015).
60 Zychowski, K. E. *et al.* Serum from obstructive sleep apnea patients induces inflammatory responses in coronary artery endothelial cells. *Atherosclerosis* **254**, 59-66, doi:10.1016/j.atherosclerosis.2016.09.017 (2016).
61 Luyts, K. *et al.* Nanoparticles in the lungs of old mice: Pulmonary inflammation and oxidative stress without procoagulant effects. *Sci Total Environ* **644**, 907-915, doi:10.1016/j.scitotenv.2018.06.301 (2018).
62 Liao, H. Y. *et al.* Six-month follow-up study of health markers of nanomaterials among workers handling engineered nanomaterials. *Nanotoxicology*, doi:10.3109/17435390.2013.858793 (2013).
63 Simko, M. & Mattsson, M. O. Risks from accidental exposures to engineered nanoparticles and neurological health effects: a critical review. *Part Fibre Toxicol* **7**, 42, doi:10.1186/1743-8977-7-42 (2010).
64 Elder, A. *et al.* Translocation of inhaled ultrafine manganese oxide particles to the central nervous system. *Environ Health Perspect* **114**, 1172-1178 (2006).

65 Paul, J., Strickland, S. & Melchor, J. P. Fibrin deposition accelerates neurovascular damage and neuroinflammation in mouse models of Alzheimer's disease. *The Journal of experimental medicine* **204**, 1999-2008, doi:10.1084/jem.20070304 (2007).
66 Rawlings, N. D., Barrett, A. J. & Finn, R. Twenty years of the MEROPS database of proteolytic enzymes, their substrates and inhibitors. *Nucleic Acids Res* **44**, D343-350, doi:10.1093/nar/gkv1118 (2016).
67 Petersen, T. N., Brunak, S., von Heijne, G. & Nielsen, H. SignalP 4.0: discriminating signal peptides from transmembrane regions. *Nat Methods* **8**, 785-786, doi:10.1038/nmeth.1701 (2011).
68 Wenger, C. D. & Coon, J. J. A proteomics search algorithm specifically designed for high-resolution tandem mass spectra. *J Proteome Res* **12**, 1377-1386, doi:10.1021/pr301024c (2013).
69 Strohalm, M., Kavan, D., Novak, P., Volny, M. & Havlicek, V. mMass 3: a cross-platform software environment for precise analysis of mass spectrometric data. *Anal Chem* **82**, 4648-4651, doi:10.1021/ac100818g (2010).
70 Chen, J., Bardes, E. E., Aronow, B. J. & Jegga, A. G. ToppGene Suite for gene list enrichment analysis and candidate gene prioritization. *Nucleic Acids Res* **37**, W305-311, doi:10.1093/nar/gkp427 (2009).
71 Szklarczyk, D. *et al.* The STRING database in 2017: quality-controlled protein-protein association networks, made broadly accessible. *Nucleic Acids Res* **45**, D362-D368, doi:10.1093/nar/gkw937 (2017).
72 Erdely, A. *et al.* Carbon nanotube dosimetry: from workplace exposure assessment to inhalation toxicology. *Part Fibre Toxicol* **10**, 53, doi:10.1186/1743-8977-10-53 (2013).
73 Saeed, A. I. *et al.* TM4: a free, open-source system for microarray data management and analysis. *Biotechniques* **34**, 374-378, doi:10.2144/03342mt01 (2003).
74 Benjamini, Y. & Hochberg, Y. Controlling the False Discovery Rate - a Practical and Powerful Approach to Multiple Testing. *J R Stat Soc B* **57**, 289-300, doi:DOI 10.1111/j.2517-6161.1995.tb02031.x (1995).
75 Govender, P., Dunn, M. J. & Donnelly, S. C. Proteomics and the lung: Analysis of bronchoalveolar lavage fluid. *Proteomics Clin Appl* **3**, 1044-1051, doi:10.1002/prca.200900032 (2009).
76 Jeong, K., Kim, S. & Bandeira, N. False discovery rates in spectral identification. *BMC Bioinformatics* **13 Suppl 16**, S2, doi:10.1186/1471-2105-13-S16-S2 (2012).
77 Ricard-Blum, S. & Salza, R. Matricryptins and matrikines: biologically active fragments of the extracellular matrix. *Exp Dermatol* **23**, 457-463, doi:10.1111/exd.12435 (2014).
78 Mu, Q., Broughton, D. L. & Yan, B. Endosomal leakage and nuclear translocation of multiwalled carbon nanotubes: developing a model for cell uptake. *Nano letters* **9**, 4370-4375, doi:10.1021/nl902647x (2009).
79 Colombo, M., Raposo, G. & Thery, C. Biogenesis, secretion, and intercellular interactions of exosomes and other extracellular vesicles. *Annu Rev Cell Dev Biol* **30**, 255-289, doi:10.1146/annurev-cellbio-101512-122326 (2014).
80 Park, J. A. *et al.* Tissue factor-bearing exosome secretion from human mechanically stimulated bronchial epithelial cells in vitro and in vivo. *J Allergy Clin Immunol* **130**, 1375-1383, doi:10.1016/j.jaci.2012.05.031 (2012).
81 Mandler, W. K., Nurkiewicz, T. R., Porter, D. W. & Olfert, I. M. Thrombospondin-1 mediates multi-walled carbon nanotube induced impairment of arteriolar dilation. *Nanotoxicology* **11**, 112-122, doi:10.1080/17435390.2016.1277275 (2017).
82 Asch, A. S., Silbiger, S., Heimer, E. & Nachman, R. L. Thrombospondin sequence motif (CSVTCG) is responsible for CD36 binding. *Biochemical and biophysical research communications* **182**, 1208-1217, doi:10.1016/0006-291x(92)91860-s (1992).
83 Klenotic, P. A. *et al.* Molecular basis of antiangiogenic thrombospondin-1 type 1 repeat domain interactions with CD36. *Arterioscler Thromb Vasc Biol* **33**, 1655-1662, doi:10.1161/ATVBAHA.113.301523 (2013).
84 Prudova, A., auf dem Keller, U., Butler, G. S. & Overall, C. M. Multiplex N-terminome analysis of MMP-2 and MMP-9 substrate degradomes by iTRAQ-TAILS quantitative proteomics. *Mol Cell Proteomics* **9**, 894-911, doi:10.1074/mcp.M000050-MCP201 (2010).
85 Seif, K. *et al.* Neutrophil-Mediated Proteolysis of Thrombospondin-1 Promotes Platelet Adhesion and String Formation. *Thromb Haemost* **118**, 2074-2085, doi:10.1055/s-0038-1675229 (2018).
86 Lee, N. V. *et al.* ADAMTS1 mediates the release of antiangiogenic polypeptides from TSP1 and 2. *EMBO J* **25**, 5270-5283, doi:10.1038/sj.emboj.7601400 (2006).

87 Butler, G. S., Dean, R. A., Tam, E. M. & Overall, C. M. Pharmacoproteomics of a metalloproteinase hydroxamate inhibitor in breast cancer cells: dynamics of membrane type 1 matrix metalloproteinase-mediated membrane protein shedding. *Mol Cell Biol* **28**, 4896-4914, doi:10.1128/MCB.01775-07 (2008).
88 Lawler, J., Connolly, J. E., Ferro, P. & Derick, L. H. Thrombin and chymotrypsin interactions with thrombospondin. *Ann N Y Acad Sci* **485**, 273-287, doi:10.1111/j.1749-6632.1986.tb34589.x (1986).
89 Bonnefoy, A. & Legrand, C. Proteolysis of subendothelial adhesive glycoproteins (fibronectin, thrombospondin, and von Willebrand factor) by plasmin, leukocyte cathepsin G, and elastase. *Thromb Res* **98**, 323-332, doi:10.1016/s0049-3848(99)00242-x (2000).
90 Chen, C. Y. *et al.* N-Terminomics identifies HtrA1 cleavage of thrombospondin-1 with generation of a proangiogenic fragment in the polarized retinal pigment epithelial cell model of age-related macular degeneration. *Matrix Biol* **70**, 84-101, doi:10.1016/j.matbio.2018.03.013 (2018).
91 El Rayes, T. *et al.* Lung inflammation promotes metastasis through neutrophil protease-mediated degradation of Tsp-1. *Proc Natl Acad Sci U S A* **112**, 16000-16005, doi:10.1073/pnas.1507294112 (2015).
92 Song, J. *et al.* PROSPER: an integrated feature-based tool for predicting protease substrate cleavage sites. *PLoS One* **7**, e50300, doi:10.1371/journal.pone.0050300 (2012).
93 Tyler, C. R. *et al.* Surface area-dependence of gas-particle interactions influences pulmonary and neuroinflammatory outcomes. *Part Fibre Toxicol* **13**, 64, doi:10.1186/s12989-016-0177-x (2016).
94 Oudin, A. *et al.* Traffic-Related Air Pollution and Dementia Incidence in Northern Sweden: A Longitudinal Study. *Environ Health Perspect* **124**, 306-312, doi:10.1289/ehp.1408322 (2016).
95 Clifford, A., Lang, L., Chen, R., Anstey, K. J. & Seaton, A. Exposure to air pollution and cognitive functioning across the life course--A systematic literature review. *Environ Res* **147**, 383-398, doi:10.1016/j.envres.2016.01.018 (2016).
96 Brockmeyer, S. & D'Angiulli, A. How air pollution alters brain development: the role of neuroinflammation. *Transl Neurosci* **7**, 24-30, doi:10.1515/tnsci-2016-0005 (2016).
97 Schindelin, J. *et al.* Fiji: an open-source platform for biological-image analysis. *Nat Methods* **9**, 676-682, doi:10.1038/nmeth.2019 (2012).
98 Bodaleo, F. J., Montenegro-Venegas, C., Henriquez, D. R., Court, F. A. & Gonzalez-Billault, C. Microtubule-associated protein 1B (MAP1B)-deficient neurons show structural presynaptic deficiencies in vitro and altered presynaptic physiology. *Sci Rep* **6**, 30069, doi:10.1038/srep30069 (2016).
99 Bouquet, C. *et al.* Microtubule-associated protein 1B controls directionality of growth cone migration and axonal branching in regeneration of adult dorsal root ganglia neurons. *J Neurosci* **24**, 7204-7213, doi:10.1523/JNEUROSCI.2254-04.2004 (2004).
100 Kravtsov, V., Oren-Suissa, M. & Podbilewicz, B. The fusogen AFF-1 can rejuvenate the regenerative potential of adult dendritic trees by self-fusion. *Development* **144**, 2364-2374, doi:10.1242/dev.150037 (2017).
101 Oren-Suissa, M., Gattegno, T., Kravtsov, V. & Podbilewicz, B. Extrinsic Repair of Injured Dendrites as a Paradigm for Regeneration by Fusion in Caenorhabditis elegans. *Genetics* **206**, 215-230, doi:10.1534/genetics.116.196386 (2017).
102 Peng, C. *et al.* Vps18 deficiency inhibits dendritogenesis in Purkinje cells by blocking the lysosomal degradation of Lysyl Oxidase. *Biochemical and biophysical research communications* **423**, 715-720, doi:10.1016/j.bbrc.2012.06.021 (2012).
103 Tortosa, E. *et al.* Microtubule-associated protein 1B (MAP1B) is required for dendritic spine development and synaptic maturation. *J Biol Chem* **286**, 40638-40648, doi:10.1074/jbc.M111.271320 (2011).
104 Bitoun, E. & Davies, K. E. The robotic mouse: understanding the role of AF4, a cofactor of transcriptional elongation and chromatin remodelling, in purkinje cell function. *Cerebellum* **8**, 175-183, doi:10.1007/s12311-009-0101-0 (2009).
105 Bitoun, E., Finelli, M. J., Oliver, P. L., Lee, S. & Davies, K. E. AF4 is a critical regulator of the IGF-1 signaling pathway during Purkinje cell development. *J Neurosci* **29**, 15366-15374, doi:10.1523/JNEUROSCI.5188-09.2009 (2009).
106 Peng, C. *et al.* Ablation of vacuole protein sorting 18 (Vps18) gene leads to neurodegeneration and impaired neuronal migration by disrupting multiple vesicle transport pathways to lysosomes. *J Biol Chem* **287**, 32861-32873, doi:10.1074/jbc.M112.384305 (2012).

107 Yamada, M. *et al.* Loss of hippocampal CA3 pyramidal neurons in mice lacking STAM1. *Mol Cell Biol* **21**, 3807-3819, doi:10.1128/MCB.21.11.3807-3819.2001 (2001).
108 Kimura, M. *et al.* Homeobox A4 suppresses vascular remodeling by repressing YAP/TEAD transcriptional activity. *EMBO Rep* **21**, e48389, doi:10.15252/embr.201948389 (2020).
109 Chen, X. *et al.* Terazosin activates Pgk1 and Hsp90 to promote stress resistance. *Nat Chem Biol* **11**, 19-25, doi:10.1038/nchembio.1657 (2015).
110 Schousboe, A. *et al.* Neuron-glia interactions in glutamatergic neurotransmission: roles of oxidative and glycolytic adenosine triphosphate as energy source. *J Neurosci Res* **89**, 1926-1934, doi:10.1002/jnr.22746 (2011).
111 Mannini, B. *et al.* Differential Interactome and Innate Immune Response Activation of Two Structurally Distinct Misfolded Protein Oligomers. *ACS Chem Neurosci* **10**, 3464-3478, doi:10.1021/acschemneuro.9b00088 (2019).
112 Rao, S. K. *et al.* Differential proteomic and behavioral effects of long-term voluntary exercise in wild-type and APP-overexpressing transgenics. *Neurobiol Dis* **78**, 45-55, doi:10.1016/j.nbd.2015.03.018 (2015).
113 Allen, J. L. *et al.* Cognitive Effects of Air Pollution Exposures and Potential Mechanistic Underpinnings. *Curr Environ Health Rep* **4**, 180-191, doi:10.1007/s40572-017-0134-3 (2017).
114 Costa, L. G., Pellacani, C., Dao, K., Kavanagh, T. J. & Roque, P. J. The brominated flame retardant BDE-47 causes oxidative stress and apoptotic cell death in vitro and in vivo in mice. *Neurotoxicology* **48**, 68-76, doi:10.1016/j.neuro.2015.03.008 (2015).
115 Heusinkveld, H. J. *et al.* Neurodegenerative and neurological disorders by small inhaled particles. *Neurotoxicology* **56**, 94-106, doi:10.1016/j.neuro.2016.07.007 (2016).
116 Power, M. C., Adar, S. D., Yanosky, J. D. & Weuve, J. Exposure to air pollution as a potential contributor to cognitive function, cognitive decline, brain imaging, and dementia: A systematic review of epidemiologic research. *Neurotoxicology* **56**, 235-253, doi:10.1016/j.neuro.2016.06.004 (2016).
117 An, L., Liu, S., Yang, Z. & Zhang, T. Cognitive impairment in rats induced by nano-CuO and its possible mechanisms. *Toxicology letters* **213**, 220-227, doi:10.1016/j.toxlet.2012.07.007 (2012).
118 Hartz, A. M., Bauer, B., Block, M. L., Hong, J. S. & Miller, D. S. Diesel exhaust particles induce oxidative stress, proinflammatory signaling, and P-glycoprotein up-regulation at the blood-brain barrier. *FASEB J* **22**, 2723-2733, doi:10.1096/fj.08-106997 (2008).
119 Chen, L., Yokel, R. A., Hennig, B. & Toborek, M. Manufactured aluminum oxide nanoparticles decrease expression of tight junction proteins in brain vasculature. *J Neuroimmune Pharmacol* **3**, 286-295, doi:10.1007/s11481-008-9131-5 (2008).
120 Oppenheim, H. A. *et al.* Exposure to vehicle emissions results in altered blood brain barrier permeability and expression of matrix metalloproteinases and tight junction proteins in mice. *Part Fibre Toxicol* **10**, 62, doi:10.1186/1743-8977-10-62 (2013).
121 Harmon, M. E. *et al.* Residential proximity to abandoned uranium mines and serum inflammatory potential in chronically exposed Navajo communities. *J Expo Sci Environ Epidemiol* **27**, 365-371, doi:10.1038/jes.2016.79 (2017).
122 Cheng, W. *et al.* Carbon content in airway macrophages and genomic instability in Chinese carbon black packers. *Arch Toxicol* **94**, 761-771, doi:10.1007/s00204-020-02678-6 (2020).
123 Tang, J. *et al.* Occupational exposure to carbon black nanoparticles increases inflammatory vascular disease risk: an implication of an ex vivo biosensor assay. *Part Fibre Toxicol* **17**, 47, doi:10.1186/s12989-020-00378-8 (2020).